ELECTROCHEMISTRY APPLICATIONS

FOR SUSTAINABLE ENERGY

ELECTROCHEMISTRY APPLICATIONS FOR SUSTAINABLE ENERGY

By WENDY HUANG, M.A.Sc., B.A.Sc.

Faculty of Engineering

Civil Engineering

A Thesis

Submitted to the School of Graduate Studies

in Partial Fulfillment of the Requirements

for the Degree

Doctor of Philosophy

McMaster University DOCTOR OF PHILOSOPHY (2017) Hamilton, Ontario (Civil Engineering)

TITLE: Electrochemistry Applications for Sustainable Energy AUTHOR: Wendy Huang, M.A.Sc. (McMaster University), B.A.Sc. (University of Regina) SUPERVISOR: Dr. Younggy Kim NUMBER OF PAGES: xvi, 149

Abstract

While the terms reduce, reuse, and recycle are common concepts in minimizing resource waste, most people do not think twice about energy as a resource or the large amounts of wasted energy in wastewater treatment and industrial processes. Recovery of wasted energy or reducing the net energy consumption of such processes would save resources and reduce energy costs. This research investigated emerging energy systems for handling wastewater (bioelectrochemical systems) and waste heat (ion exchange membrane systems) to elucidate and quantify thermodynamic and kinetic phenomena in biological and electrochemical reactions.

Bioelectrochemical systems utilize exoelectrogenic microorganisms for wastewater treatment energy recovery in the form of electricity or biogas. The substrate utilization and electron transfer by exoelectrogens to the bioanode have not been clearly explained and thus there are no commonly accepted models for bioanode performance. A comprehensive model for bioanode operation was proposed including equilibrium, kinetics, and microbiological characteristics. The utilization and preference of different organic substrates were also assessed with electrochemical techniques and it was found that linear sweep voltammetry and exchange current are good indicators of whether a substrate is directly or indirectly utilized by exoelectrogenic microorganisms.

This research also investigated ion exchange membrane systems for energy recovery from waste-grade heat, such as that wasted in the steel refinery and power industries, using

concentration gradients of ammonium bicarbonate solutions. Estimation of the junction potential (amount of concentration gradient energy) has significant technical difficulties for highly concentrated ammonium bicarbonate solutions (e.g., unknowns in equilibrium speciation and activity coefficient determination). A straightforward estimation method was proposed and found to be able to reliably determine the junction potential across an ion exchange membrane based on conductivity measurement, simplifying the model for junction potential determination.

Acknowledgments

I would like to express my heartfelt gratitude to my mentor Dr. Younggy Kim for his endless support, guidance, and supervision over the course of my doctorate studies, without whom I would not have been able to achieve this milestone in my life.

I would also like to thank my supervisory committee, Dr. Sarah Dickson and Dr. Carlos Filipe, for their valuable input and advice, and taking time out of their busy schedules for supervisory committee meetings.

I appreciate the assistance and support from our wonderful lab technicians Ms. Anna Robertson, Mr. Peter Koudys, and Ms. Monica Han who have been so helpful with the construction and operation of devices in the lab. I would also like to thank all the members of the Kim Lab, past and present, for their friendship and support over the years.

I also acknowledge the financial support from the Natural Science and Research Council of Canada (NSERC), Ontario Graduate Scholarship, and the Department of Civil Engineering at McMaster University.

Last but not least, I forever grateful to my family and friends for their love, encouragement, and support as I pursued my goals.

Declaration of Academic Achievement

This thesis has been prepared in accordance with the regulations for a sandwich thesis format as a compilation of papers stipulated by the Faculty of Graduate Studies at McMaster University and as such, the publications that comprise Chapters 2, 3, 4 of this thesis have been co-authored.

Chapter 2: Huang, W., & Kim, Y. Enzyme kinetic model for exoelectrogenic electron transfer in bioelectrochemical systems. Submitted to Bioelectrochemistry.

The methodology, development, model formulation, solution of the model, and calibration of the model were completed by W. Huang with the supervision and consultation of Dr. Y. Kim. The manuscript was prepared by W. Huang and edited by Dr. Y. Kim.

Chapter 3: Huang, W., & Kim, Y. (2016). Electrochemical techniques for evaluating short-chain fatty acid utilization by bioanodes. Environmental Science and Pollution Research, 1-7. doi:10.1007/s11356-016-8026-x

The methodology and experimental procedures were developed by W. Huang with the advice and consultation of Dr. Y. Kim. The experimental work was carried out by W. Huang with the consultation of Dr. Y. Kim. The manuscript was written by W. Huang and edited by Dr. Y. Kim in 2016 and published in Environmental Science and Pollution Research in 2017.

Chapter 4: Huang, W., Walker, W. S., & Kim, Y. (2015). Junction potentials in thermolytic reverse electrodialysis. Desalination, 369, 149-155.

The methodology, model development, and experimental work was developed and carried out by W. Huang with the assistance and consultation of Drs. Y. Kim and S. Walker. The paper was written by W. Huang and edited by Dr. Y. Kim in 2015 and published in Desalination in 2015.

Table of Contents

List of Figures

List of Tables

List of Abbreviations and Symbols

AEM	Anion exchange membrane
ATP	Adenosine triphosphate
BES	Bioelectrochemical system
CE	Coulombic efficiency
CEM	Cation exchange membrane
E_{ap}	Applied potential (V)
EIS	Electrochemical impedance spectroscopy
ETC	Electron transfer chain
F	Faraday's constant
HC	High concentration
I	Electric current (mA or A)
IEM	Ion exchange membrane
LC	Low concentration
LSV	Linear sweep voltammetry
MEC	Microbial electrolysis cell
MFC	Microbial fuel cell
PMF	Proton motive force
R	Ideal gas constant
RED	Reverse electrodialysis
V	Volts

CHAPTER 1 Introduction

Management and disposal of waste can be an energy intensive process and a large part of municipal resources goes in to the management of waste streams such as wastewater. The wastewater treatment technologies we use today are decades old and may not be the best option for efficient wastewater treatment. Conventional wastewater treatment technology is both energy intensive and requires a large footprint, and there are emerging technologies being researched to reduce the energy cost of wastewater, recovering resources from wastewater, and reducing space requirements by decreasing treatment time. In this thesis, methods for low-energy wastewater treatment are explored theoretically and experimentally. Another source of energy from waste is from waste heat. Waste heat recovery methods can reduce energy input requirements by converting waste heat from anthropological activities such as steel processing to electrical power. This thesis presents three papers on wastewater as a potential resource for energy, waste heat recovery and address some of the challenges of implementing these technologies.

1.1 Research objectives

The research presented in this thesis aims to present novel methods using techniques from electrochemistry to study the recovery of energy from wastewater and waste heat using both models and experimental techniques.

The following specific objectives were set to be achieved:

- Develop, validate and calibrate a model for electron transfer in BES that includes the electron transfer chain. The electron transfer chain is an important process that

cells undergo in the conversion of substrate to usable energy that has been overlooked or considered indirectly by previous models (Chapter 2).

- Evaluate substrate utilization and preference in BES by using electrochemical techniques to investigate their oxidation. This study develops electrochemical methods to systematically examine how readily a substrate is utilized, direct and indirect oxidation, and substrate concentration effects on current generation (Chapter 3).
- Create and verify a tool for determining the junction potential across an ion exchange membrane for modeling of thermolytic reverse electrodialysis with ammonium bicarbonate for waste heat recovery applications. The lack of thermodynamic information for high concentration ammonium bicarbonate solutions makes it challenging to model junction potential. This study proposes a method to overcome this difficulty by developing an equation correlating conductivity to junction potential (Chapter 4).

1.2 Bioelectrochemical systems for wastewater treatment

Wastewater treatment is an energy and space intensive process, requiring many pumps, aerators, tanks and reservoirs. With increasingly more stringent water discharge requirements and public concern for what is going into natural receiving waters, it is of interest to look into other methods of wastewater treatment. One of these alternatives is the use of bioelectrochemical systems (BESs). In a BES, organic matter is broken down by anaerobic bacteria and energy is produced either as direct electric current or hydrogen gas.

BESs also offer resource recovery options, such as the recovery of nutrients and metals through reduction and precipitation.

Challenges to the practical implementation of BESs in wastewater treatment include substrate availability, size and scale, methanogenesis, a lack of any widely accepted models and understanding of the microbiological details of the microorganisms involved. There are two types of BESs: microbial fuel cells (MFC) and microbial electrolysis cells (MEC). While they share the same type of bioanode, they differ in their cathodes. MFCs use an air cathode where oxygen reduction occurs at the cathode, and the MFC acts as a galvanic cell and produces electric current directly (Logan et al., 2006; Wang et al., 2009; Liu et al., 2004; Rabaey et al., 2003). MFCs require no external energy source and are more well-known than the electrolytic cell, or microbial electrolysis cell (Tartakovsky et al., 2009; Call et al., 2009; Logan et al., 2008). An MEC is anaerobic with a submerged cathode. The cathode reaction in an MEC reduces water to hydrogen gas. The reduction of water to H_2 gas normally requires 1.23V applied voltage. However, the use of a bioanode lowers this voltage substantially. H_2 gas can be produced in an MEC with as low as 0.4V, effectively reducing energy requirement for H_2 production over 60%.

In addition to energy recovery during wastewater treatment, MECs can be used for the removal and recovery of other resources. MECs have been shown to be capable of removing and recovering heavy metals such as lead and cadmium (Colantonio & Kim, 2016a; Colantonio & Kim, 2016b) as well as nutrients such as phosphate (Tice & Kim, 2014), making them useful for not just wastewater treatment, but also recovery of resources.

Models for the performance of the bioanode is important to the development of bioelectrochemical systems as it allows for us to predict performance and to better understand the detailed mechanisms of electron transfer. While some models have been developed for BESs, there is still no one accepted best model, and there is still a lot to be learned about the behaviour of the bacteria species involved in BESs and improvement to be made on existing models. Another major challenge to the implementation of BESs is limited substrate availability. Most research presently has been at bench scale with synthetic wastewater. However, the substrates used in this synthetic wastewater is not representative of the constituents of real wastewater. Exoelectrogenic bacteria in BESs use a limited range of substrates and substrate preference and the mechanisms involved in substrate utilization require further investigating

One of the main limitations of BESs is that they are still new and in the research stage. The first studies on BESs were done in the 1960s (Davis & Yarbrough, 1962), but most research and advancement on this technology has been in the last twenty years. Relative to conventional activated sludge, this technology is fairly new. The bioanode is also a complex microbial community and there is still much to be learned about optimizing the anode. At a bench-scale, common anode materials include graphite brushes, carbon felt, or carbon cloth connected to wires. Scale-up of the anode to hold a biofilm capable of handling typical wastewater treatment plant flow is one of many challenges facing practical implementation

of BESs at a full scale. Another challenge is the limitations in our knowledge of the behaviour of the bacterial community of the bioanode.

Exoelectrogens are anaerobic bacteria ubiquitous in anaerobic environment, including wastewater collection systems. They are easily enriched in a lab, generally requiring two weeks of operation to develop a biofilm capable of generating stable electric current. For practical purposes, the research for this thesis was performed using mixed cultures enriched from a local wastewater treatment plant. This decision was made with the engineering end-goal of implementation in wastewater treatment in mind. In practical application, it would be impossible to maintain a pure culture of bacteria as the biofilm comes into contact with wastewater during the treatment process. Furthermore, *Geobacter* spp. is very specific in their substrate preferences and a study found that mixed culture biofilms are more robust and capable of handling more substrates (Freguia et al., 2010).

While a mixed culture can break down some short chain fatty acids, the performance of BESs is better when operated with acetic acid than with other short chain fatty acids (Sun et al., 2009). However, acetic acid is not an accurate representation of the organic substrates found in municipal wastewater, which consists of various particulate and complex organics (Tchobanoglous et al., 2003). Studies on substrate utilization have shown that while bioelectrochemical systems have limited capability to break down propionic and butyric acids compared to acetic acid; as a result, organic removal was incomplete and the coulombic efficiency was relatively low (Cheng et al., 2007; Kiely et al., 2011; Freguia et

al., 2010). Partial utilization of other short chain fatty acids, such as butyric and propionic acid occurs, however, it is unknown whether these are broken down directly by exoelectrogens, or if other bacteria in the biofilm first.

1.2.1 Evaluation of bioelectrochemical systems performance

The performance of a biofilm is monitored by the electric current it produces under steady operation and compared to the concentration of substrate provided. Coulombic efficiency is the ratio of coulombs generated by the BES to the coulombs given by the provided substrate and calculated as

$$CE = \frac{32 \int_0^t I dt}{4FV\Delta COD} \quad \text{(Eq 1-1)}$$

where t is time, F is the Faraday constant, V is reactor volume, and ΔCOD is change in the COD over time t.

Theoretically, the coulombic efficiency for an MEC is 100%. However, experimentally, values of over 100% are frequently observed during the operation of a single-celled MEC with no membrane separating the anode and cathode. This is due to the consumption of hydrogen by the anode biofilm. The hydrogen produced at the cathode is used as an electron donor by the anode bacteria, thus producing more electrons than what is provided by the substrate.

1.3 Modeling of bioelectrochemical systems

Three electron transfer mechanisms have been proposed for the transfer of electrons from a biofilm to the anode. In the direct electron transfer model, the cell membrane contains cytochromes that transfer electrons from the bacteria cells to the anode they are attached to. Direct electron transfer requires the bacteria to be in contact with the anode. Enzymes on the membrane of the bacteria transfer electrons to the electrode. This type of transfer requires direct contact of the cell membrane to the electrode surface, and thus is very surface area dependent. Another type of transfer is indirect, through soluble mediators. Electrons are passed through an electron transfer chain with soluble exocellular enzymes. Assay experiments have been performed to show that this type of transfer is possible (Li et al., 2012). The third mechanism is through a conductive matrix. Microorganisms produce extracellular structures, such as pili, that act as nanowires to connect them to the electrode. Electrons are transferred through these pili nanowires to the bioanode (Reguera et al., 2005). It is believed that electron transfer in BES occurs through a combination of mechanisms. *Geobacter* species has been shown to transfer electrons through a conductive matrix of conductive pili (Reguera et al., 2005) while *Shewanella* species have been shown to transfer electrons through a combination of extracellular electron shuttles as well as conductive pili.

The three key components in modeling of BESs are kinetic, equilibrium, and transfer equations. In this section we will discuss the equations and their relevance in BES models. Models in BES modeling involve concepts from biology, microbiology, electrochemistry, fluid mechanics, and thermodynamics.

1.3.1 Kinetic models

Michaelis-Menton kinetics is often used in BES modeling. One equation very commonly used in BES modeling is the Monod equation for microbial growth and substrate utilization (Zhang & Halme, 1995; Torres et al., 2007; Kato-Marcus et al., 2007). The Monod equation relates growth rate to substrate concentration and is commonly used to describe bacteria growth in both suspended and attached systems. The Monod equation assumes soluble electron donors and acceptors, and is described by two constants: the maximum specific growth rate and half-saturation constant. Since the Monod equation is accepted as a model for describing microbial growth, it is reasonable to expect that it has been applied in BES modeling as well. In BES modeling, a modified form of the Monod equation is used because the electron acceptor is a solid electrode and does not have a concentration and must be modified. One modification commonly seen is the addition of Nernst equation (Zhang & Halme, 1995; Torres et al., 2007) which will be discussed in a later section.

However, there are some limitations to how applicable the Monod equation is for use in BES. While the models fit experimental data, the Monod equation is not valid in some conditions. Notably, Monod growth does not fit with the electric current profile typical of a BES. When assuming Monod equation, one would expect electric current to gradually decline as substrate is depleted; however, this is hardly the case. Electric current in BES stays steady and sharply decline when substrate is depleted. Monod-based models have been fitted to experimental results in a number of studies. However, Monod models cannot describe conditions where substrate concentration is not the limiting factor. Since the

Monod equation is for substrate utilization, in excess of substrate when other factors are limiting to electric current, the Monod equation is inadequate. Additionally, when substrate concentrations are high (>30 g/L), substrate inhibition can occur and as a result Monod models cannot describe the system (Jafary et al., 2013; Peng et al., 2013).

Another kinetic equation used in BES modeling is the Butler-Volmer equation, commonly used in describing electrode kinetics. The equation has been used to model electron transfer by a mediator, such as NAD+/NADH, cytochromes, quinones (Shcroder, 2007), or any other recyclable electron carrier or enzyme. Models based on the Butler-Volmer equation can be used for modeling both direct electron transfer and indirect electron transfer through exocellular mediators. In models utilizing the Butler-Volmer equation, the models assume that at least one redox enzyme governs the electron transfer. While many enzymes are involved in transferring electrons from inside the cell to the outer membrane, and then to the electrode, it is necessary to assume that only one enzyme needs to be modeled and it governs the rate.

A limitation to the validity of the Butler-Volmer equation in BESs is the reversibility of the reaction. The Butler-Volmer equation describes a reversible system, but the reactions in BES are not reversible. The anode consumes organics, breaking organic compounds down to CO_2 and energy is released as part of their metabolic processes, and this reaction is not reversible. While the overall reaction of substrate utilization to release electrons is irreversible, there are reversible steps within the series of reactions. The Butler-Volmer

equation is applied specifically to model the transfer of electrons by the mediator enzymes. Under these conditions, if the total concentration of mediators in both its oxidized and reduced forms stays constant, the Butler-Volmer equation can be valid for that step of the reaction. In models using the Butler-Volmer equation, the equation is applied to model the transfer of one electron by one enzyme in its oxidized and reduced states (Hamelers et al., 2011; Korth et al, 2015). Since the enzyme is reduced upon receiving an electron and oxidized when releasing the electron, this reaction is reversible. For this to be applicable for an entire biofilm, however, the concentration of redox enzymes must remain constant; that is, the active biomass on the bioanode must also remain constant with cell growth rate equal to the rate of cell decay.

Electron transfer is accomplished through redox enzymes, and enzyme kinetics-based models have been used to simulate BES systems. The ping-pong model (Peng et al., 2013) used an enzyme based model to model current density in BES. Enzyme kinetic equations were used to model substrate utilization, electron transfer within the cells, and extracellular transfer from the cell to the anode. The ping-pong model addressed both low and high substrate conditions and reflected the inhibition effect under high substrate conditions.

Substrate inhibition and toxic inhibition models have also been applied to BES models (Jafary et al., 2012; Stein et al., 2012). The Haldane inhibition model was applied to results from a MFC using yeast as the biocatalyst, and the model was able to predict the inhibition effects of high substrate concentrations.

1.3.2 Equilibrium models

The Nernst equation is used to determine the electrochemical cell potentials under non-standard state conditions. In BES models, the Nernst equation is often found in the Nernst-Monod model, where the Monod equation for substrate utilization is coupled with the Nernst equation for electron transfer. The Nernst-Monod model was proposed by Zhang (1995), and has since been used in a number of models. While this type of models has been shown to fit experimental data well, it was not valid at high substrate concentrations due to substrate inhibition effects. The Nernst model is also used to describe electron transfer via electron shuttle, with each enzyme involved having an oxidized and reduced form with an equilibrium potential. One limitation of the Nernst equation is that it requires the redox potential of the enzymes in the metabolic pathways used by the microorganisms, and there is limited knowledge on this front.

1.3.3 Transport models

The third component in BES modeling is transport equations, including mass transport through the biofilm, charge transfer, proton transport, and heat transport. The Nernst-Planck equation is used to model diffusion of substrate through the biofilm (Renslow et al., 2013; Oliviera et al., 2013). Oliveira et al. developed a steady-state one-dimensional model for determining current density in MFCs. In this study, one dimensional model refers to transfer only on the x-axis and diffusion is assumed to be the only transport mechanism and convection is negligible. The model uses Fick's diffusion to model mass transfer through

the MFC including diffusion of oxygen through the air cathode, carbon dioxide at the anode, and substrate transfer through the biofilm. Heat transfer is modeled by Fourier's law for differential thermal energy conservation. The steady state assumption assumes that biomass remains constant, where biofilm growth through substrate utilization is equal to the loss by decay. While over a long term this assumption is not valid since biomass does not stay constant, over a short period of time this assumption can be valid. In another model, it was found that for biofilms of relatively uniform thickness, one-dimensional transfer is sufficient for BES models (Picioreanu et al., 2010). However, convection must be considered for complex electrode geometry since without consideration for convection, performance of porous electrodes could not be modeled accurately.

The importance of mass transport models in BES is dependent on anode geometry. For high surface area anodes, such as a brush anode, mass transfer through the biofilm may not be rate-limiting. For anodes with lower surface area, such as flat anodes, mass transfer may play an important role. The effect of anode geometry and biofilm thickness have been modeled by computational dynamics (Picioreanu et al., 2010), and it was found that while electrode geometry does affect current production in BESs, highly porous electrodes with high surface area do not necessarily correlate to better performance. Through modeling fluid dynamics, it was found that if there was no flow through the pores, higher surface area did not increase current density compared to a planar electrode under the same operating conditions. When convection through the pores did occur, higher current densities were observed (Picioreanu et al., 2010). The study also modeled proton transfer through the

biofilm. In BESs, protons are released during substrate oxidation at the anode, resulting in a pH gradient. The microorganisms involved in exoelectrogenic electron transfer have been shown to be sensitive to pH conditions, with their performance decreasing dramatically when pH is low. Thus, proton transport models have been used to simulate the release of protons in acetate oxidation (Kato-Marcus et al., 2011). The model used the proton condition and mass transfer to model proton transport in the biofilm, and the model showed that the protons released due to acetate oxidation at the anode deactivate portions of the biofilm. Alkalinity present in the bulk solution is consumed as it transports protons from the biofilm to the bulk liquid, lowering the pH in the bulk liquid near the biofilm. Since the pH gradient between bulk liquid and biofilm is lower, proton transfer from the biofilm to the liquid decreases, causing more protons to accumulate in the biofilm and lowering the pH in the biofilm, thus deactivating the biofilm. Increasing bicarbonate concentration to increase the buffer capacity has been shown, both experimentally and in models, to be effective for mitigating this effect.

1.3.4 Fluid dynamics models

Typical BESs do not involve mixing while some experiments included mixing in the reactor to ensure homogeneous conditions in the liquid of the reactors (Oliveira, 2013). In general, the movement of the fluid in reactors is not considered to be important in BES models and few studies have addressed this aspect. However, fluid dynamics has been used to model the effect of electrode geometry on biofilm growth, thickness, and evenness. In one model, Picioreanu et al (2010) used fluid dynamics to model how a biofilm forms on different

anode geometries and pH effects, and the model was also applied to a case that involved multiple microorganisms species including exoelectrogens, fermenting bacteria, and methanogens.

1.3.5 Combined models

Bioelectrochemical systems are complex and involve both kinetic and equilibrium components. Kinetic and equilibrium models have been combined in models such as the Nernst-Monod model first introduced by Zhang et al. (1995) and verified with microbial fuel cells. The Nernst-Monod models replace the half saturation constant in the Monod equation with electric potential from the Nernst equation, as there is no concentration or saturation constant for a solid electrode. Since its introduction, the model has been further developed to model transfer by soluble mediators (Picioreanu et al., 2010), to model redox potentials in biofilms and electron transfer (Snider et al., 2012) and to model the effects of electron transfer with varying electric potential (Yoho et al., 2014).

The model fits experimental data gathered from both steady-state and non-steady-state experiments; however, the model has limitations. The Nernst equation is an equilibrium model while the Monod model is a kinetic model. While the model does fit some experimental results the combination of equilibrium and kinetic equations as one equation is technically not reasonable. In order for the Nernst-Monod model to be valid, the system is assumed to be governed by bacteria growth kinetics, which may not be always true,

especially in high substrate conditions. It has also been shown that Nernst-Monod models cannot accurately predict equilibrium current.

Another limitation of the Nernst-Monod model is that it requires a detailed understanding of the biofilm, the microorganisms species involved, and the metabolic pathways used. The Nernst term is dependent on the metabolic pathways used to transfer electrons (Torres et al., 2008; Shroder et al., 2007). The application of the Nernst equation requires the redox potentials of all enzymes involved; however, there is limited knowledge of what enzymes are used in the metabolic pathways, concentrations of enzymes, whether enzymes change based on the operating conditions, and many other factors. While this term can be experimentally measured as half saturation coefficient (Kato-Marcus et al., 2007), it varies from one biofilm to another and thus this equation would be difficult to apply a model verified on one biofilm to another biofilm for which we have no information.

The Butler-Volmer-Monod model was proposed as a model that, unlike the Nernst-Monod model, can predict equilibrium current. The Butler-Volmer-Monod model combines the Butler-Volmer equation for electrode reactions with the Monod equation for biomass production and substrate utilization (Hamelers et al., 2011; Picioreanu et al., 2007; Zeng et al., 2010). The model is based on kinetic equations, so unlike the Nernst-Monod model it does not mix equilibrium and kinetic equations. However, the Butler-Volmer equation fundamentally assumes that all reactions are reversible, which is not the case with substrate utilization, as substrate is depleted and the reaction at the bioanode is not reversible. The

Butler-Volmer-Monod model involves, at minimum, two kinetic processes – substrate utilization, modeled by the Monod model, and electron transfer from the microbe to the electrode. The Butler-Volmer-Monod model assumes that the intermediate processes are not rate limiting, and that the rate of electron transfer is not dependent on these processes (Hamelers et al., 2011).

Picioreanu et al (2010) used fluid dynamics and an extended Nernst-Planck equation to model biofilm growth and pH effects. This model uses a set of fluid dynamic equations, and uses the Nernst-Planck equation to model diffusion and mass transfer of substrate and electrons. The Nernst-Ping-Pong model proposed by Peng (2013) uses enzyme kinetics to describe substrate utilization by a ping-pong electron transfer mechanism, and the Nernst equation to represent the exocellular electron transfer from microbe to the anode. This model found that at low substrate concentrations, where substrate can reasonably be assumed to be rate limiting, the model matched results obtained from a Monod-based model, while at high substrate concentrations the model showed substrate inhibition effects.

1.3.6 Model development

While many models have been proposed and are capable of capturing the trends seen in BESs, the research on model development in this research looks into the biological steps occurring in a cell as it consumes substrate and releases electrons to the bioanode. The model developed in this research is novel in its addition of the electron transfer chain, the process by which cells convert high-energy carrier molecules (NADH) into usable energy

molecules (ATP). The model presented in Chapter 2 utilizes an enzyme kinetic model to model substrate utilization, Nernst equilibrium to model a simplified electron transfer chain consisting of one enzyme pair, and the Butler-Volmer equation to model the transfer of electrons to the solid terminal electron acceptor, or bioanode. This model was verified with experimental results under both fixed and non-steady state conditions and found to be capable of capturing the key features of BESs.

1.3.7 Governing factors on electric current

Exoelectrogenic bacteria utilize a limited range of substrates. Studies have shown that BESs perform best with simple substrates, such as acetate, and that performance and efficiency decrease with more complex substrates such as glucose and short chain fatty acids. Other electron donors that have been modeled in BESs include glucose (Picioreanu et al., 2010), sulfide (Fischer et al., 2015; Liu et al., 2015), brewery wastewater (Wen et al., 2009), fruit sugars such as date syrup (Jafary et al., 2012). For high concentrations of a single substrate type, it was found that inhibition kinetics can be used to model the current and power density. In Jafary's study, they found higher current and power densities for a MFC fed with a high concentration of date syrup in comparison to one fed with a high concentration of glucose. This is due to date syrup containing a diverse mix of sugars, while glucose is one single type of sugar, thus, inhibition effects are less significant in date syrup.

BESs are sensitive to environmental conditions, showing inactivation due to oxygen, low substrate, competition with methanogens, and low pH. Known exoelectrogens, such as

Geobacter spp, are inactivated at pH lower than 6.5. While pH sensitivity is a critical aspect of BES performance, few models have addressed the issue. One pH model (Picioreanu et al., 2010) used Nernst-Planck equation and mass balance to model diffusion, electromigration and pH effects in BESs under different pH buffer concentrations. This model found that in a BES with a cation exchange membrane, proton transport was found to be negligible, and there was a buildup of protons at the anode, leading to lowering pH and current density. Thus, increasing the bicarbonate concentration could counter this effect.

Both pure culture and mixed culture BESs have been used in the verification of electron transfer models (Lee et al., 2009; Renslow et al., 2013; Rousseau et al., 2014). Most models that modeled overall performance of BESs were verified with mixed cultures using wastewater as the inoculum. Experiments with pure cultures used known exoelectrogens, namely *Geobacter sulfurreducens* and *Shewanella oneidensis* MR-1. Yeasts, such as *Sacchoromyces cerevisiae,* have also been shown to exhibit exoelectrogenic capabilities and inhibition models have been fitted to the results of a yeast-catalyzed MFC (Jafary et al., 2012).

Most previous studies did not address interaction between different types of microorganisms that populate anaerobic environments, such as methanogens. One study (Picioreanu et al., 2008) combined a computational fluid dynamic model for microbial fuel cells with the International Water Association's ADM1 (Anaerobic Digestion Model No.1) to model the performance microbial fuel cells containing multiple types of microbes,

including exoelectrogens, fermenters, and methanogens. This model was able to model the utilization of more complex substrates such as glucose, to short-chain fatty acids by glucose-consuming microorganisms. Methanogens and acetate-producing bacteria further break down short-chain fatty acids to methane and acetate, and exoelectrogens utilize acetate for current production.

In pure-culture experiments, *Geobacter* species were often used for verifying direct transfer and conductive matrix models. This is due to it being commonly accepted that *Geobacter* transfers electrons mainly through direct electron transfer. *Shewanella* species transfer electrons through a combination of conductive matrix and soluble mediator mechanisms, thus, models that investigate electron transfer through soluble mediators used *Shewanella* in their model verification. In one experiment, a colour changing mediator was used where the oxidized and reduced forms of the enzyme had different colours, and the study found that when plated there was a visible diameter where the colour changed, indicating that there was a range where electron transfer could occur through these soluble mediators (Li et al., 2012).

Some exoelectrogens obtain energy from inorganic sources, such as sulfur. Sulfur oxidizing bacteria known as *Desulfobulbacaea* spp. are marine sediment bacteria that produce long filmaments that are capable of transferring electrons over a distance up to 2 mm. These bacteria oxidize sulfur as their electron source, and produce electrons. Their behavior has been modeled by a 3-part reaction to represent metabolism, electron transfer, and electron

conduction (Liu et al., 2015; Fischer et al., 2014). The oxidation of sulfide as a substrate for biomass growth is modeled by Michaelis-Menton kinetics, and the transfer of electrons within the cell is described by the Butler-Volmer equation with enzymes to cycle the electrons within the cell. Extracellular conduction and long-range electron transfer is achieved by a conductive matrix consisting of long, conductive extracellular filaments.

1.4 Thermolytic reverse electrodialysis

Another source of wasted energy is waste heat from industrial processes. Heat is generated in many processes, by mechanical motion or heating. Even with insulation, heat will be lost to the ambient surroundings, resulting in loss of energy and money. An estimated 220 TWh of energy is lost as heat from slag production worldwide in the steel manufacturing process (Barati et al., 2011). Through energy recovery from waste heat, we can lower the net energy cost by producing a small amount of electrical power from heat that would be otherwise dissipated.

One method of energy recovery is through reverse electrodialysis (RED), where a stack of ion exchange membranes is used to convert the concentration difference of two electrolyte solutions into electric current. In RED, ion exchange membranes (IEMs) are used to extract energy from a salinity difference. Ion exchange membranes are polymer membranes containing fixed charges that allow selective ion movement, rather than separating by particle size as with filtration membranes. A stack of alternating anion exchange membranes (AEM) and cation exchange membranes (CEM) is placed between high and

low concentration electrolyte solutions (Fig 1-1). Due to the concentration gradient, cations from the higher concentration solution migrate across the cation exchange membranes into the lower concentration solution and anions through the anion exchange membranes, resulting in the accumulation of cations and anions on either side of the stack. Electric current can be produced across a stack of IEMs in this manner.

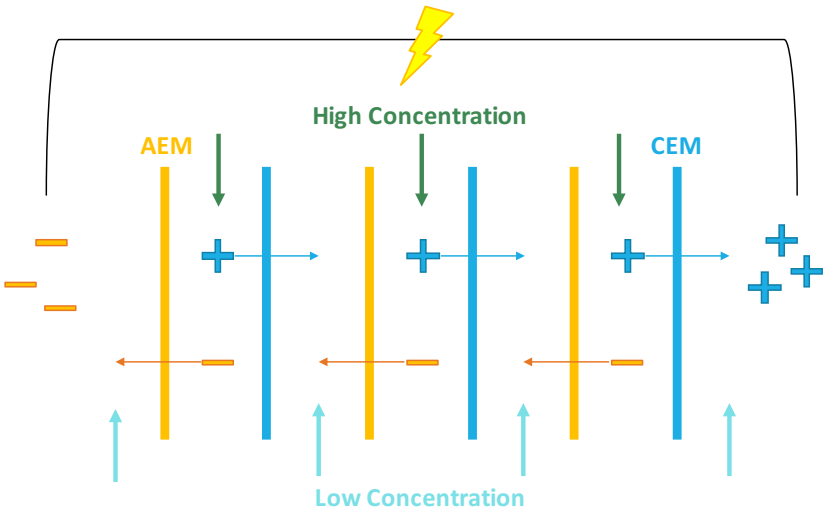

Figure 1-1 Reverse electrodialysis across three ion exchange membrane pairs

RED has been used to extract energy the salinity difference between seawater and fresh water (Dlugolecki et al., 2009; Post et al., 2008; Weinstein et al., 1976). This technology can also be used to generate electric power from any electrolyte solutions, and ammonium bicarbonate (NH_3HCO_3) is of particular interest. Ammonium bicarbonate is a soluble salt with properties that make it appealing for use in RED for waste heat energy recovery, as it converts to gas and separates from solution at 60ºC (Cath et al., 2006), a temperature that is easily reached in manufacturing processes such as that of steel. After the high and low

concentration solutions have passed through the RED stack, the concentration gradient between the solutions becomes too small to generate power and must be regenerated. In order to maintain current, these solutions must be returned to their original high and low concentrations. With a small amount of heat, ammonium bicarbonate can be vaporized and removed from the low concentration stream and put back into the high concentration stream, regenerating that energy potential gradient. Waste heat is an ideal application for this. As its name implies, this heat is normally wasted as the temperatures are generally insufficient for use again in the tasks that generated this heat, but by directing this heat into solution regeneration, it is possible to convert a portion of this heat into electrical energy. RED with ammonium bicarbonate solutions has been shown to produce energy as electricity (Cusick et al., 2012; Luo et al., 2012; Liu et al., 2014) and hydrogen gas (Nam et al., 2012; Hatzell et al., 2014).

One of the difficulties with ammonium bicarbonate for RED operation is that the chemical properties of its solution make it difficult to model the energy potential across an energy gradient. Ammonium bicarbonate in solution contains ammonia, ammonium, carbonate, carbamate and bicarbonate in equilibrium. It is not practical to determine the equilibrium concentrations of all of these ion species at all times. The activity coefficient of the individual ionic species is also unknown in ammonium carbonate solution and literature values for the thermodynamic constants required do not exist. It is thus highly difficult to determine the energy between a low and high concentration solution across an IEM, known as the junction potential (ϕ_{jct}), using the definition of the junction potential (Eq 2-1).

$$\left|\phi_{jct}\right| = \frac{RT}{F}\sum_i \frac{t_i}{z_i} ln \frac{a_i^{HC}}{a_i^{LC}} \quad \text{(Eq 1-2)}$$

where R is the gas constant, T is the temperature, t_i is the transport number of ion species i, z is the charge of i, and a_i is the activity of i. The calculation for the junction potential requires the activity coefficients of all ions in the solution, which is nearly impossible to determine in high concentration ammonium bicarbonate solutions. However, the junction potential can be measured across one ion exchange membrane using reference electrodes and a two-chamber cell separated with a cation or anion exchange membrane. Conductivity of electrolyte solutions is related to activity, and also easily measured experimentally. Thus, in Chapter 4, a new method to use conductivity to estimate junction potential is proposed and this correlation was experimentally verified.

1.5 References

Barati, M., Esfahani, S., & Utigard, T. A. (2011). Energy recovery from high temperature slags. *Energy*, *36*(9), 5440-5449.

Bell, L. E. (2008). Cooling, heating, generating power, and recovering waste heat with thermoelectric systems. *Science*, *321*(5895), 1457-1461.

Call, D. F., Wagner, R. C., & Logan, B. E. (2009). Hydrogen production by Geobacter species and a mixed consortium in a microbial electrolysis cell. *Applied and environmental microbiology*, *75*(24), 7579-7587.

Cath, T. Y., Childress, A. E., & Elimelech, M. (2006). Forward osmosis: principles, applications, and recent developments. *Journal of membrane science*, *281*(1), 70-87.

Colantonio, N., & Kim, Y. (2016a). Cadmium (II) removal mechanisms in microbial electrolysis cells. *Journal of hazardous materials*, *311*, 134-141.

Colantonio, N., & Kim, Y. (2016b). Lead (II) Removal at the Bioanode of Microbial Electrolysis Cells. *ChemistrySelect*, *1*(18), 5743-5748.

Davis, J. B., & Yarbrough, H. F. (1962). Preliminary experiments on a microbial fuel cell. *Science*, *137*(3530), 615-616.

Długołęcki, P., Gambier, A., Nijmeijer, K., & Wessling, M. (2009). Practical potential of reverse electrodialysis as process for sustainable energy generation. *Environmental science & technology*, *43*(17), 6888-6894.

Fischer, K. M., Batstone, D. J., van Loosdrecht, M. C., & Picioreanu, C. (2015). A mathematical model for electrochemically active filamentous sulfide-oxidising bacteria. *Bioelectrochemistry*, *102*, 10-20.

Freguia, S., Teh, E. H., Boon, N., Leung, K. M., Keller, J., & Rabaey, K. (2010). Microbial fuel cells operating on mixed fatty acids. *Bioresource Technology*, *101*(4), 1233-1238.

Hamelers, H. V., Ter Heijne, A., Stein, N., Rozendal, R. A., & Buisman, C. J. (2011). Butler–Volmer–Monod model for describing bio-anode polarization curves. *Bioresource technology*, *102*(1), 381-387.

Jafary, T., Ghoreyshi, A. A., Najafpour, G. D., Fatemi, S., & Rahimnejad, M. (2013). Investigation on performance of microbial fuel cells based on carbon sources and kinetic models. *International Journal of Energy Research*, *37*(12), 1539-1549.

Kato Marcus, A., Torres, C. I., & Rittmann, B. E. (2007). Conduction-based modeling of the biofilm anode of a microbial fuel cell. *Biotechnology and Bioengineering*, *98*(6), 1171-1182.

Korth, B., Rosa, L. F., Harnisch, F., & Picioreanu, C. (2015). A framework for modeling electroactive microbial biofilms performing direct electron transfer. *Bioelectrochemistry*, *106*, 194-206.

Li, R., Tiedje, J. M., Chiu, C., & Worden, R. M. (2012). Soluble electron shuttles can mediate energy taxis toward insoluble electron acceptors. *Environmental science & technology*, *46*(5), 2813-2820.

Li, Y., Wu, Y., Liu, B., Luan, H., Vadas, T., Guo, W., & Li, B. (2015). Self-sustained reduction of multiple metals in a microbial fuel cell–microbial electrolysis cell hybrid system. *Bioresource technology*, *192*, 238-246.

Liu, H., Ramnarayanan, R., & Logan, B. E. (2004). Production of electricity during wastewater treatment using a single chamber microbial fuel cell. *Environmental science & technology*, *38*(7), 2281-2285.

Liu, Y., Peng, L., Gao, S. H., Dai, X., & Ni, B. J. (2015). Mathematical modeling of microbial extracellular electron transfer by electrically active microorganisms. *Environmental Science: Water Research & Technology*, *1*(6), 747-752.

Logan, B. E., Call, D., Cheng, S., Hamelers, H. V., Sleutels, T. H., Jeremiasse, A. W., & Rozendal, R. A. (2008). Microbial electrolysis cells for high yield hydrogen gas production from organic matter. *Environmental Science & Technology*, *42*(23), 8630-8640.

Logan, B. E., Hamelers, B., Rozendal, R., Schröder, U., Keller, J., Freguia, S., & Rabaey, K. (2006). Microbial fuel cells: methodology and technology. *Environmental science & technology*, *40*(17), 5181-5192.

Madigan, M. T., Martinko, J. M., Bender, K. S., Buckley, D. H., & Stahl, D. A. (2015). *Brock biology of microorganisms* (Fourteenth edition.). Boston: Pearson.

Oliveira, V. B., Simões, M., Melo, L. F., & Pinto, A. M. F. R. (2013). A 1D mathematical model for a microbial fuel cell. *Energy*, *61*, 463-471.

Peng, S., Liang, D. W., Diao, P., Liu, Y., Lan, F., Yang, Y., ... & Xiang, Y. (2013). Nernst-ping-pong model for evaluating the effects of the substrate concentration and anode potential on the kinetic characteristics of bioanode. *Bioresource technology*, *136*, 610-616.

Picioreanu, C., Head, I. M., Katuri, K. P., van Loosdrecht, M. C., & Scott, K. (2007). A computational model for biofilm-based microbial fuel cells. *Water Research*, *41*(13), 2921-2940.

Picioreanu, C., Katuri, K. P., Head, I. M., van Loosdrecht, M. C., & Scott, K. (2008). Mathematical model for microbial fuel cells with anodic biofilms and anaerobic digestion. *Water science and technology*, *57*(7), 965-971.

Picioreanu, C., Katuri, K. P., van Loosdrecht, M. C., Head, I. M., & Scott, K. (2010). Modelling microbial fuel cells with suspended cells and added electron transfer mediator. *Journal of applied electrochemistry*, *40*(1), 151.

Picioreanu, C., van Loosdrecht, M. C., Curtis, T. P., & Scott, K. (2010). Model based evaluation of the effect of pH and electrode geometry on microbial fuel cell performance. *Bioelectrochemistry*, *78*(1), 8-24.

Picioreanu, C., van Loosdrecht, M. C., Curtis, T. P., & Scott, K. (2010). Model based evaluation of the effect of pH and electrode geometry on microbial fuel cell performance. *Bioelectrochemistry*, *78*(1), 8-24.

Post, J. W., Hamelers, H. V., & Buisman, C. J. (2008). Energy recovery from controlled mixing salt and fresh water with a reverse electrodialysis system. *Environmental science & technology*, *42*(15), 5785-5790.

Rabaey, K., Lissens, G., Siciliano, S. D., & Verstraete, W. (2003). A microbial fuel cell capable of converting glucose to electricity at high rate and efficiency. *Biotechnology letters*, *25*(18), 1531-1535.

Reguera, G., McCarthy, K. D., Mehta, T., Nicoll, J. S., Tuominen, M. T., & Lovley, D. R. (2005). Extracellular electron transfer via microbial nanowires. *Nature*, *435*(7045), 1098-1101.

Renslow, R., Babauta, J., Kuprat, A., Schenk, J., Ivory, C., Fredrickson, J., & Beyenal, H. (2013). Modeling biofilms with dual extracellular electron transfer mechanisms. *Physical Chemistry Chemical Physics*, *15*(44), 19262-19283.

Schröder, U. (2007). Anodic electron transfer mechanisms in microbial fuel cells and their energy efficiency. *Physical Chemistry Chemical Physics*, *9*(21), 2619-2629.

Snider, R. M., Strycharz-Glaven, S. M., Tsoi, S. D., Erickson, J. S., & Tender, L. M. (2012). Long-range electron transport in Geobacter sulfurreducens biofilms is redox gradient-driven. *Proceedings of the National Academy of Sciences*, *109*(38), 15467-15472.

Sun, M., Sheng, G. P., Mu, Z. X., Liu, X. W., Chen, Y. Z., Wang, H. L., & Yu, H. Q. (2009). Manipulating the hydrogen production from acetate in a microbial electrolysis cell–microbial fuel cell-coupled system. *Journal of Power Sources*, *191*(2), 338-343.

Stein, N. E., Hamelers, H. V., van Straten, G., & Keesman, K. J. (2012). Effect of toxic components on microbial fuel cell-polarization curves and estimation of the type of toxic inhibition. *Biosensors*, *2*(3), 255-268.Tartakovsky, B., Manuel, M. F., Wang, H., & Guiot, S. R. (2009). High rate membrane-less

microbial electrolysis cell for continuous hydrogen production. *International Journal of Hydrogen Energy*, *34*(2), 672-677.

Tice, R. C., & Kim, Y. (2014). Energy efficient reconcentration of diluted human urine using ion exchange membranes in bioelectrochemical systems. *Water research*, *64*, 61-72.

Torres, C. I., Marcus, A. K., Parameswaran, P., & Rittmann, B. E. (2008). Kinetic experiments for evaluating the Nernst− Monod model for anode-respiring bacteria (ARB) in a biofilm anode. *Environmental science & technology*, *42*(17), 6593-6597.

Torres, C. I., Marcus, A. K., & Rittmann, B. E. (2007). Kinetics of consumption of fermentation products by anode-respiring bacteria. *Applied microbiology and biotechnology*, *77*(3), 689-697.

Wang, X., Feng, Y., Ren, N., Wang, H., Lee, H., Li, N., & Zhao, Q. (2009). Accelerated start-up of two-chambered microbial fuel cells: effect of anodic positive poised potential. *Electrochimica Acta*, *54*(3), 1109-1114.

Weinstein, J. N., & Leitz, F. B. (1976). Electric power from differences in salinity: the dialytic battery. *Science*, *191*(4227), 557-559.

Wen, Q., Wu, Y., Cao, D., Zhao, L., & Sun, Q. (2009). Electricity generation and modeling of microbial fuel cell from continuous beer brewery wastewater. *Bioresource Technology*, *100*(18), 4171-4175.

Yoho, R. A., Popat, S. C., & Torres, C. I. (2014). Dynamic Potential-Dependent Electron Transport Pathway Shifts in Anode Biofilms of Geobacter sulfurreducens. *ChemSusChem*, *7*(12), 3413-3419.

Zeng, Y., Choo, Y. F., Kim, B. H., & Wu, P. (2010). Modelling and simulation of two-chamber microbial fuel cell. *Journal of Power Sources*, *195*(1), 79-89.

Zhang, X. C., & Halme, A. (1995). Modelling of a microbial fuel cell process. *Biotechnology Letters*, *17*(8), 809-814.

CHAPTER 2 Enzyme Kinetic Model for Exoelectrogenic Electron Transfer in Bioelectrochemical Systems

Paper I: *: Huang, W., & Kim, Y. Bioanode model based on Butler-Volmer and enzyme kinetics. Submitted to Bioelectrochemistry..*

This paper presents a comprehensive model for exoelectrogens electron transfer in bioanodes. The model is novel in its addition of the electron transfer chain as well as the more commonly found Nernst and Butler-Volmer equations to simulate bioanode performance in BES (bioelectrochemical systems). Existing models utilize a series of equilibrium and kinetic equations that mathematically work; however, the shortcoming of these models is that they do not follow the electrons the way they flow through the cell as a bacterium consumes substrate. In this research, an electron transfer chain was added as a method to follow electron flow through a cell. In the framework of this thesis, this model contributes to the development of estimation tools for the performance of BES, as well as furthering the exploration and understanding of the behaviour of bioanodes for potential applications in wastewater treatment.

The topics covered in this paper were as follows:

- Develop and calibrate a model using enzyme kinetics and a simplified electron transfer chain consisting of one enzyme pair to illustrate the electron transfer chain in a model
- Comparison of the model to experimental results

- Discussion of sensitivity to the kinetic constants and concentrations involved, through which it was found that the model was highly sensitive to the constants and concentrations directly linked to the electron transfer chain

Abstract

This paper presents a new model for exocellular electron transfer involving modified Michaelis-Menten and enzyme kinetics and a representation of the electron transfer chain. This model incorporates the concept of the electron transfer chain for extracting energy from the adenosine triphosphate (ATP) produced during substrate oxidation. Using this model, it was found the model is highly sensitive to the concentration of the enzyme representing the electron transfer chain. This finding agrees with the actual reactions, in which the electron transfer chain accounts for a large portion of the energy produced by the cell. As we increased the enzyme concentration, electrons are released to the anode at a higher rate, resulting in increased current generation. It was also found that the model was not highly sensitive to the constants that only the kinetics governing substrate intake. The model is able to capture key features of bioanodes under non-steady state operation, and it was found that most kinetic parameters were more sensitive under non-steady state operation.

Keywords

Bioelectrochemical; Bioanode; Model; Enzyme Kinetics; Electron Transfer Chain

2.1 Introduction

Bioelectrochemical systems (BESs) are an emerging alternative to conventional wastewater treatment. In BESs, organic matter is oxidized by exoelectrogenic bacteria. These bacteria form biofilms and consume organic matter in the process they release electrons. When the biofilm is attached to a conductive material, we create a bioanode through which electrons can be fed into an electrical circuit to generate a small electric current [1]. This study proposes a bioelectrocatalysis-based model to model the transfer of electrons from organic substrate to the bioanode in bioelectrochemical systems. We utilized modified Michaelis-Menten and Butler-Volmer kinetics along with Nernst equilibrium to develop a model that considers substrate breakdown as well as the electron transfer chain in the electron transfer process.

Previous models proposed for BES models often consider Michaelis-Menten kinetics (i.e., Monod kinetics) for microbiological growth as biofilm growth is an important factor in electron transfer [2–8]. Furthermore, the implementation of the Monod equation requires a soluble electron acceptor (e.g., dissolved oxygen) while BESs have a solid acceptor, thus, the Monod model is often coupled with the Nernst equation [2,4,7]. However, these Monod-based models are governed by growth rate. With a Monod-based model, we would expect to see electric current production to reflect a typical Monod growth (Fig 2-1 A, 2B), which is not the case in bioelectrochemical systems.

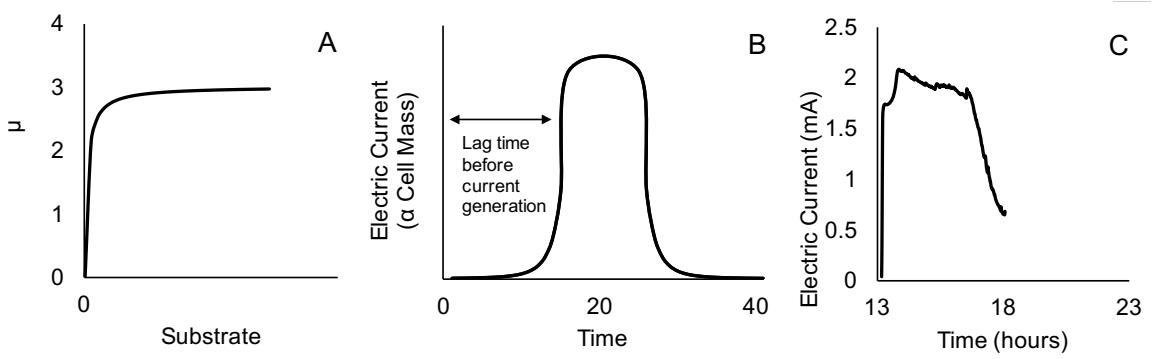

Fig 2-1 (A) Monod kinetics (B) expected electric current if current generation is mainly governed by Monod kinetics and (C) typical electric current observed in bioelectrochemical systems

Microbial electrolysis cells (MECs) are a type of BESs. In MECs, a rapid increase in electric current is commonly observed shortly after substrate addition and steady current production as long as substrate concentration is above a threshold level. When available substrate concentration drops below approximately 0.1 g/L COD, a rapid drop in current is observed (Fig 1C). This effect is not well modeled by Monod kinetics alone; thus, previous model studies have introduced electrode kinetics such as the Butler-Volmer equation [8–11].

There are other modeling approaches to BES modeling. These include mass transfer models which include proton and mass balance [12], COD change [13], and diffusion [14]. Another approach is computational fluid dynamics to account for variation in

surface texture [15]. There are also kinetic models such inhibition kinetics [16] and other enzyme kinetics [5].

In this study, a modified equation based on Michaelis-Menten kinetics and enzyme kinetics involving the electron transfer respiratory chain is used to model bioanode electron transfer. This type of enzyme model is similar to mediated bioelectrocatalysis, where an enzyme mediator assists in the transfer of electron to an acceptor. This paper applies these concepts to modeling bioelectrochemical systems. This model adds a simplified version of the electron transfer respiratory chain to Michaelis-Menten kinetics for substrate utilization. In microbial metabolism, the final steps in obtaining energy from a food source is the electron transfer chain in which adenosine triphosphate (ATP) molecules are produced by phosphorylation or proton motive force as electrons are cycled through a series of enzymes [17]. Due to limited knowledge of the enzymes involved, we simplified the model to one enzyme pair. This model is capable of simulating both steady and varying applied voltage conditions. It models current production under depleting substrate concentrations in a microbial electrolysis cell, as well as linear sweep voltammetry and cyclic voltammetry results.

2.2 Methodology

2.2.1 Model development

A two stage electron transfer model was developed using principles from Michaelis-Menten kinetics, Nernst equation and Butler-Volmer equation. This process is also known

as mediated bioelectrocatalysis where a mediator assists the transfer of electrons from an enzyme to an electrode [18,19]. This study extends the concepts of mediated bioelectrocatalysis to bioelectrochemical systems by introducing current density to the model. This set of equations estimates the concentration of substrate, product, enzymes, and electric current density at any given time. Using this model, we are able to model both constant (steady state) and varying applied potential conditions (non-steady state) of microbial electrolysis cell operation.

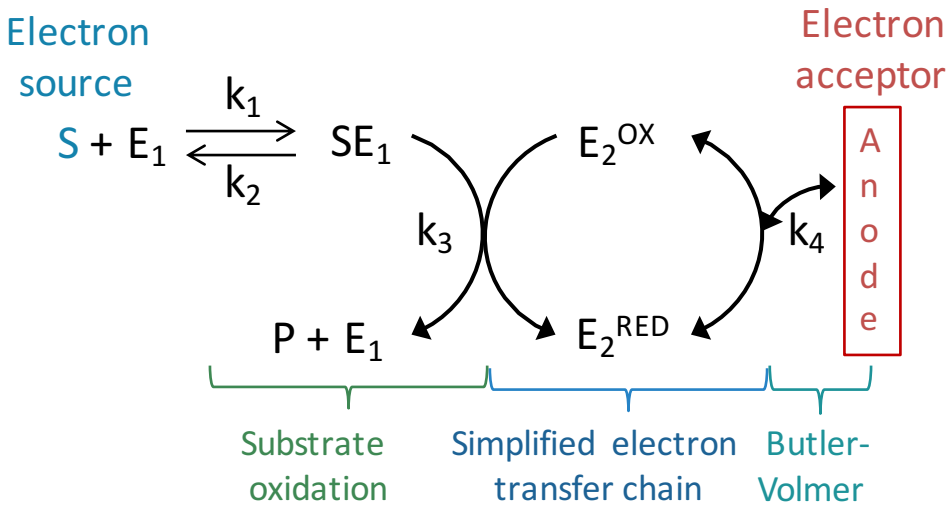

Figure 2-2 Proposed enzyme kinetic model with electron transfer chain

Michaelis-Menten kinetics was used to model electron transfer from the substrate into the cell. The substrate (S) forms an intermediate compound (SE_1) with enzyme E_1 through a reversible reaction governed by constants k_1 and k_2. SE_1 then undergoes an irreversible reaction by kinetic constant k_3 to produce product P and E_1.

$$\frac{d[S]}{dt} = -k_1[S][E_1] + k_2[SE_1] \quad \text{(Eq 2-1)}$$

$$\frac{d[SE_1]}{dt} = -k_1[S][E_1] + k_2[SE_1] - k_3[SE_1][E_2^0] \quad \text{(Eq 2-2)}$$

$$\frac{dP}{dt} = -k_3[SE_1][E_2^0] \quad \text{(Eq 2-3)}$$

Equations 2-2 and 2-3 involve an electron transfer mediator, E_2, to consider the electron transfer to a solid anode through the electron transfer chain (ETC). The mediator, E_2, is one of a series of enzymes found in the electron transfer respiratory chain in cells. For the purposes of this model, it is assumed that E_2 is a rate-limiting enzyme and representative of the electron transfer respiratory system. Monod-equation based models such as the Nernst-Monod model for bacteria electron transfer proposed by Zhang and Halme [2], combined the Nernst equilibrium equation into the Monod model in order to account for a solid electron receiver that has no concentration. In our model, we also utilize the Nernst equation, however, the enzyme being reduced is involved further down in the model as part of the electron transfer chain, rather than using the potential of a solid electrode as the Nernst-Monod model had used. The kinetic constants k_1, k_2, k_3 were estimated based on the range of values in [20–22] and enzyme concentration values were estimated from the typical range of enzymes found in [23,24] The differential equations were discretized using backwards iteration.

The electron transfer chain is modeled by two equations (Eq 2-2, 2-3), one based on enzyme kinetics and another with Nernst equilibrium. The ETC consists of several

enzymes of decreasing potential, and cells generate energy storage molecules (i.e., ATP, adenosine triphosphate) and/or create proton motive force (PMF) as the electrons pass through the electron transfer chain. In reality the ETC involves a series of enzymes, but for the purposes of this model, we have simplified the ETC to a single enzyme (E_2) with oxidation-reduction potential E_0, under the assumption that there is a rate-limiting enzyme in the electron transfer chain.

$$\frac{d[E_2^0]}{dt} = \frac{1}{n} k_3 [SE_1][E_2^0] + \frac{I}{nF} \quad \text{(Eq 2-4)}$$

$$E_{an}^{eq} = E^0 - \frac{RT}{nF} \ln \left(\frac{E_2^{red}}{E_2^{ox}} \right) \quad \text{(Eq 2-5)}$$

For the transfer of the electron to the terminal electron acceptor (i.e., bioanode), the Butler-Volmer equation for electrode kinetics was used. This reaction is irreversible and drives the electron towards the electrode. While the Butler-Volmer equation describes a reversible electrode reaction, due to the lower potential of the electrode compared to that of the electron transfer chain, the net flow of electrons will always be towards the electrode.

$$I = nFk_4 E_2^{red} exp\left[(1-\alpha)\frac{F}{RT}\left(E_{an} - E_{an}^{eq}\right)\right] - E_2^{ox} exp\left[(-\alpha)\frac{F}{RT}\left(E_{an} - E_{an}^{eq}\right)\right] \quad \text{(Eq 2-6)}$$

2.2.2 Experimental methods

A single-chamber microbial electrolysis cell (MEC) was used for model validation. The MEC was constructed using a low density polyethylene block and consisted of a single cylindrical chamber with an internal volume of 40 mL. The bioanode was inoculated with

primary clarifier effluent from a local wastewater treatment plant, and the MEC was operated at 0.6 V batch cycles until steady current production was observed. The feed solution consisted of 25 mM phosphate buffer solution (4.32g/L $Na_2HPO_4 \cdot 7H_2O$, 1.07 g/L NaH_2PO_4, 0.16 g/L NH_4Cl, 0.07 g/L KCl) and 1 g/L sodium acetate, vitamins and minerals.

After the MECs were producing steady current, we performed linear sweep voltammetry (LSV) (BioLogic VSP, BioLogic, France) under different substrate, product, and applied potential conditions for model verification. Experimental and model data were compared for the peak current and peak location in LSV operation. For constant applied potential operation we used the steady operation peak current and operation time for comparison.

For LSV operation we used a Ag/AgCl reference electrode (BASi Liquid Chromatography) and performed LSV from -0.4 to +0.6 V vs. Ag/AgCl at a scan rate of 0.1 mV/s. Constant mixing was provided to minimize losses due to diffusion and mass transfer in the bulk solution.

The model was fit to experimental results through changing constants k_1, k_2, k_3, k_4, and enzyme concentrations E_{1tot} and E_{2tot}. E^0 was set at -0.2V vs. SHE, the redox potential of the enzyme Cytochrome-C which is thought to play a key role in exocellular electron transfer (Bonanni et al., 2013). The key features matched were the size and location of the LSV peak and the magnitude of electric current under steady applied potential conditions.

2.3 Results and discussion

2.3.1 Validation

The model captures the typical pattern of electric current produced under both steady and non-steady applied potential conditions. Parameter values obtained through the models are shown in Table 2-1. The model parameters were estimated by visually determining the peak current magnitude and peak locations for LSV and current for fixed potential conditions, while remaining within literature parameter ranges (Table 2-1). Under non-steady state operation (Fig 3-3A) the oxidation peak magnitude and location matches with the experimental LSV scan peak. The current after the peak drops in the model results due to the use of only one enzyme pair to represent the electron transfer chain. In an actual cell, a series of enzyme pairs are involved, allowing the current to remain higher throughout the LSV scan.

For fixed potential, the model reproduced a typical MEC current profile, with the electric current picking up rapidly after substrate addition and holding steady at a peak current, and dropping rapidly when substrate is depleted, which occurs at about 1 mol/m^3 (0.82 g/L sodium acetate, which matches when current drops off in lab-scale MEC operation). The model results also show a steady peak current that does not vary significantly as substrate is depleted at a constant rate. The addition of the electron transfer chain regulates this, as without the ETC we would see the pattern of Monod growth, with exponential growth and decay as substrate is added and depleted.

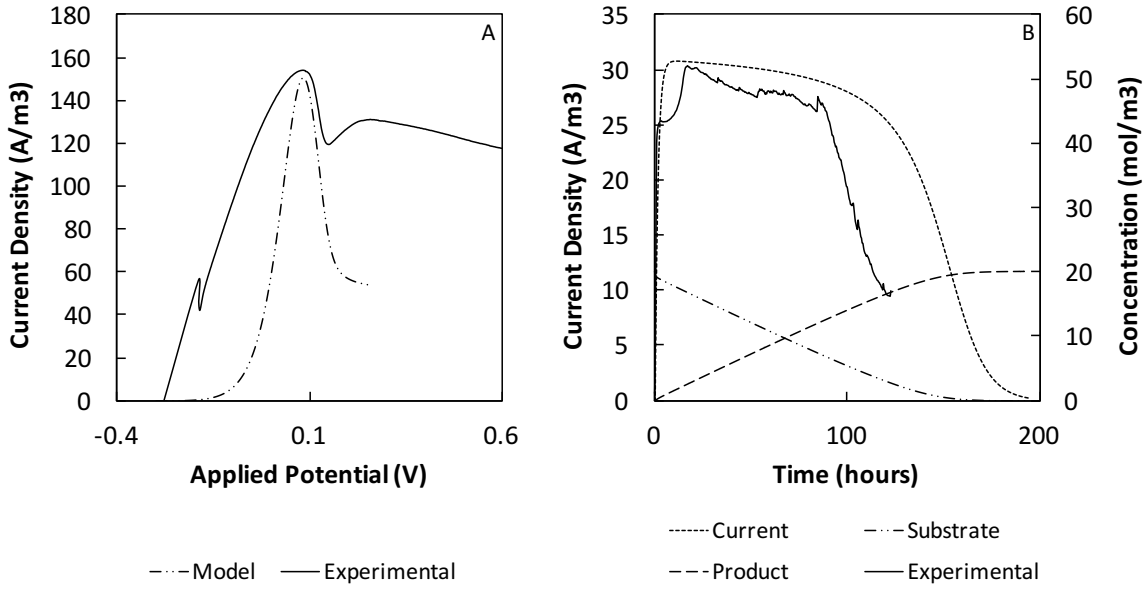

Figure 2-3 Model results compared with experimental results under (A) linear sweep voltammetry and (B) fixed anode potential of 0.6V

Table 2-1 Parameter values used in model

Parameter	Type	Model	Literature	
k_1	Kinetic constant	0.0007	$1 \cdot 10^{-4}$ - $1 \cdot 10^{-3}$ [a]	$m^3 \cdot mol^{-1} \cdot s^{-1}$
k_2	Kinetic constant	0.001	$1 \cdot 10^{-4}$ - $1 \cdot 10^{-3}$ [a]	s^{-1}
k_3	Kinetic constant	0.00013	$1 \cdot 10^{-5}$ - $1 \cdot 10^{-4}$ [a]	$m^3 \cdot mol^{-1} \cdot s^{-1}$
k_4	Kinetic constant	0.00012	n/a	$m^{-3} s^{-1}$
E^0	Equilibrium potential of E_2	-0.2	-0.24 [b]	V vs SHE
E_1	Enzyme concentration	0.71	$1 \cdot 10^{-3}$ - 10^{1} [c,d]	$mol \cdot m^{-3}$
E_2	Enzyme concentration	0.8	$1 \cdot 10^{-3}$ - 10^{1} [c,d]	$mol \cdot m^{-3}$

[a] Calculated from Tchonbanoglous et al., 2003

[b] Madigan et al., 2015

[c] Novick & Weiner, 1957

[d] Albe et al., 1990

The equilibrium potential of enzyme E_2, the enzyme representative of the electron transfer chain, was set to -0.2 V vs. standard hydrogen electrode (SHE). Cytochrome-C has been found to be a key electron transfer mediator in exoeletrogenic electron transfer [25]. The equilibrium potential for the model was fixed to -0.2 V for sensitivity on the kinetic parameters and enzyme concentrations. When the equilibrium potential of E_2 is varied, a shift in LSV peak location is observed (Fig 2-4A) due to the change in the equilibrium potential at which the enzyme is active. Peak magnitude also changes due to a change in overpotential when the equilibrium potential changes. It can be seen in Fig 2-4B that the fixed potential model is highly sensitive to changes in equilibrium potential.

With different equilibrium potentials, the model results are unreasonable and other kinetic constants must be adjusted around the equilibrium potential.

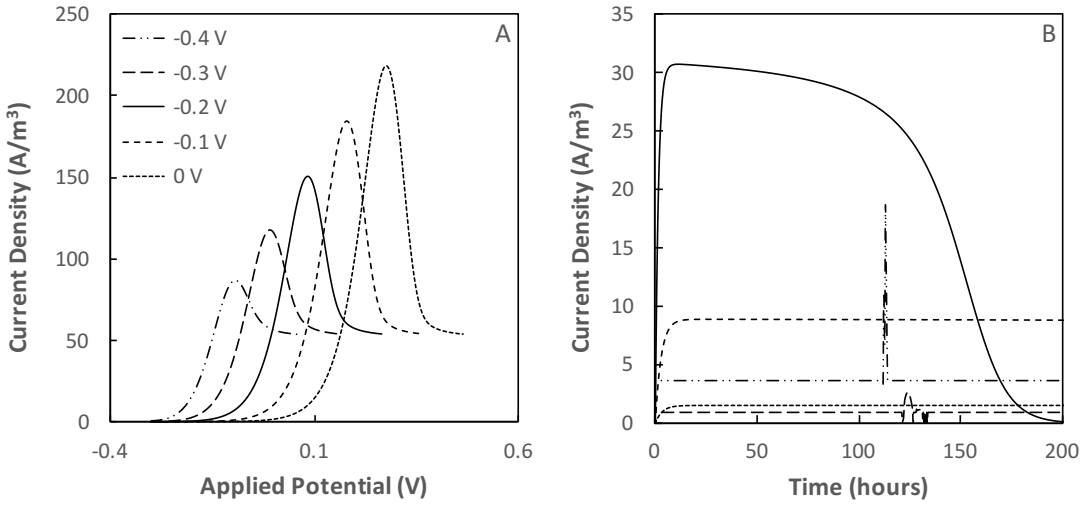

Figure 2-4 Model results changing equilibrium potential of E_2

2.3.2 Linear Sweep Voltammetry Model Results

Constants k_1, k_2, and k_3 are involved in the Michaelis-Menten or Monod aspect of the model reaction. In sensitivity analysis, it can be seen that as k_1 increases, the magnitude of the peak increases, as expected for a forward reaction. The effect of k_2 on electric current is seen to have a threshold value. Below 0.0001, the values are relatively similar, but increasing k_2 above this threshold causes a notable drop in the peak current, indicating that the backward drive of k_2 is in effect, thus slowing the reversible reaction that forms the enzyme-substrate intermediate SE_1.

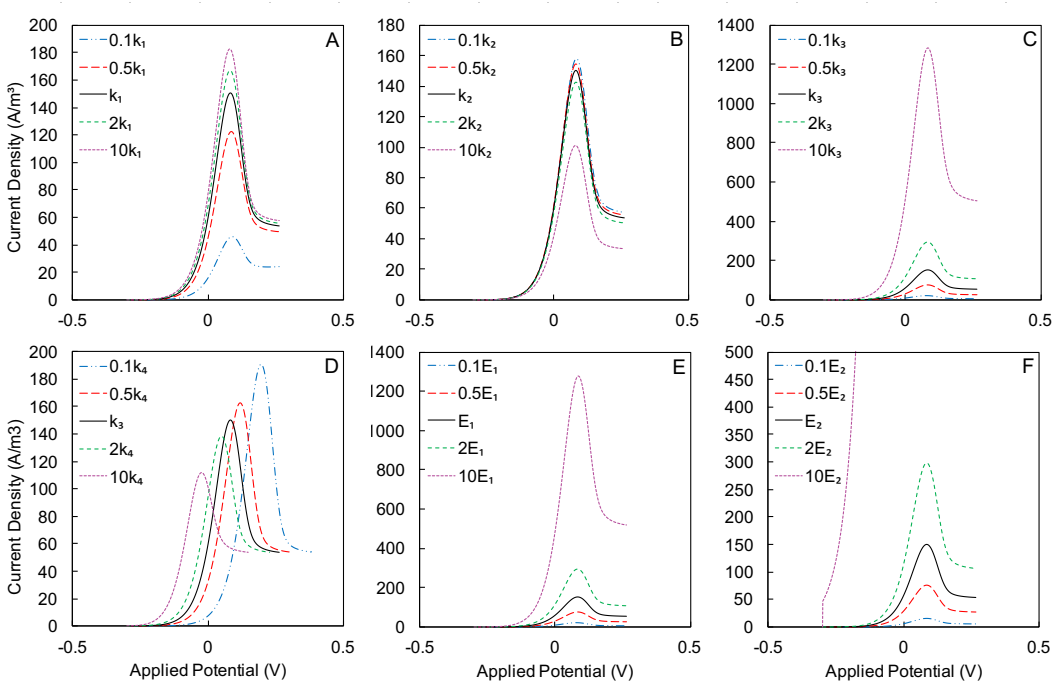

Figure 2-5 Sensitivity analysis on linear sweep voltammetry results on (A) k_1, (B) k_2, (C) k_3, (D) k_4, (E) E_1, (F) E_2

Sensitivity analysis on the variables shows that the kinetic constant k_4 is the only constant that alters the location of the peak. As k_4 increases, the peak appears at more negative applied voltage and the magnitude of current is lower. This implies that as we increase the rate of transfer of electrons to the anode without changing other aspects of the reaction, the oxidation of substrate occurs at more negative potential but the rate of electron transfer decreases, resulting in a lower peak current. The increase in k_4 shifts the peak location shifts to a more negative applied potential, indicating that the anode pulls electrons away from the biofilm more rapidly, resulting in a more negative potential at the anode. It can be noted that while changing k_4 also shifts the magnitude of the peak, this can be attributed to anode overpotential. As k_4 increases, peak magnitude decreases. It

can be seen in Fig 4 that as the equilibrium potential of the enzyme increases, peak magnitude increases and shifts towards the right.

Enzyme concentration also affects the magnitude of the peak. Enzyme E_2 total concentration strongly shifts the peak along the y-axis with subtle changes (Fig 2-5F) while E_1 has less of an effect. The enzyme E_2 is the enzyme involved in the final electron transfer to the electrode, modeled by the Butler-Volmer equation. The high sensitivity to E_2 concentration indicates that the current producing reactions are extremely sensitive to the concentration of enzyme E_2. The E_1 and E_2 concentrations in the model denotes the total concentration of E_1 and E_2, so $E_2 = E_{2+} E_2$. For the purposes of this model, it is assumed that the total active biomass does not change, and thus, total enzyme concentration remains constant and shifts between the oxidized and reduced states. This enzyme is involved in the electron transfer chain portion of the model, which contributes a large portion of the energy extracted from substrate. In both aerobic and anaerobic respiration, energy is produced and stored as adenosine triphosphate (ATP) by the enzymes found in cells. During the oxidation of organic substrates through the Citric Acid Cycle, NADH and $FADH_2$ molecules are produced, which are then passed through the electron transfer chain where a series of enzymes produces 4 and 2 ATP from each NADH and $FADH_2$ molecule, respectively (Madigan et al., 2015). Proportionally, a larger amount of ATP molecules were produced through the ETC than through Glycolysis and the Citric Acid Cycle, thus, it is expected that the model is more sensitive to E_2 concentration, as this enzyme in our model is representative of the entire ETC.

Cytochrome-C is a redox enzyme found in high concentrations in exoelectrogenic bacteria and thought to be a key component of exocellular electron transfer, thus, the redox potential of Cytochrome-C was used for enzyme E_2 as a representation of the electron transfer chain.

This model shows the key features of LSV results. Typically, MEC experimental results from cycle to cycle have some variation due to the complexities and numerous changing conditions in an MEC, thus, an identical fit is not necessary. Additionally, this model only utilizes one enzyme pair as a representation of the electron transfer chain, when the electron transfer chain should of several enzyme pairs, and implementing additional enzyme pairs may address this issue. However, our goal for this model was to introduce the concept, and in model fitting we aimed to fit the LSV oxidation peak magnitude and location, while producing a fixed-potential electric current magnitude that is typical for the substrate concentration.

2.3.3 Fixed Anode Potential Model Results

In the fixed potential condition, it can be seen that k_1 and k_2 have opposite trends (Fig 2-6A, B), which is expected as k_1 represents the forward reaction and k_2 the backward reaction. While increasing k_1 and decreasing k_2 shifts the duration of high current production, the magnitude of the current hardly changes except in $0.1k_1$ and $10k_2$. It can also be noted that the current drop when substrate is depleted become more abrupt with higher k_1 and lower k_2. This indicates this first reaction with the substrate provides

sufficient substrate-enzyme intermediates for the reaction, other kinetic constants govern the rate at which electrons are extracted from the intermediates.

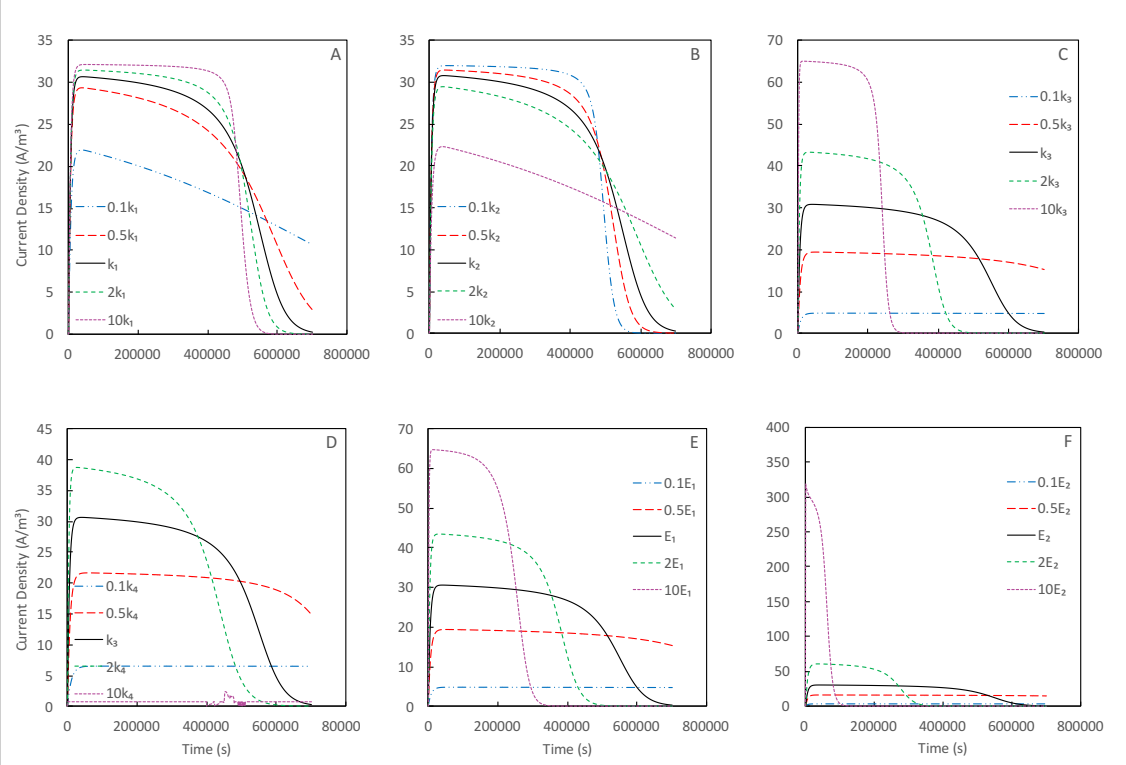

Figure 2-6 Sensitivity analysis on fixed anode potential results on (A) k_1, (B) k_2, (C) k_3, (D) k_4, (E) E_1, (F) E_2

Kinetic constant k_3 and equilibrium constant k_4 both shift the magnitude of current along the y-axis (Fig 2-6C, D), which indicates that the rate oxidation of substrate to collect electrons is governed by these constants. As to satisfy Coulombic efficiency where electrons produced must equal electrons provided, the duration of high current production decreases as the magnitude of current increases. Futhermore, at $10k_4$ the model fails to converge and is incapable of simulating fixed potential conditions (Fig 2-6D) and the modeled electric current becomes near zero.

The concentrations of both enzymes affect the magnitude of current as well though E_2 has a much stronger effect. A subtle change in the concentration of enzyme E_2 results in a very dramatic shift in the magnitude of the current. This is similar to the large shift in peak current in the LSV results with a slight change in enzyme concentration. As the E_2 concentration increases, electrons are cycled through more rapidly, resulting in a higher rate of electrons being released to the terminal electron acceptor, or the bioanode.

2.3.4 Constant estimation

Comparison between the sensitivity analyses of the model under fixed and LSV conditions (Fig 2-5, 2-6) shows which operation is more sensitive to changes in the parameters, and between the two types of model operation a range for kinetic constants can be estimated.

The parameters related to the Michaelis-Menten part of the model were more sensitive to LSV than fixed anode operation. When k_1 and k_2 are shifted by two orders of magnitude in fixed anode potential operation, the current generation changed by approximately 50%, while the same change in LSV operation resulted in a difference of nearly 500%. Similarly, k_3 current generation under fixed potential changed by an order of magnitude, while LSV peak increased by three orders of magnitude. Enzyme E_1 is involved in Michaelis-Menten and similar to k_3, slight changes in k_3 results in much larger differences in LSV than in fixed anode operation.

The fixed potential model was more sensitive to k_4 than LSV in terms of current magnitude. The change in LSV peak current with changes in k_4 were within an order of magnitude, while fixed potential changed by an order of magnitude.

The model was very sensitive to changes in enzyme E_2 both in LSV and fixed anode potential operation, which is expected as E_2 represents the electron transfer chain, which accounts for a large fraction of the ATP produced by a cell, and thus E_2 concentration should be highly important to electron transfer. A range of parameter values was established based on the sensitivity analysis and are summarized below.

Table 2-2 Parameter value estimation

Parameter	**Model**	**Range**			
k_1	0.0007	0.0005	-	0.001	$m^3 \cdot mol^{-1} \cdot s^{-1}$
k_2	0.001	1×10^{-10}	-	0.001	s^{-1}
k_3	0.00013	0.0001	-	0.00018	$m^3 \cdot mol^{-1} \cdot s^{-1}$
k_4	0.00012	0.00008	-	0.0005	$m^{-3} s^{-1}$
E^0	-0.2	-0.2	-	-0.2	V vs S.H.E
E_1	0.71	0.61	-	0.81	$mol \cdot m^{-3}$
E_2	0.8	0.7	-	0.9	$mol \cdot m^{-3}$

2.4 Conclusions

A new model for exocellular electron transfer in bioelectrochemical systems was proposed and validated to experimental results. The key features of the model are the addition of an electron transfer chain (ETC) and the capability to capture the characteristics of non-steady state operation such as linear sweep voltammetry. It was found that the model was highly sensitive to the concentration of the enzyme representative of the ETC, supporting the hypothesis that the ETC is a highly important aspect of energy production from bioelectrochemical systems. Future work includes further refine the model with the addition of additional enzyme pairs to better model the electron transfer chain and further narrowing down the kinetic constants and enzyme concentrations.

2.6. References

Albe, K. R., Butler, M. H., & Wright, B. E. (1990). Cellular concentrations of enzymes and their substrates. *Journal of theoretical biology*, *143*(2), 163-195.

Bonanni, P. S., Massazza, D., & Busalmen, J. P. (2013). Stepping stones in the electron transport from cells to electrodes in Geobacter sulfurreducens biofilms. *Physical Chemistry Chemical Physics*, *15*(25), 10300-10306.

Čech, J. S., Chudoba, J., & Grau, P. (1985). Determination of kinetic constants of activated sludge microorganisms. *Water Science and Technology*, *17*(2-3), 259-272.

Hamelers, H. V., Ter Heijne, A., Stein, N., Rozendal, R. A., & Buisman, C. J. (2011). Butler–Volmer–Monod model for describing bio-anode polarization curves. *Bioresource technology*, *102*(1), 381-387.

Kato Marcus, A., Torres, C. I., & Rittmann, B. E. (2007). Conduction-based modeling of the biofilm anode of a microbial fuel cell. *Biotechnology and Bioengineering*, *98*(6), 1171-1182.

Korth, B., Rosa, L. F., Harnisch, F., & Picioreanu, C. (2015). A framework for modeling electroactive microbial biofilms performing direct electron transfer. *Bioelectrochemistry*, *106*, 194-206.

Jafary, T., Ghoreyshi, A. A., Najafpour, G. D., Fatemi, S., & Rahimnejad, M. (2013). Investigation on performance of microbial fuel cells based on carbon sources and kinetic models. *International Journal of Energy Research*, *37*(12), 1539-1549.

Lee, H. S., Torres, C. I., & Rittmann, B. E. (2009). Effects of substrate diffusion and anode potential on kinetic parameters for anode-respiring bacteria. *Environmental science & technology*, *43*(19), 7571-7577.

Li, R., Tiedje, J. M., Chiu, C., & Worden, R. M. (2012). Soluble electron shuttles can mediate energy taxis toward insoluble electron acceptors. *Environmental science & technology*, *46*(5), 2813-2820.

Logan, B. E., Call, D., Cheng, S., Hamelers, H. V., Sleutels, T. H., Jeremiasse, A. W., & Rozendal, R. A. (2008). Microbial electrolysis cells for high yield hydrogen gas production from organic matter. *Environmental Science & Technology*, *42*(23), 8630-8640.

Madigan, M. T., Martinko, J. M., Bender, K. S., Buckley, D. H., & Stahl, D. A. (2015). *Brock biology of microorganisms* (Fourteenth edition.). Boston: Pearson.

Marcus, A. K., Torres, C. I., & Rittmann, B. E. (2011). Analysis of a microbial electrochemical cell using the proton condition in biofilm (PCBIOFILM) model. *Bioresource technology*, *102*(1), 253-262.

Novick, A., & Weiner, M. (1957). Enzyme induction as an all-or-none phenomenon. *Proceedings of the National Academy of Sciences*, *43*(7), 553-566.

Peng, S., Liang, D. W., Diao, P., Liu, Y., Lan, F., Yang, Y., ... & Xiang, Y. (2013). Nernst-ping-pong model for evaluating the effects of the substrate concentration and anode potential on the kinetic characteristics of bioanode. *Bioresource technology*, *136*, 610-616.

Picioreanu, C., Head, I. M., Katuri, K. P., van Loosdrecht, M. C., & Scott, K. (2007). A computational model for biofilm-based microbial fuel cells. *Water Research*, *41*(13), 2921-2940.

Picioreanu, C., van Loosdrecht, M. C., Curtis, T. P., & Scott, K. (2010). Model based evaluation of the effect of pH and electrode geometry on microbial fuel cell

Pinto, R. P., Srinivasan, B., Manuel, M. F., & Tartakovsky, B. (2010). A two-population bio-electrochemical model of a microbial fuel cell. *Bioresource technology*, *101*(14), 5256-5265.

Renslow, R., Babauta, J., Kuprat, A., Schenk, J., Ivory, C., Fredrickson, J., & Beyenal, H. (2013). Modeling biofilms with dual extracellular electron transfer mechanisms. *Physical Chemistry Chemical Physics*, *15*(44), 19262-19283.

Robinson, J. A., & Tiedje, J. M. (1983). Nonlinear estimation of Monod growth kinetic parameters from a single substrate depletion curve. *Applied and Environmental Microbiology*, *45*(5), 1453-1458.

Rousseau, R., Délia, M. L., & Bergel, A. (2014). A theoretical model of transient cyclic voltammetry for electroactive biofilms. *Energy & Environmental Science*, *7*(3), 1079-1094.

Song, Y. C., Lim, H. J., & Woo, J. H. (2015). Influence of applied voltage and COD on the bioelectrochemical degradation of organic matter. *Desalination and Water Treatment*, *53*(10), 2732-2739.

Tchobanoglous G, Burton FL, Stensel HD Eds. (2003) Metcalf & Eddy Wastewater Treatment and Reuse 4th ed. McGraw-Hill, Boston

Torres, C. I., Marcus, A. K., Parameswaran, P., & Rittmann, B. E. (2008). Kinetic experiments for evaluating the Nernst− Monod model for anode-respiring bacteria (ARB) in a biofilm anode. *Environmental science & technology*, *42*(17), 6593-6597.

Zeng, Y., Choo, Y. F., Kim, B. H., & Wu, P. (2010). Modelling and simulation of two-chamber microbial fuel cell. *Journal of Power Sources*, *195*(1), 79-89.

CHAPTER 3 Electrochemical Techniques for Evaluating Substrate Utilization by Bioanodes

Paper II: Huang, W., & Kim, Y. (2016). Electrochemical techniques for evaluating short-chain fatty acid utilization by bioanodes. Environmental Science and Pollution Research, 1-7. doi:10.1007/s11356-016-8026-x

This paper examines the use of electrochemical techniques to assess the utilization of a number of short-chain fatty acids (SCFA) in a MEC. One of the limitations of practical application of MECs is their limited range of usable substrate and decrease in performance in the absence of preferred substrate. In this study, the utilization of n-butyric and iso-butyric acid, two substrates known to be difficult for MECs to process, was systematically investigated with various electrochemical techniques. Key findings in this study were:

- Using fixed potential operation while monitoring concentration change of SCFA over time, it was found that iso-butyric acid utilization is affected by applied potential while n-butyric acid was unaffected.
- Linear sweep voltammetry can be used to identify whether or not a substrate is favourable
- Electrochemical impedence spectroscopy can be used to identify substrate favourability. However, exchange current is a better indicator of substrate preference than charge transfer resistance

3.1 Abstract

The utilization of propionic, n-butyric and iso-butyric acids in microbial electrolysis cells (MECs) was examined by monitoring individual short-chain fatty acid concentration and using electrochemical techniques, such as linear sweep voltammetry (LSV) and electrochemical impedance spectroscopy (EIS). When n- or iso-butyrc acid was provided as a single substrate, acetic acid was consistently observed in experiments, indicating that acetic acid was produced as a byproduct and utilized by exoelectrogenic bacteria as an additional substrate in MECs. When iso-butyric acid was given as a sole substrate, the applied potential governed the electric current (i.e., rate of substrate utilization). In addition, the coulombic efficiency was substantially high (90%), indicating direct utilization of iso-butyric acid by exoelectrogenic bacteria. However, the coulombic efficiency was relatively low (30-60%) when n-butyric acid was provided as a sole substrate. In another experiment, the magnitude of electric current was more dependent on the concentration of acetic acid than that of other short-chain fatty acids. In the EIS analysis, the exchange current was found to be a more reliable indicator of substrate favorability than the charge transfer resistance.

Keywords

Bioelectrochemical systems; wastewater treatment; exoelectrogenic bacteria; volatile fatty acids; electrochemical techniques; potentiostat; acetic acid

3.2 Introduction

Bioelectrochemical systems (BESs) are an alternative wastewater treatment method that utilizes exoelectrogenic bacteria to oxidize organic matter in wastewater while recovering energy. The removal of organics from wastewater prior to discharge into the environment is important as a high organic loading can lead to undesired biological growth and dissolved oxygen depletion. Microbial electrolysis cells (MECs) are a type of BESs where the electrons released by exoelectrogens are used for the electrolysis of water to produce hydrogen gas (Call et al, 2008, 2009; Cheng et al., 2007; Liu et al. 2005b; Logan et al., 2008). Microbial electrolysis cells can rapidly remove soluble organics in wastewater with low voltage requirements (Call et al., 2008; Cheng et al., 2007; Liu et al., 2005). These findings are reliable for acetic acid, which has been shown to be the most favorable substrate for bioelectrochemical systems for high energy recovery rates. Many studies used acetic acid as a substrate and demonstrated its consistently favorable utilization (Cheng et al., 2007; Freguia et al., 2010; Lee et al., 2008; Liu et al., 2005b; Sharma et al., 2013; Sun et al., 2009). Bioelectrochemical systems can also decompose other organic substrates, including glucose (Chae et al., 2009; Lee et al., 2008; Liu et al., 2005a), short chain fatty acids (Cheng et al., 2007; Freguia et al.; 2010, Sharma et al., 2013), real or synthetic domestic wastewater and sludge (Asztalos and Kim, 2015b; Ditzig et al., 2007; Gil-Carrera et al., 2013; Zeppilli et al, 2015), as well as the waste byproducts of industrial processes such as petroleum refining (Sevda et al, 2016), brewery wastewater (Feng et al., 2008; Wang et al., 2008; Zhuang et al., 2012), food processing wastewater (ElMekawy et al., 2015) such as that from molasses production (Zhang et al., 2009) and cereal processing (Oh

and Logan, 2005), or a combination of wastewaters such as food wastes mixed with municipal wastewater (Pant et al., 2013). While these substrates can be treated by MEC to an extent, they showed lower energy recovery due to slow degradation of available substrate. Thus, these substrates may undergo indirect oxidation by non-exoelectrogenic microorganisms to acetic acid, which is readily utilized byexoelectrogens (Pant et al., 2010).

The main focus of this study is the utilization of short-chain fatty acids (SCFA) in bioelectrochemical systems. Organic substrates in real wastewaters are more difficult for BESs to utilize than acetic acid (Sun et al., 2009), and acetic acid is not representative of organic substrates in municipal wastewater which consists of various particulate and complex organics (Tchobanoglous et al., 2003). Furthermore, wastewater sludge initially contains a high concentration of long- and short-chain fatty acids rather than acetic acid and thus requires pretreatment to increase the concentration of readily biodegradable organics, such as heat pre-treatment (Pilli et al., 2015) and electro-oxidation with hydrogen peroxide (Feki et al, 2015). Studies on substrate utilization have shown that while bioelectrochemical systems have limited capability to break down propionic and butyric acids compared to acetic acid; as a result, organic removal was incomplete and the coulombic efficiency was relatively low (Cheng et al., 2007; Kiely et al., 2011; Freguia et al., 2010). These previous studies determined substrate utilization by measuring electric current generation and chemical oxygen demand (COD) removal for a given organic substrate in BESs (Cheng et al, 2007; Freguia et al, 2010; Nevin et al, 2008). However, none of the previous studies have monitored individual substrate compounds and their

changes with time. For instance, acetic acid concentration was not monitored in experiments when relatively complex organics (e.g., glucose and butyric acid) were used as a substrate. As a result, it is unclear whether the given organic substrates are directly utilized or there exists intermediate compounds, such as acetic acid, indicating multi-step reactions at the bioanode. Thus, in this study, we monitored all individual short-chain fatty acids, including acetic acid, propionic acid, n- and iso-butyric acids, and n- and iso-valeric acids in our experiments.

Another important objective of this study is to use sophisticated electrochemical techniques, such as linear sweep voltammetry (LSV) and electrochemical impedance spectroscopy (EIS), as tools to identify the favorability of a given substrate in BESs. These electrochemical techniques have been used to characterize various aspects of the bioanode reaction for substrate oxidation (Fricke et al, 2008; He & Mansfeld, 2009). However, none of the previous studies have utilized LSV or EIS to quantify the favorability of a given organic substrate. We focused on developing a method to interpret LSV and EIS analysis results in better understanding substrate utilization by the bioanode in BESs.

3.3 Materials and Methods

3.3.1 Reactor construction and operating conditions

The single-chamber MEC reactors were constructed from low-density polyethylene blocks with a cylindrical internal chamber of 40 mL. The bioanode was prepared with a graphite-

fiber brush pre-treated at 450 °C for 30 minutes (Wang et al., 2009) and inoculated with primary clarifier effluent from a local municipal wastewater treatment plant. The bioanode brush and inner surfaces of the reactor were pre-treated with a surfactant to accelerate biofilm growth and maturation (Guo et al., 2014). Two layers of stainless steel mesh (AISI 304, 100 mesh; McMaster-Carr, OH) were used as the cathode and no additional catalysts were applied to the cathode. A total of three reactors were constructed for the experiments and each was acclimated to a designated substrate among n-butyric acid, iso-butyric acid, and a mixture of SCFAs (propionic acid, n-butyric acid, iso-butyric acid, n-valeric acid, iso-valeric acid, and hexanoic acid).

The MEC feed solution was prepared with 25 mM phosphate buffer solution (8.65 g/L $Na_2HPO_4 \cdot 7H_2O$, 2.13 g/L NaH_2PO_4, 0.31 g/L NH_4Cl, and 0.13 g/L KCl) with a trace amount of vitamins and minerals (Cheng et al., 2009). The MECs were run with 1000 mg/L sodium acetate (780 mg COD/L) as substrate at 0.6 V applied potential (GW Instek GPS-1850D Laboratory DC Power Supply; Good Will Instruments, CA) for about 6 months before the bioanode was exposed to the given SCFA substrates. After the SCFA substrates were fed as a substrate, the MECs were allowed to acclimate to the new substrates for 2 weeks before the EIS analysis was performed. Following EIS, the MECs were fed with the SCFAs for an additional month before performing analysis of SCFA utilization. The applied voltage was 0.6 V unless otherwise noted. Electric current data was determined by monitoring the voltage drop across a 10-ohm resistor using digital multimeter and data acquisition system (Keithley 2700; Keithley Instruments, OH). All reactors were fed by

batch cycles. During acclimation period, the reactors were fed when the current dropped below 1 mA, approximately once every 3 days.

3.3.2 Operational conditions for evaluating substrate utilization

To evaluate substrate utilization at high and low applied potential, we applied electric potential and monitored electric current with multi-channel potentiostat (Bio-Logic VSP, Bio-Logic Science Instruments; TN). We applied 0.6 and 1.2 V to the bioanode versus the cathode to compare low and high voltage applications. Substrate utilization tests were done over a period of 44 hours, with the first condition lasting 20 hours and second condition lasting 24 hours. All experiments were conducted in a temperature controlled laboratory (21 ± 1°C).

3.3.3 Experimental analysis for substrate concentration

Individual SCFA concentrations were determined by flame ionization detector gas chromatography (FID GC) (Varian CP3800; Varian, CA; equipped with StabilWax-DA polyethylene glycol column, Restek, PA). For the FID GC analysis, 0.1 mL samples were taken directly from the reactor and acidified with phosphoric acid (3% v/v) (Fisher Scientific, Pittsburgh, PA). For the experiment, we analyzed influent concentration and the concentration at 0, 4, 20, 24, and 44 hours. The influent concentration is the concentration of the prepared feed solution. After the feed solution was introduced to the reactor, it rested at open circuit for 1 hour to allow adsorption to the bioanode or reactor surfaces, and the 0 hour sample was taken after this open circuit period in order to ensure that any

concentration changes between 0 and 4 hours were not affected by adsorption. Coulombic efficiencies (CE) were determined from the current recorded from the potentiostat and change in chemical oxygen demand (COD) as determined by gas chromatography of the fed substrate.

3.3.4 Linear sweep voltammetry

Linear sweep voltammetry (LSV) tests were performed using a potentiostat (Bio-Logic VSP, Bio-Logic Science Instruments, France). An Ag/AgCl reference electrode (MW-2030; BASi Liquid Chromatography, IN) was inserted between the bioanode and cathode. The bioanode was set as the working electrode and the cathode as the counter electrode. We chose a scan range of -0.5 V to +0.4 V vs. Ag/AgCl at a scan-rate of 0.1 mV/s. Preliminary experiments found that a scan rate of 0.1 mV/s was most successful in capturing clear oxidation peaks. Prior to each LSV test, a 30-minute chronoamperometry was conducted at -0.4 V versus Ag/AgCl and the reactor was left open circuit for 120 minutes.

3.3.5 Electrochemical impedance spectrometry

Electrochemical impedance spectrometry (EIS) was performed using a potentiostat (Bio-Logic VSP, Bio-Logic Science Instruments, France). The EIS frequency ranged from 0.1 Hz to 1 MHz. For each substrate tested, the reactor was operated at -0.4 V vs Ag/AgCl for 40 minutes, followed by 10 consecutive EIS analyses.

The charge transfer resistance (R_{CT}) was determined from EIS. When the charge transfer resistance was found, the exchange current (I_0) was calculated using Equation 1 (Bard and

Faulkner, 2001):

$$I_0 = \frac{RT}{nFR_{CT}} \quad \text{(Eq 3-1)}$$

where R is the ideal gas constant, T is temperature, n is the number of electrons provided by a given substrate (8 for acetic acid; 14 for propionic acid; 20 for butyric acid), and F is the Faraday constant. The exchange current (I_0) is the electron transfer occurring under zero net current, and the backward and forward transfer is equal. In BES, I_0 is determined by the rate at which exoelectrogens utilize the substrate and release electrons, and is dependent on how well and quickly they can utilize the given substrate.

3.4 Results and Discussion

3.4.1 Utilization of n-butyric acid

When n-butyric acid or iso-butyric acid was provided as the sole substrate, acetic acid production was observed under both the high and low (1.2 and 0.6 V) voltage application conditions (Fig 1A, 1B, 2A, 2B). This observation suggests that there was electric current production through indirect oxidation of the given substrate where acetic acid was used for current production. Previous studies have shown the importance of acetic acid preferred *Geobacter sulferreducens* in BESs and found that a high population of *G. sulferreducen*s usually produced higher coulombic efficiencies and power densities when the substrate provided is acetic acid (Nevin et al., 2008; Kiely et al., 2011). A study also showed that for a mixed culture MEC fed with acetic acid, *G. sulferreducens* becomes dominant (Kiely et al., 2011) and the MEC exhibits performance similar to an MEC with a pure culture of *G. sulferreducens* (Call et al., 2009; Kiely et al., 2011). While *Geobacter* species are the most

effective at producing high coulombic efficiency, they are not as robust at handling varied substrate alone (Freguia et al., 2010). A study found that a mixed-culture bioanode fed with propionic and butyric acids produced relatively low current and the bioanode showed a lack of *Geobacter* species in the biofilm, suggesting that *Geobacter* species are not responsible for electric current production from propionic and butyric acids (Freguia et al., 2010). In our experiment, the MEC fed with butyric acid produced relatively low current, but an increase in electric current was observed as acetic acid was accumulated (Fig 3-1), suggesting that presence of acetic acid is highly important for high current production.

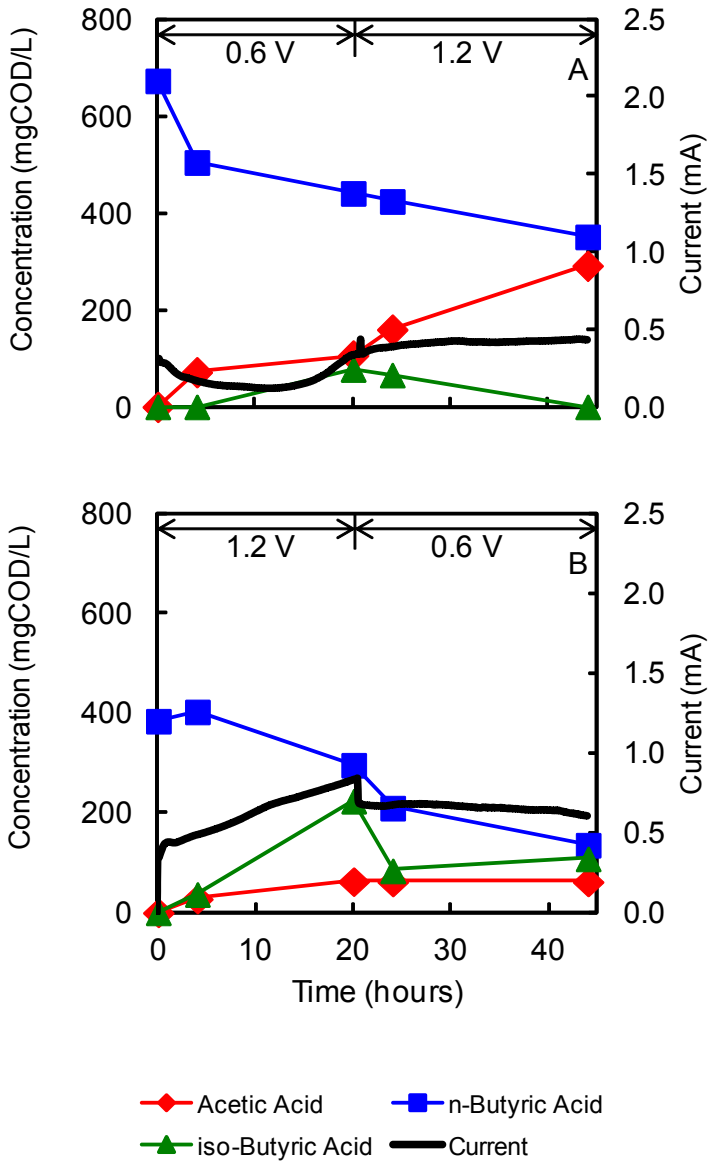

Figure 3-1(A) 500 mg COD/L n-butyric acid, E_{ap} = 0.6 V to 1.2 V, CE = 28.67%. (B) 500 mg COD/L n-butyric acid, E_{ap} = 1.2 V to 0.6 V, CE = 59.14% (the MEC reactor was fed with only n-butyric acid for 2 weeks prior to the shown fed-batch cycle).

In the reactor fed with n-butyric acid, low current production corresponded with low acetic acid concentration and high current corresponded to increased acetic acid concentrations (Fig 3-1). This result suggests that the charge transfer at the bioanode is mainly driven by

oxidation of acetic acid. Even though the n-butyric acid concentration was consistently high, current stays low until sufficient acetic acid has accumulated in the reactor. Also, the change in the applied potential (E_{ap}) had little impact on the magnitude of electric current for n-butyric acid. When E_{ap} increased from 0.6 to 1.2 V at 20 hours, the increase in current was almost negligible (Fig 3-1A). Similarly, the decrease in current with the decreased E_{ap} from 1.2 to 0.6 V at 20 hours was relatively small (Fig 3-1B). This finding implies that n-butyric acid was indirectly oxidized and the electric current production was limited by the rate of acetic acid accumulation.

3.4.2 Utilization of iso-butyric acid

Acetic acid production was also observed in the MEC fed with iso-butyric acid and iso-butyric acid appeared to be a more favorable substrate for exoelectrogenic utilization than n-butyric acid (Fig 3-2). Iso-butyric acid produced higher current and the time required to achieve high current production was shorter compared to n-butyric acid. The iso-butyric acid reactor reached peak current at 10 hours (Fig 3-2B) while n-butyric acid required over 20 hours (Fig 3-1B). Furthermore, the iso-butyric acid reactor showed higher coulombic efficiencies under all conditions than the reactor fed with either n-butyric acid or a mixture of SCFAs. The coulombic efficiencies (CE) for reactor fed with iso-butyric acid ranged from 89.7 to 99.8%, depending on the experimental conditions while all other substrates resulted in lower CE, with n-butyric acid ranging from 29.7 to 59.1%. Based on the short time to current production, high current, and high CE results, iso-butyric acid appears to be directly utilized by exoelectrogens. Iso-butyric acid removal was also dependent on the

applied voltage. A more rapid depletion of iso-butyric acid was observed at the higher applied potential (1.2 V) (Fig 3-2B and 3-2A).

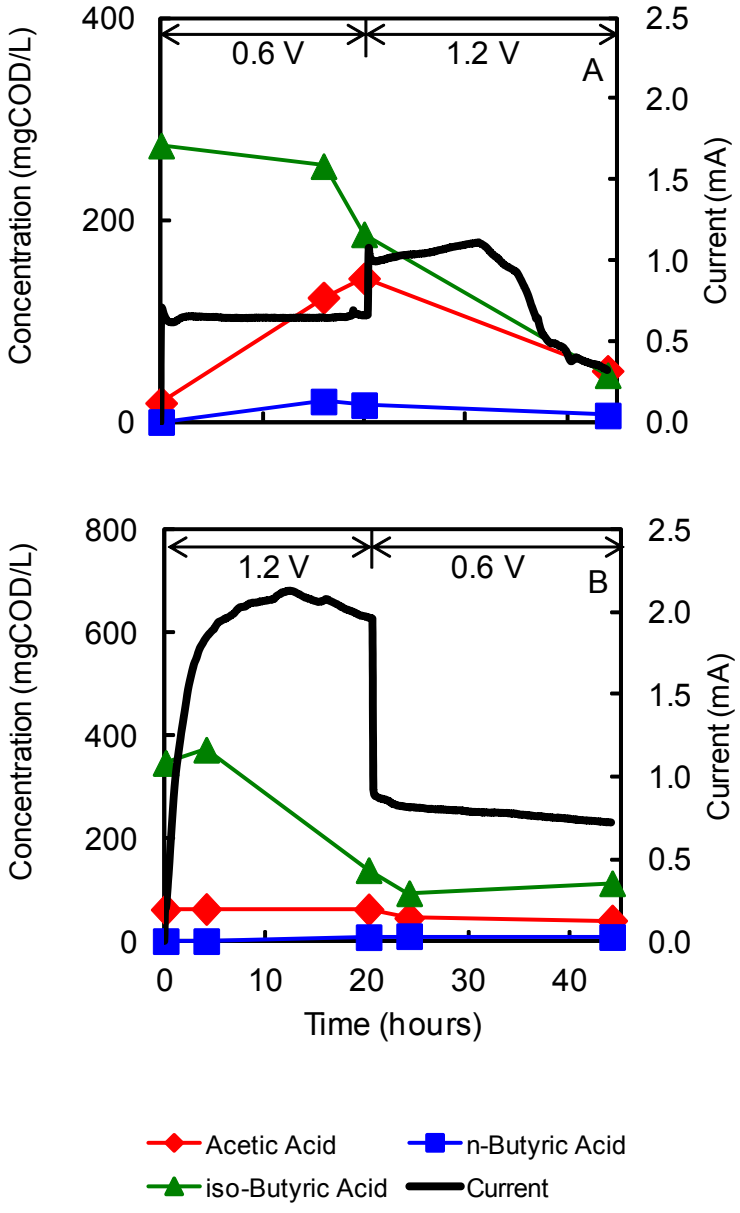

Figure 3-2(A) 500 mgCOD/L iso-butyric, 0.6V to 1.2V, CE = 89.73%. (B) 500 mgCOD/L iso-butyric, 1.2 V to 0.6 V, CE = 99.82% (the MEC reactor was fed with only iso-butyric acid for 2 weeks prior to the shown fed-batch cycle).

3.4.3 Utilization of mixed SCFA

When multiple substrates (acetic acid, propionic acid, n-butyric acid, and iso-butyric acid) were provided simultaneously in the MEC, acetic acid was preferentially used. The preferential oxidation of acetic acid over other SCFA is particularly noticeable in Fig 3-3. After the initial drop in all acids in the first 4 hours, the SCFA concentrations remained relatively stable while acetic acid concentration decreased over the course of the experiment cycle. While the combined COD from all SCFA available in the reactor was sufficient for current generation, the current generation was relatively low, indicating that the COD was not in a readily utilizable form. High current was observed in the first 15 hours, followed by a drop for the remainder of the experiment despite the increase in applied voltage at 20 hours. This result can be attributed to the limited amount of acetic acid in the reactor. After acetic acid was depleted, the high COD and high applied voltage are insufficient to sustain high current (Fig 3-3).

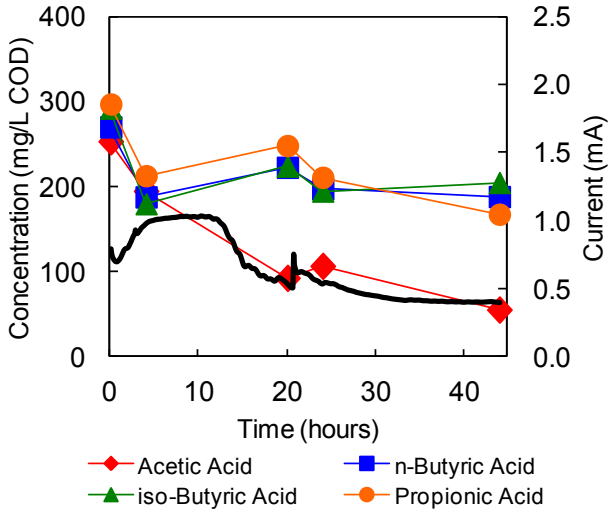

Figure 3-3 Mixed acids reactors, high substrate 200-400 mgCOD/L of each, 0.6V to 1.2V, CE = 46.51% (the MEC reactor was fed with the multiple substrates over 2 weeks prior to the 50-hr fed batch cycle).

3.4.4 LSV with butyric acids

Both n-butyric and iso-butyric acids are less easily oxidized by exoelectrogens (Fig 4). The acetic acid feed exhibited a much higher peak (~4 mA) than when fed with n-butyric or iso-butyric acid (~2 mA for 100 and 500 mg/L and ~1 mA for 50 mg/L). In LSV, there is a strong dependency of electric current on the concentration of n- and iso-butyric acid, though the dependency was not clear for concentration above 100 mg/L. It needs to be emphasized that, for 50 mg/L, the current started to decrease after the initial peak at -0.3 V vs. Ag/AgCl (Fig 3-4A & 3-4B) for both n- and iso-butyric acids. This finding implies direct oxidation of the substrates because the exoelectrogenic activity was affected by the substrate concentration. For comparison, LSV was performed in the n- and iso- butyric acid reactors with a feed solution of acetic acid. The reactors had been exposed to SCFA for

several weeks and the biofilms have been able to break down SCFA. When the feed substrate was switched to acetic acid, both reactors showed improved current generation (Fig3-4A, B).

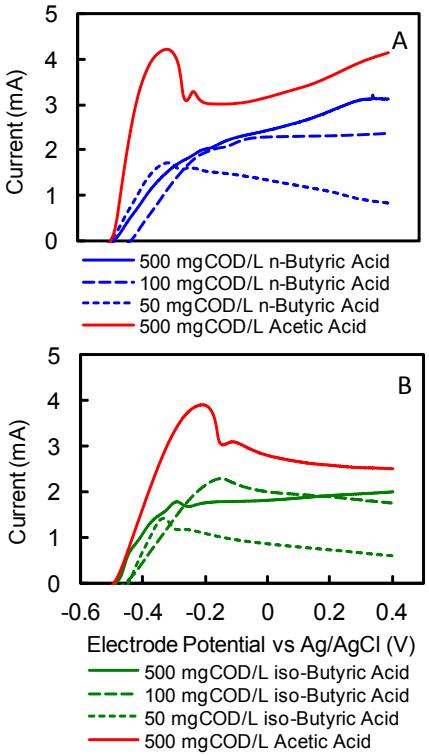

Figure 3-4(A) LSV results for n-butyric acid reactor and (B) LSV results for iso-butyric acid reactor (the reactor was fed with n-butyric acid (A) and iso-butyric acid (B) and run at 1.2 V Eap for 2 weeks prior to LSV).

3.4.5 Exchange current (I_0) for evaluating substrate favorability

The exchange current (I_0) was found to be a more reliable indicator of substrate preference than the charge transfer resistance (R_{CT}) in EIS tests performed using propionic, n-butyric, iso-butyric, n-valeric, iso-valeric and hexanoic acids. It is well known that acetic and propionic acids are readily utilized in the bioanode compared butyric, valeric, and hexanoic

acids (Cheng and Logan, 2007; Lee et al, 2014; Kaur et al, 2013). The found I_0 values are consistent with this trend: I_0 is the highest for acetic acid (47.1 μA) and propionic acid has the second largest I_0 (16.6 μA) while I_0 for the longer chain fatty acids are consistently below 10 μA (Table 3-1). The charge transfer resistance has the similar trend with the smallest value for acetic acid (68 Ω). However, R_{CT} of n-valeric acid (161 Ω) is much smaller than that of n-butyric acid (280 Ω) and iso-butyric acid (417 Ω). In addition, it is even comparable to that of propionic acid (111 Ω). Thus, this observation indicates that the charge transfer resistance cannot be used as a reliable indicator for substrate preference.

Table 3-1 Charge transfer resistance (R_{CT}) and exchange current (I_0)

	R_{CT} (Ω)	n	I_0 (μA)
Acetic Acid	68.12	8	47.1
Propionic Acid	110.73	14	16.6
n-Butyric Acid	279.76	20	4.6
iso-Butyric Acid	416.50	20	3.1
n-Valeric Acid	161.05	26	6.1
iso-Valeric Acid	452.33	26	2.2
Hexanoic Acid	334.09	32	2.4

The charge transfer resistance is a direct parameter measuring the difficulty of electron transfer in an electrode reaction. If a large number of electrons are involved in the electrode reaction, the charge transfer resistance decreases regardless of the difficulty of electron transfer. For instance, oxidation of one molecule of n-valeric acid releases 26 electrons while propionic acid discharges only 14 electrons. As a result, the R_{CT} values of propionic and n-valeric acids are not very different even though propionic acid is more easily utilized

at the bioanode. On the other hand, the exchange current is a normalized parameter by the number of electrons that are involved in the electrode reaction (Equation 1). Thus, the exchange current is more reliable to determine the substrate preference at the bioanode. In many previous studies, the charge transfer resistance was commonly used to quantify the bioanode performance for a single substrate where the number of electrons is constant. However, when various substrates are examined in bioelectrochemical systems, it is recommended that the exchange current should be used to determine the bioanode performance.

3.5 Conclusions

This study investigated the utilization of short chain fatty acids (SFCA) in microbial electrolysis cells (MEC) and applied electrochemical techniques to evaluate how SCFA are broken down by bioanodes and determine substrate favorability. We detected acetic acid in all reactors when n- and iso-butyric acids were provided as the sole substrate, indicating that acetic acid is an intermediate product that can contribute electric current generation in MECs. We found that the reactor fed with n-butyric acid produced high current when sufficient acetic acid accumulated in the reactor, and that electric current magnitude was unaffected by applied potential. The electric current with iso-butyric acid showed a strong dependency on applied potential, implying direct oxidation of iso-butyric acid by the bioanode. We used linear sweep voltammetry (LSV) and electrochemical impedance spectroscopy (EIS) to evaluate how readily a substrate is utilized. The exchange current (I_0) was found to be a more effective indicator for substrate favorability than charge transfer

resistance (R_{CT}) because it is independent on the number of electrons released by oxidation a given substrate.

3.6 Acknowledgments

This research was supported by Discovery Grants (435547-2013, Natural Sciences and Research Council of Canada), Canada Research Chairs Program (950-2320518, Government of Canada), Leaders Opportunity Fund (31604, Canadian Foundation of Innovation), Ontario Research Fund-Research Infrastructure (31604, Ontario Ministry of Economic Development and Innovation), Clifton F. Sherman Scholarship (Ontario Graduate Scholarship), and Alexander Graham Bell Canada Graduate Scholarship (Natural Sciences and Research Council of Canada, Canada Graduate Scholarship - Doctoral). The authors also thank Mr. Peter Koudys, Ms. Anna Robertson, and Ms. Monica Han for their assistance in reactor construction and operation of laboratory equipment.

3.7 References

Asztalos JR, Kim Y (2015a) Enhanced digestion of waste activated sludge using microbial electrolysis cells at ambient temperature. Water Res 87:503-512.

Asztalos JR, Kim Y (2015b) Lab-scale experiment and model study on enhanced digestion of wastewater sludge using bioelectrochemical systems. J Environ Informatics doi:10.3808/jei.201500308

Bard AJ, Faulkner LR (2001) Electrochemical Methods 2nd Ed. Wiley & Sons, New York

Call D, Logan BE (2008) Hydrogen production in a single chamber microbial electrolysis cell lacking a membrane. Environ Sci Technol 42:3401-3406

Call DF, Wagner RC, Logan BE (2009) Hydrogen production by Geobacter species and a mixed consortium in a microbial electrolysis cell. Appl Environ Microbiol 75:7579-7587

Chae K, Choi MJ, Lee JW, Kim KY, Kim IS (2009) Effect of different substrates on the performance bacterial diversity and bacterial viability in microbial fuel cells. Bioresour Technol 100:3518-3525

Cheng S, Logan BE (2007) Sustainable and efficient biohydrogen production via electrohydrogenesis. Proc Natl Acad Sci USA 104:18871-18873

Cheng S, Xing D, Call DF, Logan BE (2009) Direct biological conversion of electrical current into methane by electromethanogenesis. Environ Sci Technol 43:3953-3958

Ditzig J, Liu H, Logan BE (2007) Production of hydrogen from domestic wastewater using a bioelectrochemically assisted microbial reactor (BEAMR). Int J Hydrogen Energy 32:2296-2304

ElMekawy A, Srikanth S, Bajracharya S, Hegab HM, Nigam PS et al (2015) Food and agricultural wastes as substrates for bioelectrochemical system (BES): The synchronized recovery of sustainable energy and waste treatment. Food Res Int 73:213-225

Feki E, Khoufi S, Loukil S, Sayadi S (2015) Improvement of anaerobic digestion of waste-activated sludge by using H2O2 oxidation, electrolysis, electro-oxidation and thermo-alkaline pretreatments. Environ Sci Pollut R 22:14717-14726.

Feng Y, Wang X, Logan BE, Lee H (2008) Brewery wastewater treatment using air-cathode microbial fuel cells. Appl Microbio Biotechnol 78:873-880

Freguia S, Teh EH, Boon N, Leung KM, Keller J, Rabaey K, (2010). Microbial fuel cells operating on mixed fatty acids. Bioresour Technol 101:1233-1238

Fricke K, Harnisch F, Schröder U (2008) On the use of cyclic voltammetry for the study of anodic electron transfer in microbial fuel cells Energy Environ Sci 1:144-147

Gil-Carrera L, Escapa A, Mehta P, Santoyo G, Guiot SR, Morán A, Tartakovsky B (2013) Microbial electrolysis cell scale-up for combined wastewater treatment and hydrogen production. Bioresour Technol 130:584-591

Guo K, Soeriyadi AH, Patil SA, Prévoteau A, Freguia S, Gooding JJ, Rabaey K (2014) Surfactant treatment of carbon felt enhances anodic microbial electrocatalysis in bioelectrochemical systems. Electrochem Commun 39:1-4

He Z, Mansfeld F (2009) Exploring the use of electrochemical impedance spectroscopy (EIS) in microbial fuel cell studies. Energy Environl Sci 2: 215-219

Hu Z (2008) Electricity generation by a baffle-chamber membraneless microbial fuel cell. J Power Sources 179: 27-33

Kaur A, Kim JR, Michie I, Dinsdale RM, Guwy AJ, Premier GC (2013) Microbial fuel cell type biosensor for specific volatile fatty acids using acclimated bacterial communities. Biosens Bioelectron 47:50-55

Kiely P. D. Regan J. M. & Logan B. E. (2011) The electric picnic: synergistic requirements for exoelectrogenic microbial communities. Current Opinion in Biotechnology 22:378-385

Lee HS, Parameswaran P, Kato-Marcus A, Torres CI, Rittmann BE (2008) Evaluation of energy-conversion efficiencies in microbial fuel cells (MFCs) utilizing fermentable and non-fermentable substrates. Water Res 42:1501-1510

Lee WS, Chua ASM, Yeoh HK, Ngoh GC (2014) A review of the production and applications of waste-derived volatile fatty acids. Chem Eng J 235:83-99

Liu H, Cheng S, Logan BE (2005a) Production of electricity from acetate or butyrate using a single-chamber microbial fuel cell. Environ Sci Technol 39:658-662

Liu H, Grot S, Logan BE (2005b) Electrochemically assisted microbial production of hydrogen from acetate. Environ Sci Technol 39:4317-4320

Logan BE, Call D, Cheng S, Hamelers HV, Sleutels TH, Jeremiasse AW, Rozendal RA (2008) Microbial electrolysis cells for high yield hydrogen gas production from organic matter. Environ Sci Technol 42:8630-8640

Nevin KP, Richter H, Covalla SF, Johnson JP, Woodard TL, Orloff AL, Jia H, Zhang M, Lovley DR (2008) Power output and coulombic efficiencies from biofilms of Geobacter sulfurreducens comparable to mixed community microbial fuel cells Environ Microbiol 10:2505-2514

Oh S, Logan BE (2005). Hydrogen and electricity production from a food processing wastewater using fermentation and microbial fuel cell technologies. Water Res 39: 4673-4682

Pant D, Arslan D, Van Bogaert G, Gallego YA, De Wever H, Diels L, Vanbroekhoven K (2013) Integrated conversion of food waste diluted with sewage into volatile fatty

acids through fermentation and electricity through a fuel cell. Environ Technol 34: 1935-1945

Pant D, Van Bogaert G, Diels L, Vanbroekhoven K (2010) A review of the substrates used in microbial fuel cells (MFCs) for sustainable energy production. Bioresour Technol 101:1533-1543

Pilli S, More T, Yan S, Tyagi RD, Surampalli RY (2015) Anaerobic digestion of thermal pre-treated sludge at different solids concentrations–Computation of mass-energy balance and greenhouse gas emissions. J Environ Manage 157:250-261

Sevda S, Abu-Reesh IM, Yuan H, He Z (2016) Bioelectricity generation from treatment of petroleum refinery wastewater with simultaneous seawater desalination in microbial desalination cells. Energ Convers Manage doi:10.1016/j.enconman.2016.05.050

Sharma M, Aryal N, Sarma PM, Vanbroekhoven K, Lal B, Benetton XD, Pant D (2013) Bioelectrocatalyzed reduction of acetic and butyric acids via direct electron transfer using a mixed culture of sulfate-reducers drives electrosynthesis of alcohols and acetone. Chem Commun 49:6495-6497

Sharma M, Bajracharya S, Gildemyn S, Patil SA, Alvarez-Gallego Y, Pant D et al. (2014) A critical revisit of the key parameters used to describe microbial electrochemical systems. Electrochim Acta 140:191-208

Sun M, Sheng GP, Mu ZX, Liu XW, Chen YZ, Wang HL, Yu HQ (2009) Manipulating the hydrogen production from acetate in a microbial electrolysis cell–microbial fuel cell-coupled system. J Power Sources 191:338-343

Tchobanoglous G, Burton FL, Stensel HD Eds. (2003) Metcalf & Eddy Wastewater Treatment and Reuse 4th ed. McGraw-Hill, Boston

Wang X, Feng YJ, Lee H (2008) Electricity production from beer brewery wastewater using single chamber microbial fuel cell. Water Sci Technol 57:1117-1122

Wang X, Cheng S, Feng Y, Merrill MD, Saito T, Logan BE (2009) Use of carbon mesh anodes and the effect of different pretreatment methods on power production in microbial fuel cells. Environ Sci Technol 43:6870-6874

Zeppilli M, Villano M, Aulenta F, Lampis S, Vallini G, Majone M (2015) Effect of the anode feeding composition on the performance of a continuous-flow methane-producing microbial electrolysis cell. Environ Sci Pollut R 22:7349-7360.

Zhang B, Zhao H, Zhou S, Shi C, Wang C, Ni J (2009) A novel UASB–MFC–BAF integrated system for high strength molasses wastewater treatment and bioelectricity generation. Bioresour Technol 100:5687-5693

Zhuang L, Yuan Y, Wang Y, Zhou S (2012) Long-term evaluation of a 10-liter serpentine-type microbial fuel cell stack treating brewery wastewater. Bioresour Technol 123:406-412

CHAPTER 4 Junction Potentials in Thermolytic Reverse Electrodialysis

Paper III: *Huang, W., Walker, W. S., & Kim, Y. (2015). Junction potentials in thermolytic reverse electrodialysis. Desalination, 369, 149-155.*

Thermolytic reverse electrodialysis is a potential method for energy recovery from waste heat generated in industrial processes. Ammonium bicarbonate is a salt with a low vaporization temperature, making it an ideal candidate for use in this type of energy recovery. However, the complicated equilibrium of ammonium bicarbonate makes it nearly impossible to calculate the energy across each membrane pair, making modeling of such systems very challenging. In this paper, a method is proposed to quickly and accurately estimate this energy, or junction potential, from a conductivity measurement.

Key findings of this research include:

- Development of an equation that can estimate to 95% accuracy the junction potential of ammonium bicarbonate solutions across either a cation exchange membrane or anion exchange membrane.
- Investigation of operating conditions for energy production found that the concentration difference governs energy generation, rather than the actual magnitude of concentration.
- Ammonium bicarbonate is better for energy production than ammonium carbonate due to the pH equilibrium of ammonia and ammonium species

4.1 Abstract

Reverse electrodialysis (RED) can produce electric energy from waste heat using thermolytic solutions (*e.g.*, NH_4HCO_3) where waste heat is used to regenerate the high (HC) and low concentration (LC) solutions. The salinity difference between the two solutions in RED is converted into electric potential across an ion exchange membrane (IEM), exploiting the liquid junction potential. Theoretical calculation of the junction potential is cumbersome because the activity coefficients and equilibrium speciation of individual ions are complicated for highly concentrated NH_4HCO_3 solution. We used a simplification of the Planck-Henderson equation to approximate the junction potential in thermolytic RED systems based on conductivity measurements, and this approximation was consistent with experimentally measured junction potentials. The experimental results also found that NH_4HCO_3 created greater junction potentials across anion exchange membranes than $(NH_4)_2CO_3$ solution for a given molar concentration ratio. The junction potential was hardly affected by the magnitude of HC as long as the concentration ratio between HC and LC was maintained. Based on the experimental findings, we recommend that thermolytic RED systems be operated under neutral pH and high concentration ratio conditions (above 1:100 ratio). These findings provide information essential for designing and operating thermolytic RED systems for future study and practical application.

Keywords

Ion exchange membranes; junction potential; reverse electrodialysis (RED); ammonium bicarbonate; ammonium carbonate; thermolytic solution

4.2 Introduction

In reverse electrodialysis (RED), ion exchange membranes (IEMs) are used to create electric power from the salinity difference between two electrolyte solutions. For instance, the permeation of salt ions in seawater across the IEM into fresh river water generates electric potential energy in an RED stack [1-6]. In addition to seawater and river water, thermolytic solutions (*e.g.*, ammonium bicarbonate solution) can be used in RED for energy recovery from low grade heat sources (often referred to as "waste heat" in various industries) [7,8]. Ammonium bicarbonate vaporizes into gaseous ammonia and carbon dioxide at relatively low temperatures (*e.g.*, ~60 °C) [9], allowing easy regeneration of the LC (low concentration) solution by separating ammonia and carbon dioxide using waste heat energy. The separated ammonia and carbon dioxide are used to regenerate the HC (high concentration) solution to maintain sufficiently high concentration of ammonium bicarbonate (*e.g.*, > 1 M) compared to that of the LC solution. The concentration difference between the HC and LC solutions is converted into electric energy in an RED stack of anion exchange membranes (AEMs) and cation exchange membranes (CEMs). This conversion into electric energy is achieved by cations migrating through CEMs and anions through AEMs and eventually by redox reactions at the electrodes. The RED technology coupled with ammonium bicarbonate thermolytic solutions has been recently demonstrated to produce electric energy [7,8,10], H_2 gas [11,12] or CH_4 gas [13] in lab-scale experiments with the aim of eventually recovering energy from low grade waste heat sources in various industries.

The electrical voltage created by the salinity difference across an IEM is a liquid junction (diffusion) potential [15]. Note that although the junction potential across a single IEM is typically small (< 0.5 V), the total junction potential is added across an RED stack of hundreds of IEMs, generating a meaningful amount of electric energy. Thus, precise assessment of the junction potential across IEMs is critical for the estimation of electric power generation and energy recovery in RED systems. Theoretical determination of the junction potential requires extensive electrochemical information of individual ionic species. For instance, the equilibrium speciation should be clarified among NH_4^+, NH_3, H_2CO_3, HCO_3^-, CO_3^{2-}, NH_2COOH (carbamic acid) and NH_2COO^- (carbamate) in ammonia- and carbonate-based thermolytic solutions (*e.g.*, ammonium bicarbonate or ammonium carbonate electrolytes). The equilibrium constant is not also clearly defined for carbamate formation ($NH_4^+ + CO_3^{2-} \rightarrow NH_2COO^- + H_2O$) and acid dissociation of carbamic acids ($NH_2COOH \rightarrow NH_2COO^- + H^+$). In addition, the activity coefficient of these individual ionic species needs to be precisely estimated. To our knowledge, however, many of these electrochemical properties for highly concentrated ammonium bicarbonate electrolytes are unavailable in literature. As a result, accurate theoretical calculation of the junction potential is difficult for RED systems using ammonium bicarbonate solution.

The main objectives of this study are to: (1) leverage an approximation for junction potential which does not require extensive electrochemical information; and (2) verify the equation by comparing it with experimental results. Other important aspects of this study are to: (3) compare two thermolytic solutions (NH_4HCO_3 vs. $(NH_4)_2CO_3$) for their capacity of creating junction potentials; and (4) investigate the pH and concentration requirement of

the HC solution for maximizing energy creation across IEMs. Since thermolytic RED has been recently demonstrated for energy capture with waste heat recovery [8,9,12,13,14], there is insufficient experimental information to explain the effect of the relative amount of ammonia and carbonate species in thermolytic solutions (*e.g.*, NH_4HCO_3 vs. $(NH_4)_2CO_3$) on energy recovery. Also, previous studies on thermolytic RED have used relatively high ammonium bicarbonate concentration (0.95 – 1.7 M) for the preparation of the HC solution [8,9,11,16,17]. In this study, we examined whether such high concentration is necessary for effective energy production in thermolytic RED.

4.3 Methodology

4.3.1 Theoretical background: junction potential across an IEM

The electrochemical potential of an ionic species *i* ($\overline{\mu_i}$) is defined as [15]:

$$\overline{\mu_i} = \overline{\mu_i^0} + RTlna_i + z_iF\phi \qquad \text{(Eq 4-1)}$$

$\overline{\mu_i^0}$ is the standard state electrochemical potential, R is the gas constant, T is the temperature, a_i is the activity of the ionic species, z_i is the charge, F is the Faraday constant and ϕ is the electric potential. When two electrolytes of a high concentration (HC) and lower concentration (LC) are separated by an IEM, the magnitude of the electric potential difference across the IEM (*i.e.*, the junction potential, ϕ_{jct}) can be found by equating Eq. 2 for all ionic species present in the electrolytes as [15]:

$$\left|\phi_{jct}\right| = \frac{RT}{F}\sum_i \frac{t_i}{z_i} ln \frac{a_i^{HC}}{a_i^{LC}} \qquad \text{(Eq 4-2)}$$

The transport number or transference number (t_i) is defined as the fractional contribution of an individual ionic flux to the total electric current across the junction (*i.e.*, IEM). Theoretical estimation of the junction potential using this equation needs extensive information of the physical and chemical properties for both the electrolyte and IEM, such as the activity of individual ions and their transport number in the IEM. For highly concentrated ammonium bicarbonate solutions, it is cumbersome to determine the concentration and activity coefficient of individual ion species: NH_4^+, HCO_3^-, CO_3^{2-} and $NH_2CO_2^-$. In addition, the transport number of these ions in IEMs needs extensive experimental information for membrane permselectivity and competitive partitioning among these ions. As a result, Eq. 2 is not convenient for practical estimation of the junction potential in ammonium bicarbonate-based RED systems. Thus, we propose using the Planck-Henderson equation for junction potentials [15,18-23], which approximates Eq. 2 by assuming that the activity of each species is proportional to the product of molar concentration (C_i) and ionic mobility (u_i) and that there is a linear transition in concentrations from the HC to the LC:

$$\phi_{jct} \approx \frac{RT}{F} \frac{\sum \frac{|z_i|u_i}{z_i}[C_i^{LC} - C_i^{HC}]}{\sum |z_i|u_i[C_i^{LC} - C_i^{HC}]} ln \frac{\sum |z_i|u_i C_i^{HC}}{\sum |z_i|u_i C_i^{LC}} \quad \text{(Eq 4-3)}$$

Since the transport number of each species is defined by Eq. 4 [15] and the electrical conductivity (κ) of the solution is written as Eq. 5 [15], then Eq. 3 can be further simplified to Eq. 6.

$$t_i = \frac{|z_i|u_i C_i}{\sum |z_j|u_j C_j} \quad \text{(Eq 4-4)}$$

$$\kappa = F \sum |z_i| u_i C_i \quad \text{(Eq 4-5)}$$

$$\left|\phi_{jct}\right| \approx \frac{RT}{F}\left(\frac{t_{counter}}{z_{counter}} + \frac{t_{co}}{z_{co}}\right) ln \frac{\kappa^{HC}}{\kappa^{LC}} \quad \text{(Eq 4-6)}$$

The subscript *counter* denotes the counter-ions that are preferentially transported through an IEM while the subscript *co* is the co-ions that are rejected by the IEM. For instance, for a CEM (cation exchange membrane), NH_4^+ is the counter-ion and HCO_3^-, CO_3^{2-} and $NH_2CO_2^-$ are the co-ions in ammonium bicarbonate electrolytes, and vice versa for an AEM (anion exchange membrane). For an ammonium bicarbonate concentration between 0.001 and 2 M, measured pH was between 7.9 and 8.1 (Fig 4-1), indicating that the fraction of CO_3^{2-} is negligible compared to that of HCO_3^- (*pKa* of HCO_3^- is 10.3) [24]. Thus, we approximated all ionic species in the ammonium bicarbonate electrolyte (*i.e.*, NH_4^+, HCO_3^-, $NH_2CO_2^-$) as monovalent, making $z_{counter}$ and z_{co} either +1 or -1.

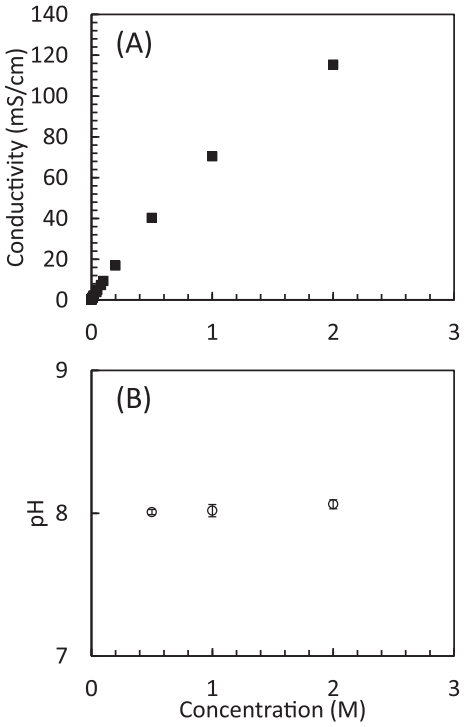

Figure 4-1 (A) Conductivity and (B) pH of NH4HCO3 solution (23 ± 1°C). (Error bars indicate the standard deviation of triplicate experiments.)

Eq. 6 can be used to estimate the junction potential across a stack of ion exchange membranes in RED for waste heat energy recovery as electricity. By finding the junction potential using Eq. 6, the maximum amount of energy available from two thermolytic solutions can be determined, allowing evaluation of energy recovery in a thermolytic RED system. Eq. 6 can also be used as a tool for modeling energy recovery and conductivity change in a thermolytic RED system.

4.3.2 Comparison of Eqs. 2 and 6 with NaCl

The activity-based junction potential (Eq. 2) was compared with the conductivity-based estimation (Eq. 6) for NaCl solution since the activity coefficient (γ_i) of Na^+ and Cl^- in

highly concentrated solution (HC = 1 M) can be found precisely using an extended Debye-Hückel equation [25]:

$$log\gamma_i = -\frac{A|z_i|^2\sqrt{I}}{1+Ba^0\sqrt{I}} - log(1 + 0.001m_iM_s) + K_iI \qquad \text{(Eq 4-7)}$$

I is the ionic strength in molality, m is the molal concentration, Ms is the molecular weight of the solvent and a^0 is the ion size parameter (3.78 Å for Na^+ and Cl^-). For NaCl solution, A = 0.5085 $mol^{-1/2}$ $kg^{1/2}$, B = 0.3282 $Å^{-1}mol^{-1/2}$ $K^{1/2}$, K_{Na} = 0.105 kg^2mol^{-2} and K_{Cl} = -0.009 kg^2mol^{-2} at 25 °C [25].

4.3.3 Thermolytic solution preparation

The HC solution was prepared by dissolving ammonium bicarbonate (NH_4HCO_3) or ammonium carbonate ($(NH_4)_2CO_3$) salt in deionized water to a designated concentration (HC = 0.5, 1.0 or 2.0 M) at room temperature. The LC solution was made by diluting the prepared HC solution for the given concentration ratios (CR = 10, 25, 50, 100, 250 and 500). Prior to the experiment for junction potential measurement, the prepared solutions were analyzed for conductivity and pH (SevenMulti; Mettler-Toledo International Inc., OH). The solution pH was not affected by the concentration while the conductivity increased with the increasing molar concentration (Fig 4-1). No pH adjustments were made to the prepared thermolytic solutions.

4.3.4 Junction potential measurement

A two-chamber reactor (HC and LC chambers) was constructed using low density polyethylene blocks with an inner cylindrical chamber (30 mL each). The HC and LC

chambers were separated by either a CEM or AEM (Selemion CMV and AMV, respectively; AGC Engineering, Japan). Two Ag/AgCl reference electrodes (MW-2030; BASi Liquid Chromatography, IN) were used to measure the junction potential across the IEM in accordance with Strathmann [26]. Note that the electrode reaction within the reference electrode ($AgCl + e^- \leftrightarrow Ag + Cl^-$) is equilibrated, *i.e.*, the net rate of the reaction is zero. In this experimental set up, each of the reference electrodes measures the electric potential level versus its equilibrated electrode reaction. Thus, the potential difference between the two identical reference electrodes can be considered as the junction potential (*i.e.*, electrical voltage created by concentration difference between two thermolytic solutions separated by an ion exchange membrane). While the HC chamber was not mixed, the LC chamber was well-mixed using a magnetic stirrer. A separate experiment confirmed that the lack of mixing condition in the HC chamber does not affect the junction potential measurement.

Electric potential between the reference electrodes was measured and recorded every 2 seconds using a digital multimeter (34970A Data Acquisition/Switch Unit; Agilent Technologies, CA). Data recorded for the first 30 seconds (*i.e.*, 15 readings) were averaged and used to determine the junction potential for a given CR and HC condition. The junction potential experiment was performed in triplicate, and all experiments were performed under room temperature in an air conditioned laboratory (23 ± 1 °C).

Note that the junction potential measurement was performed under zero electric (open circuit) current conditions. Thus, there were no working or counter electrodes in the

experimental cell. Such zero current conditions were necessary for precise measurement of the junction potential across the ion exchange membrane. With the presence of electric current (i.e., ionic flux across the ion exchange membrane), concentration polarization occurs even at very low current conditions near the ion exchange membrane surface (i.e., boundary layer or diffusion boundary layer) [26]. The concentration polarization in the diffusion boundary layer creates a substantial electric potential loss in the diffusion boundary layer and experimental measurement of the potential loss is practically impossible without knowing the thickness of the diffusion boundary layer. Also, model-based estimation of the electric potential loss in the diffusion boundary layer is not sufficiently precise because of the uncertainty involved in defining the thickness of the diffusion boundary layer [27], making it infeasible to measure the junction potential without the interference of the concentration polarization. Thus, zero current conditions were necessary for accurate estimation of the junction potential.

4.4 Results and Discussion

4.4.1 Comparison of the activity- and conductivity-based equations for simulated NaCl solution

The conductivity-based estimation for the junction potential (Eq. 6) was verified with the activity-based calculation (Eq. 2) for a theoretical IEM with NaCl solution (Fig 4-2), HC = 1 M, and where the activity of the NaCl solution was determined using Eq. 7. When compared to the activity-based calculation (Eq. 2), the conductivity-based approximation (Eq. 6) consistently overestimated the junction potential by 2.7% across an AEM (Fig 4-

2A) but underestimated the junction potential by 5.2% across a CEM (Fig 4-2B), assuming a theoretical transport number of 0.95 in both cases. These systematic discrepancies can be explained by relative differences in activity coefficients of Na^+ and Cl^- at different concentrations, which is not reflected in the conductivity-based approximation. As a result, the conductivity-based junction potential is identical for CEMs and AEMs, while the activity-based junction potential is greater for CEMs because Na^+ ions have relatively greater activity coefficients than Cl^- ions in highly concentrated NaCl solution. Even with the slight differences for individual IEMs, the conductivity-based approximation (Eq. 6) for the sum of the junction potentials across a cell pair (*i.e*, an AEM and a CEM) overestimated the activity-based junction potential (Eq. 2) by 1.4% (Fig 4-2C). Thus, the conductivity-based approximation (Eq. 6) is assumed to be relatively accurate for predicting junction potentials in RED applications (for solution concentrations up to 1 M).

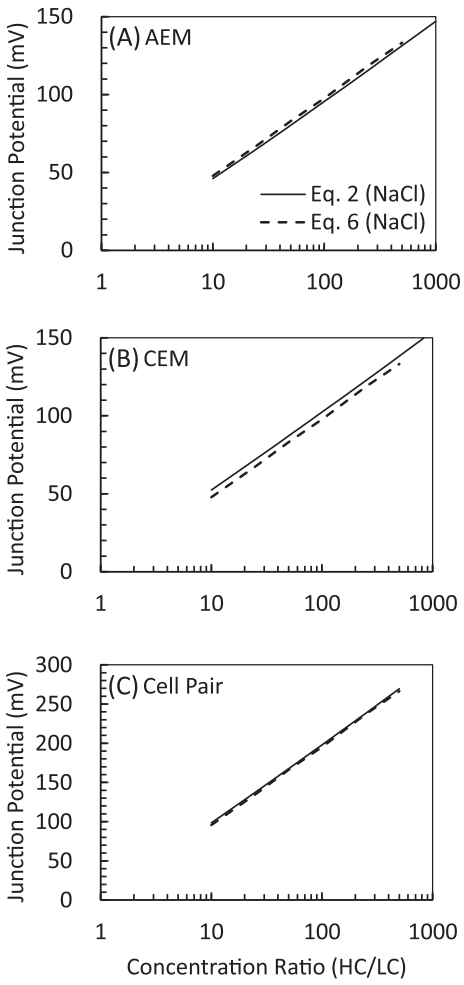

Figure 4-2 Comparison of activity-based (Eq. 2) and conductivity-based (Eq. 6) calculation for the junction potential across an IEM (t = 0.95) with NaCl solution (HC = 1 M NaCl; 25 °C).

4.4.2 Concentration requirements of ammonium bicarbonate solution and applications

From the experiments using NH_4HCO_3 solutions with an AMV or a CMV membrane, the junction potential created across the IEM increased with the increasing CR (concentration ratio, HC/LC) while the magnitude of HC hardly affected the junction potential creation for a given CR (Fig 4-3). This negligible effect of the HC magnitude implies that

thermolytic RED systems are not necessarily to be operated with highly concentrated NH_4HCO_3 solution as long as high CR conditions are effectively maintained. This result indicates that optimal HC conditions in practical RED applications should be determined by balancing the regeneration costs for HC solution and LC solution. For instance, if the HC solution regeneration (*i.e.*, increasing concentration) is more expensive than the LC solution regeneration (*i.e.*, decreasing concentration), CR should be maintained high by lowering LC rather than increasing HC.

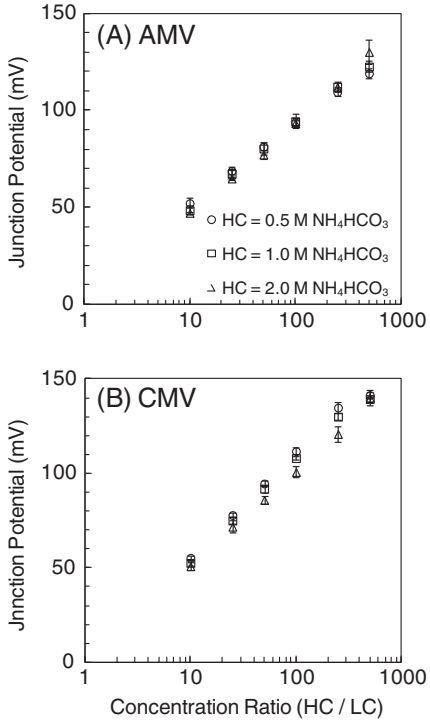

Figure 4-3 Effect of the magnitude of high concentration (HC) on junction potential creation (Experiments performed with NH4HCO3 solutions; error bars indicating the standard deviation of triplicate experiments).

4.4.3 Ammonium carbonate ($(NH_4)_2CO_3$) vs. ammonium bicarbonate (NH_4HCO_3)

Experiments found that the thermolytic solution of NH_4HCO_3 creates a greater junction potential across the AEM (AMV membrane) than that of $(NH_4)_2CO_3$ by 21-65% (Fig 4-4A). Note that the pH in NH_4HCO_3 solutions was between 7.9 and 8.1 (Fig 4-1B), while it was between 9.1 and 9.2 for $(NH_4)_2CO_3$ solutions. This relatively high pH can explain the smaller junction potential across the AEM with $(NH_4)_2CO_3$ (Fig 4-4A). For pH between 9.1 and 9.2, the concentration of hydroxide ion (OH^-) ranges between 1.3×10^{-5} and 1.6×10^{-5} M, and since this OH^- concentration is almost identical on both sides of the AEM, then the OH^- contribution to the junction potential should be negligible. Since the total amount of carbonate species in the LC solution was as small as 1×10^{-3} M (CR = 500), the amount of hydroxide ions was up to 1.3 – 1.6 % of the total anions in the LC solution. While this fraction is still small, the diffusion coefficient (and, thus, the ionic mobility) of OH^- at infinite dilution (5.273×10^{-9} m^2/s) is about 4.4 times that of HCO_3^- (1.185×10^{-9} m^2/s), increasing the transport number of OH^- [28]. Furthermore, AEMs are known to favor hydroxide ions over carbonate ions, so for example, with a selectivity coefficient of 3.0 for OH^- over HCO_3^-, the fraction of hydroxide ions in the membrane would be significantly greater [29]. As a result, the transport number of hydroxide ions increases in proportion to the fraction, making the transport number of carbonate ions small. Since the concentration ratio (or activity ratio) of hydroxide ions across the AEM is close to unity, the junction potential decreases with the increasing transport number of hydroxide ions (Eq. 2). Consequently, the junction potential with $(NH_4)_2CO_3$ is smaller than that with NH_4HCO_3 (Fig 4A). Note that the transport number of the hydroxide ion in NH_4HCO_3 is smaller than

that in $(NH_4)_2CO_3$ by an order of magnitude because the hydroxide ion concentration is smaller by an order of magnitude.

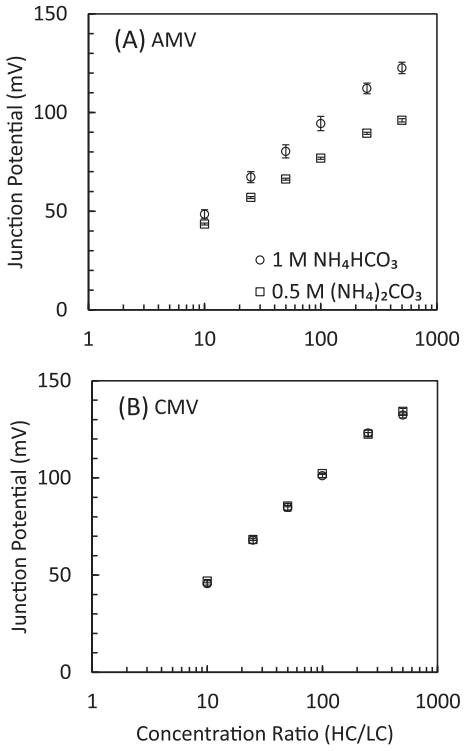

Figure 4-4 Experimental junction potential created with ammonium carbonate solution and ammonium bicarbonate solution (HC = 1 M for NH_4HCO_3 and 0.5 M for $(NH_4)_2CO_3$; Error bars indicating the standard deviation of triplicate experiments).

While the relatively high pH in $(NH_4)_2CO_3$ solutions (pH = 9.1 – 9.2) resulted in smaller junction potentials across the AEM, it hardly affected the junction potential across the CEM (Fig 4-4B). For the examined molar concentration of NH_4HCO_3 and $(NH_4)_2CO_3$, the total amount of ammonium species was the same; however, the relative amount of cationic NH_4^+ was greater in NH_4HCO_3 solution than that in $(NH_4)_2CO_3$ solution. For instance, approximately 91% of the total ammonia was NH_4^+ in the 1 M NH_4HCO_3 solution, whereas approximately 56% of the total ammonia was cationic NH_4^+ in the 0.5 M $(NH_4)_2CO_3$

solution (the remainder of the total ammonia is present as uncharged ammonia, NH_3, pK_a of NH_4^+ = 9.3 [24]). Even with this substantial difference in the amount of cationic NH_4^+, the experimental result was not affected by the speciation between NH_4^+ and NH_3 (Fig 4-4B). This result can be explained by neutral free ammonia (NH_3) being impermeable through the CEM, allowing the crossover of only ammonium ions (NH_4^+).

It is clear that NH_4HCO_3 is beneficial over $(NH_4)_2CO_3$ for the waste heat energy recovery using thermolytic RED systems since the junction potential is greater with NH_4HCO_3 due to neutral pH conditions (pH of 7.9 – 8.1 compared to 9.1 – 9.2 for $(NH_4)_2CO_3$). Similarly, thermolytic RED systems should not be operated at low pH conditions, where high H^+ concentration can decrease the junction potential across the CEM. We recommend that pH of thermolytic solutions be kept relatively neutral by balancing the amount of ammonia species and carbonate species.

4.4.4 Validity of conductivity-based estimation for ammonium bicarbonate solutions

The conductivity-based estimation (Eq. 6) was consistent with the experimentally measured junction potential (Fig. 4-5). Even with the equilibrium reactions among ammonium, carbonate and carbamate species, the assumption employed for the preparation of Eq. 6 (*i.e.*, the sum of the activity ratio terms for individual ions can be replaced by the ratio of solution conductivity) was found to be valid for the examined concentration conditions (HC = 0.5 to 2 M; CR = 10 to 500). No pH adjustments were made to the

solutions and the pH ranged between 7.9 and 8.1 (Fig 4-1B). Considering the limited information available for the ionic speciation and activity coefficient of individual ions in the thermolytic solution, Eq. 6 provides a straightforward method for precise estimation of the junction potential in thermolytic RED applications for energy recovery from waste heat.

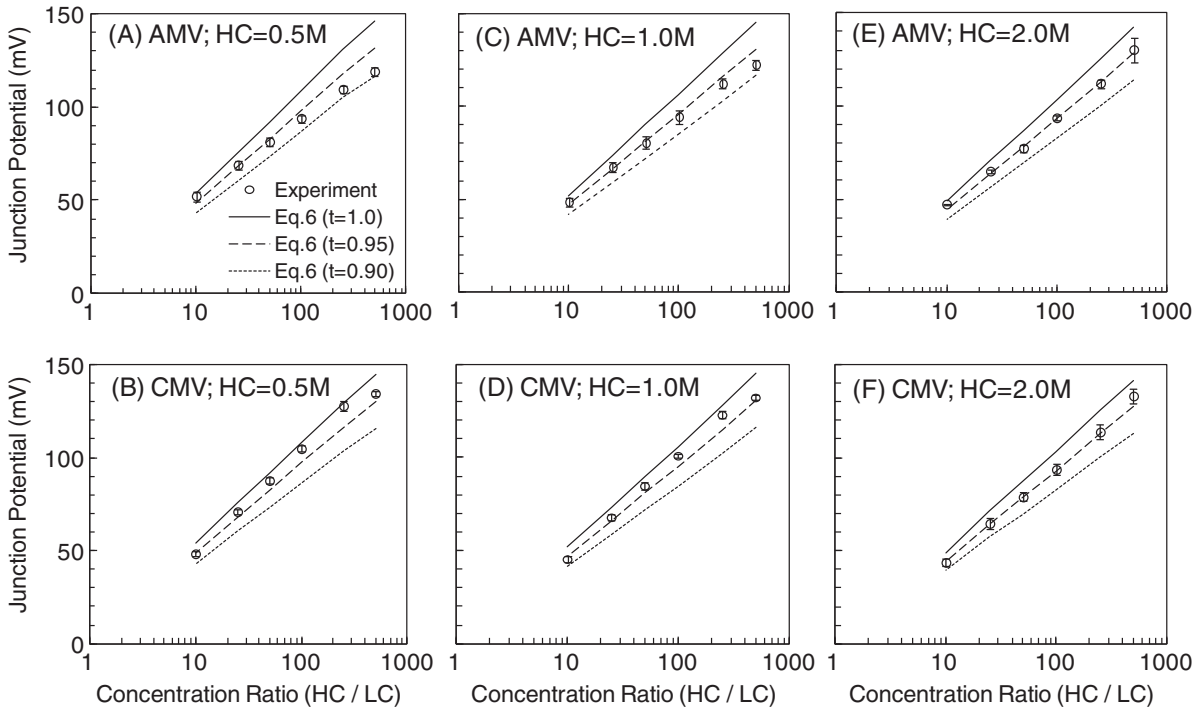

Figure 4-5 Experimental junction potential created with ammonium carbonate solution and ammonium bicarbonate solution (HC = 1 M for NH4HCO3 and 0.5 M for (NH4)2CO3; Error bars indicating the standard deviation of triplicate experiments).

The experimental junction potential across the IEM corresponds to the counter-ion transport number of approximately 0.95 (Fig 4-5). This observed transport number is consistent with previously reported values for the examined IEMs (Selemion AMV and CMV) [14,26,30-32]. When HC = 2 M, the measured junction potential fits consistently with the conductivity based estimation using a counter-ion transport of approximately 0.95

for both the CEM and AEM (Fig 4-5E and F). The counter-ion transport number of the AEM increased slightly with the increasing HC (Fig 5A, C and E) while the counter-ion transport number of the CEM decreased slightly with the increasing HC (Fig 4-5B, D and F). This correlation between the magnitude of HC and the resulting IEM transport number is summarized in Table 1. The examined commercial membranes (Selemion CMV and AMV) provide relatively consistent permselectivity for thermolytic RED applications, even with high ionic strength and relatively high levels of neutral components (*e.g.*, NH_3).

Table 4-1 Transport number of counter-ions determined by least square methods

NH_4HCO_3 concentration	AEM (R^2 value)	CEM (R^2 value)
HC = 0.5 M	0.93 (96.9%)	0.98 (99.0%)
HC = 1.0 M	0.94 (99.5%)	0.97 (99.1%)
HC = 2.0 M	0.94 (99.6%)	0.96 (99.3%)

The conductivity-based estimation of the junction potential elucidates the sensitivity of the junction potential to the transport number of IEMs in thermolytic RED systems (Fig 4-5). Regardless of the magnitude of HC and type of IEMs, the junction potential is sensitively affected by the transport number of the IEM. For instance, a 5% increase in the counter-ion transport number resulted in an 11% increase in the junction potential (Fig 4-5).

4.5 Conclusions

In this study, a conductivity-based equation (Eq. 6) was proposed for approximating the junction potential in thermolytic RED systems. We verified that the equation is consistent

with: (a) the theoretical junction potential of NaCl solutions for concentration ratios (CR) from 10 to 500 and high concentration (HC) of 1 M NaCl, and (b) experimentally measured junction potential for AMV and CMV membranes with CR from 10 to 500 and HC from 0.5 to 2 M NH_4HCO_3. The transport number of counter-ions was observed to be 0.93 to 0.95 for the AEM and 0.96 to 0.98 for the CEM (consistent with previously reported values). Both NH_4HCO_3 and $(NH_4)_2CO_3$ were initially considered, but the experimental results showed that NH_4HCO_3 is superior to $(NH_4)_2CO_3$ for creating junction potential (for a given concentration ratio). The relatively high pH of $(NH_4)_2CO_3$ solution resulted in a lesser junction potential creation across the AEM, as compared with NH_4HCO_3. However, the CEM junction potential was almost identical between $(NH_4)_2CO_3$ and NH_4HCO_3, indicating that the junction potential across the CEM is not affected by the pH-dependent speciation between ionic ammonium (NH_4^+) and free ammonia (NH_3). We also found that the junction potential was hardly affected by the magnitude of HC as long as the concentration ratio (CR) between HC and LC was maintained. We recommend that thermolytic RED systems be operated under neutral pH conditions by balancing the amount of ammonia species and carbonate species. Optimization of the thermolytic solution and operating conditions (*i.e.*, minimum necessary concentration of NH_4HCO_3 to maintain high concentration ratios, all at relatively neutral pH) is important for developing RED for energy recovery from low-grade heat sources.

4.6 References

[1] J. N. Weinstein, F. B. Leitz, Electric power from differences in salinity: the dialytic battery, *Science, 191* (1976), pp. 557-559.

[2] P. Dlugolecki, A. Gambier, K. Nijmeijer and M. Wessling, Practical potential of reverse electrodialysis as process for sustainable energy generation, *Environ. Sci. Technol., 43* (2009), pp. 6888-6894.

[3] J. W. Post, H. V. M Hamelers, C. J. N. Buisman, Energy recovery from controlled mixing salt and fresh water with a reverse electrodialysis system, *Environ. Sci. Technol., 42* (2008), pp. 5785- 5790.

[4] J. Veerman, M. Saakes, S. J. Metz and G. J. Harmsen, Reverse electrodialysis: evaluation of suitable electrode systems, *J. Appl. Electrochem.*, *40* (2010), pp. 1461–1474.

[5] J. W. Post, C. H. Goeting, J. Valk, S. Goinga, J. Veerman, H. V. M Hamelers and P. J. F. M. Hack, Towards implementation of reverse electrodialysis power generation from salinity gradients. *Desalin. Water Treat.*,*16* (2010), pp. 182-193.

[6] N. Y. Yip, D. A. Vermaas, K. Nijmeijer and M. Elimelech, Thermodynamic, Energy Efficiency, and Power Density Analysis of Reverse Electrodialyis Power Generation with Natural Salinity Gradients, *Environ. Sci. Technol., 48* (2014), pp. 4925-4936.

[7] R. D. Cusick, Y. Kim, B.E. Logan, Energy capture from thermolytic solutions in microbial reverse-electrodialysis cells, *Science, 335* (2012), pp. 1474-1477.

[8] X. Luo, X. Cao, Y. Mo, X. Zhang, P. Liang and X. Huang, Power generation by coupling reverse electrodialysis and ammonium bicarbonate: Implication for recovery of waste heat. *Electrochemistry Communications, 19* (2012), pp. 25-28.

[9] T. Y. Cath, A. E. Childress and M. Elimelech, Forward osmosis: Principles, applications, and recent developments. *J. Membr. Sci.*, *281* (2006), pp. 70-87.

[10] J. Liu, G.M. Geise, X. Luo, H. Hou, F. Zhang, Y. Feng, M. A. Hickner, B. E. Logan, Patterned ion exchange membranes for improved power production in microbial reverse-electrolysis cells. *J. Power Sources, 297* (2014), pp. 437-443.

[11] J. Y. Nam, R. D. Cusick, Y. Kim and B. E. Logan, Hydrogen generation in microbial reverse-electrodialysis electrolysis cells using a heat-regenerated salt solution. *Environ. Sci. Technol., 46* (2012), pp. 5240-5246.

[12] M. C. Hatzell, I. Ivanov, R. D. Cusick, X. Zhu and B. E. Logan, 2014, Comparison of hydrogen production and electrical power generation for energy capture in closed-loop ammonium bicarbonate reverse electrodialysis systems, *Phys. Chem. Chem. Phys, 16* (2014)*,* pp. 1632-1638.

[13] R. D. Cusick, M. C. Hatzell, F. Zhang and B. E. Logan, Minimal RED cell pairs markedly improve electrode kinetics and power production in microbial reverse-electrodialysis cells, *Environ. Sci. Technol., 47* (2013), pp. 14518-14524.

[14] J. G. Hong, B. Zhang, S. Glabman, N. Uzal, X. Dou, H. Zhang, X. Wei and Y. Chen, Potential ion exchange membranes and system performance in reverse electrodialysis for power generation: A review, *J. Membr. Sci. 486* (2015), pp. 71-88.

[15] A. J. Bard and L. R. Faulkner, in *Electrochemical Methods Fundamentals and Applications*, John Wiley & Sons Inc., 2nd edn., 2001, ch. 2, pp. 44-86.

[16] X. Luo, F. Zhang, J. Liu, X. Zhang, X. Huang and B.E. Logan, Methane production in microbial reverse-electrodialysis methanogenesis cells (MRMC) using thermolytic solutions. *Environ. Sci. Technol., 48* (2014), pp. 8911-8918.

[17] X. Luo, J. Y. Nam, F. Zhang, X. Zhang, P. Liang, X. Huang, B. E. Logan, Optimization of membrane stack configuration for efficient hydrogen production in microbial reverse-electrodialysis electrolysis cells coupled with thermolytic solutions, *Bioresource Technology, 140* (2013), pp. 399-405.

[18] M. Planck, Diffusion and Potential at Liquid-Liquid Boundaries, *Ann. Physik, 40* (1890), pp. 561.

[19] P. Henderson, An Equation for the Calculation of Potential Difference at any Liquid Junction Boundary, *Z. Phys. Chem (Leipzig), 59* (1907), pp. 118.

[20] G. Kortum and J. O'M. Bockris, in *Textbook of Electrochemistry*, Elsevier, 1951, Vol. I, ch VII, p. 272.

[21] G. Kortum, in *Treatise on Electrochemistry*, Elsevier, 1965, ch VIII, pp. 291-292.

[22] C. W. Davies, in *Electrochemistry*, Philosophical Library, 1968, ch 13, pp. 156-157.

[23] J. O'M. Bockris and A. K. N. Reddy, in *Modern Electrochemistry I: Ionics*, Plenum Press, 1998, Vol. I, ch VII, p. 272.

[24] V. L. Snoeyink and D. Jenkins, in *Water Chemistry*, John Wiley & Sons, New York, 1980, Appendix 3, pp. 446-447.

[25] K. Zhuo, W. Dong, W. Wang, and J. Wang, Activity coefficients for individual ions in aqueous solutions of sodium halides at 298.15K. *Fluid Phase Equilibria, 274* (2008), pp. 81-84.

[26] H. Strathmann in *Ion Exchange Membrane Separation Processes,* Elsevier, 1st edn., 2004.

[27] Y. Kim, W.S. Walker, D.F. Lawler, Electrodialysis with spacers: Effects of variation and correlation of boundary layer thickness, *Desalination, 274* (2011), pp. 54-63.

[28] Chemical Rubber Company, *CRC Handbook of Chemistry and Physics, 95th Ed.*, CRC Press, Cleveland, Ohio, 2014, Section 8 Ionic Conductivity and Diffusion at Infinite Dilution.

[29] S. Sodaye, G. Suresh, A. K. Pandey, A. Goswami, Determination and theoretical evaluation of selectivity coefficients of monovalent anions in anion-exchange polymer inclusion membrane, *J. Membr. Sci.* 295 (2007) pp. 108-113.

[30] R. K. Nagarale, G. S. Gohil, V. K. Shahi, Recent developments on ion-exchange membranes and electro-membrane processes, *Advances in Colloid and Interface Science, 119* (2006), pp. 97-130.

[31] Y. Kim, W. S. Walker, D. F. Lawler, Competitive separation of di- vs. mono-valent cations in electrodialysis: Effects of the boundary layer properties, *Water Research, 46* (2012), pp. 2042-2056.

[32] G. M. Geise, H. J. Cassady, D. R. Paul, B. E. Logan, M. A. Hickner, Specific ion effects on membrane potential and the permselectivity of ion exchange membranes, *Phys. Chem. Chem. Phys.,16* (2014), pp. 21673-21681.

CHAPTER 5 Conclusions and Recommendations

This thesis presented methods and techniques to implement and evaluate the recovery of energy from wastes using bioelectrochemical systems and reverse electrodialysis. These technologies are relatively new and still under research investigations, and the papers in this thesis developed tools to aid in evaluating and modeling these technologies.

5.1 Enzyme kinetic model with electron transfer chain for bioanodes

Main findings include:

- A model was developed using enzyme kinetics, electron transfer chain, and electrode kinetics to model electron transfer in a bioanode.
- Kinetic parameters were estimated and validated with experimental results and found to be within range of literature values
- The model was used for both fixed and non-steady state operation with a good fit to experimental data
- The model was highly sensitive to changes in the concentration of the enzyme representing the electron transfer chain, supporting the hypothesis that the electron transfer chain is highly important in electron transfer.

Recommended future work includes:

- Develop the model to include additional enzyme pairs in the electron transfer chain to improve the fit of linear sweep voltammetry experimental results. The current model does not fit the full range of the LSV scan due to the presence of only one

enzyme pair in the model. Additional enzyme pairs will add additional oxidation peaks, allowing for better fitting of LSV.

- The feasibility of the model needs to be assessed for a larger-scale application. Presently, the model is suitable for small reactor sizes (< 100 mL) for use with acetic acid only.

5.2 Substrate preference in bioelectrochemical systems

Main findings from this study include:

- Non-steady state experiments (linear sweep voltammetry) showed that favourable substrates responded very differently compared to non-favourable substrates
- Exchange current (calculated from electrochemical impedance spectroscopy results) was a better indicator of substrate preference than charge transfer resistance (directly read from electrochemical impedance spectroscopy results)
- Acetic acid was consumed before other short chain fatty acids
- Utilization of iso-butyric acid was dependent on the applied potential, while utilization of n-butyric acid was not

Future plans for this work includes:

- Use the electrochemical methods developed in the research to study the utilization of other short-chain fatty acids
- Investigate the conditions affecting favourability through both models and experimental methods.

- Study the factors affecting substrate removal. For instance, a minimum 100 mg/L COD of substrate was required for substrate removal to occur.

5.3 Thermolytic reverse electrodialysis with ammonium bicarbonate

The main findings from this research project were:

- A conductivity-based equation was developed and verified to estimated junction potential across ion exchange membranes allowing for junction potential estimation without requiring extensive thermodynamic data.
- Ammonium bicarbonate ($NH_4H_2CO_3$) solution produces a higher junction potential than ammonium carbonate $(NH_4)_2CO_3$
- Junction potential magnitude was more dependent on the concentration ratio between high and low concentration solutions than the concentration of the solution.

The following are recommendations for future work with the project

- Use the developed model for an RED stack. The method presented in Chapter 4 was only used to measure the junction potential across one membrane, but these equations should also be valid for a of membranes.
- Preliminary experiments with a membrane stack noted substantial losses of current, and thus the experiment direction changed towards the determination of junction potential across one membrane. With this equation, energy generation across the stack can be estimated and the losses can be calculated.
- In experiments, fresh high and low concentration solutions are prepared for each experiment. The physical process of regeneration is much easier said than done, as

a mechanism to collect vaporized ions and re-concentrate them back into a very high concentration solution is challenging. Further work is required in order to implement such waste heat recovery systems.

Appendix A – Experimental Methods

Gas Chromatography Analysis Settings

Software: *Galaxie Chromatography Data System*

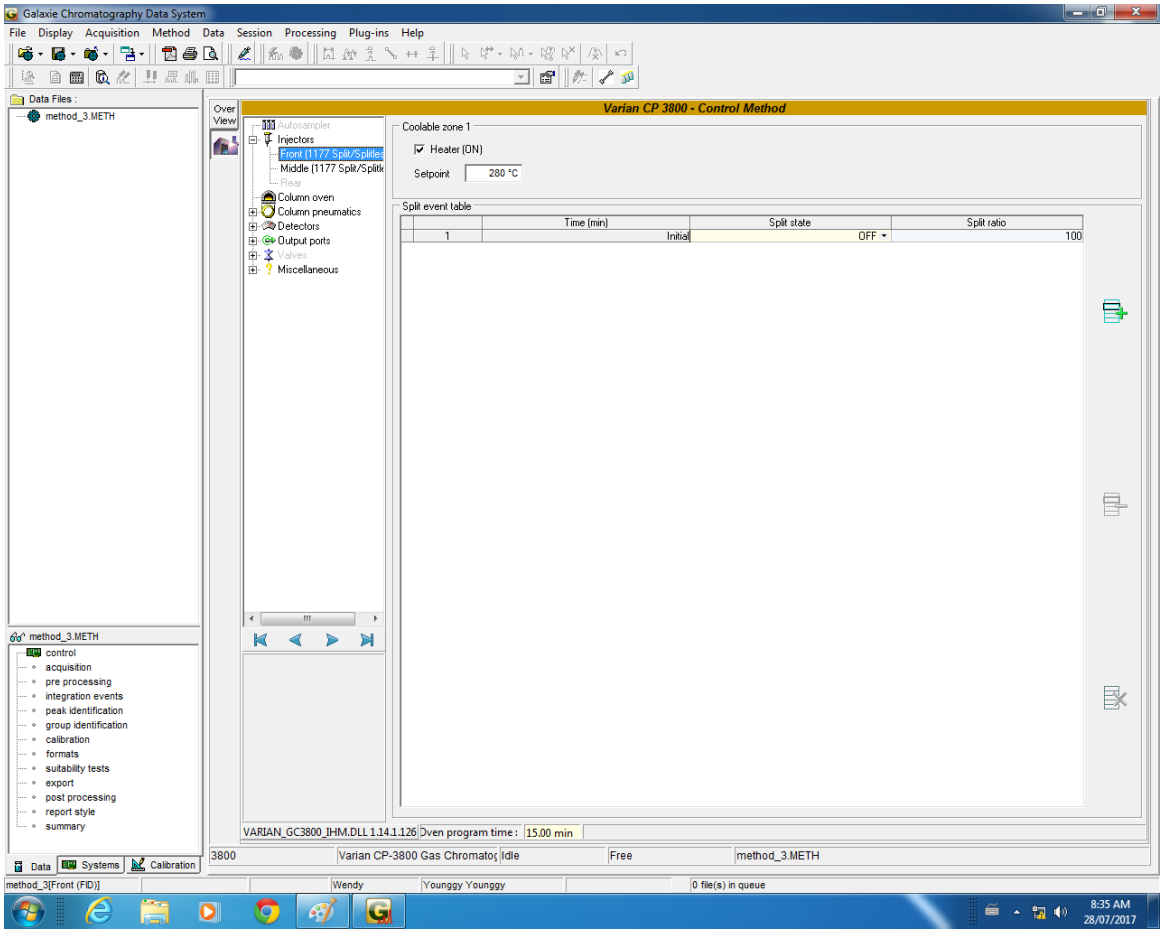

Figure A-1: Injector temperature, 280ºC, no split flow.

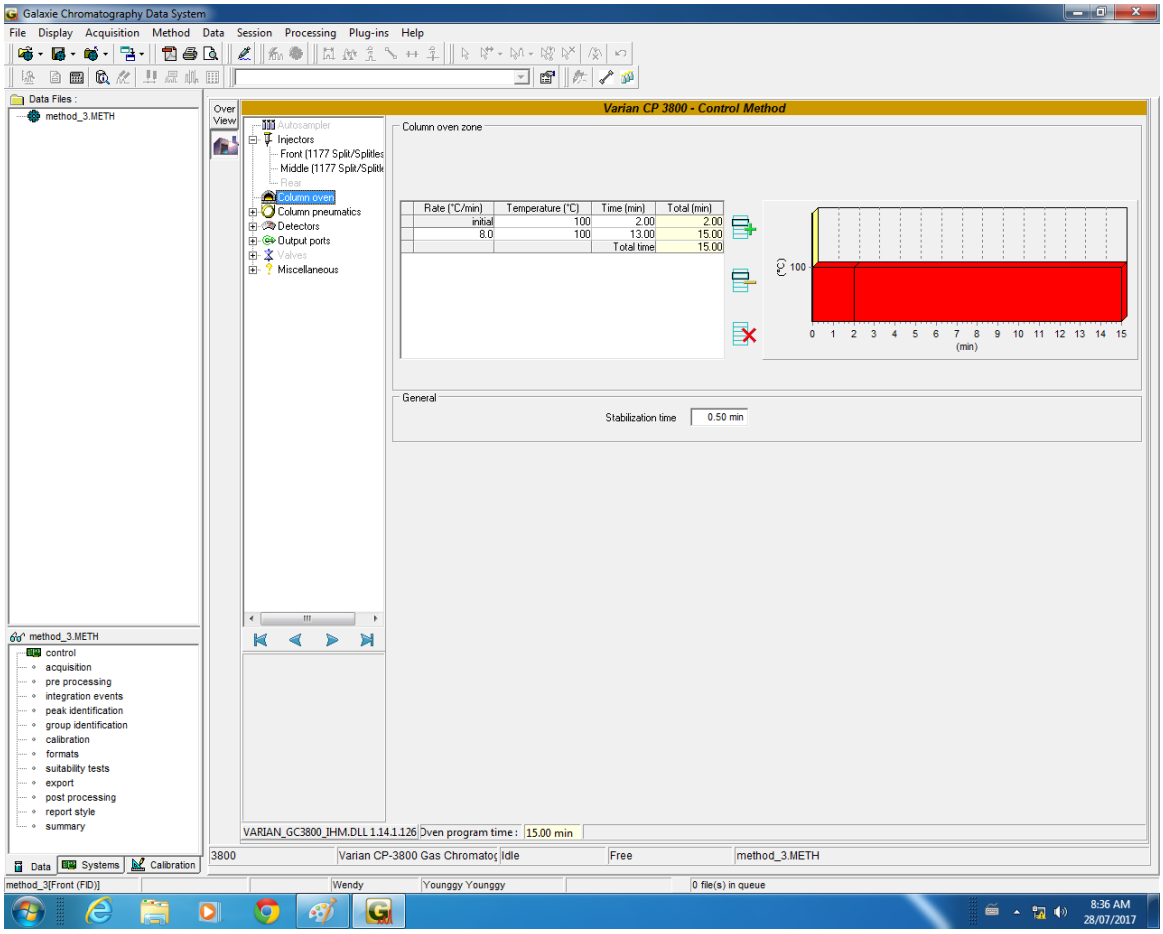

Figure A-2: Oven temperature profile, hold constant at 100°C.

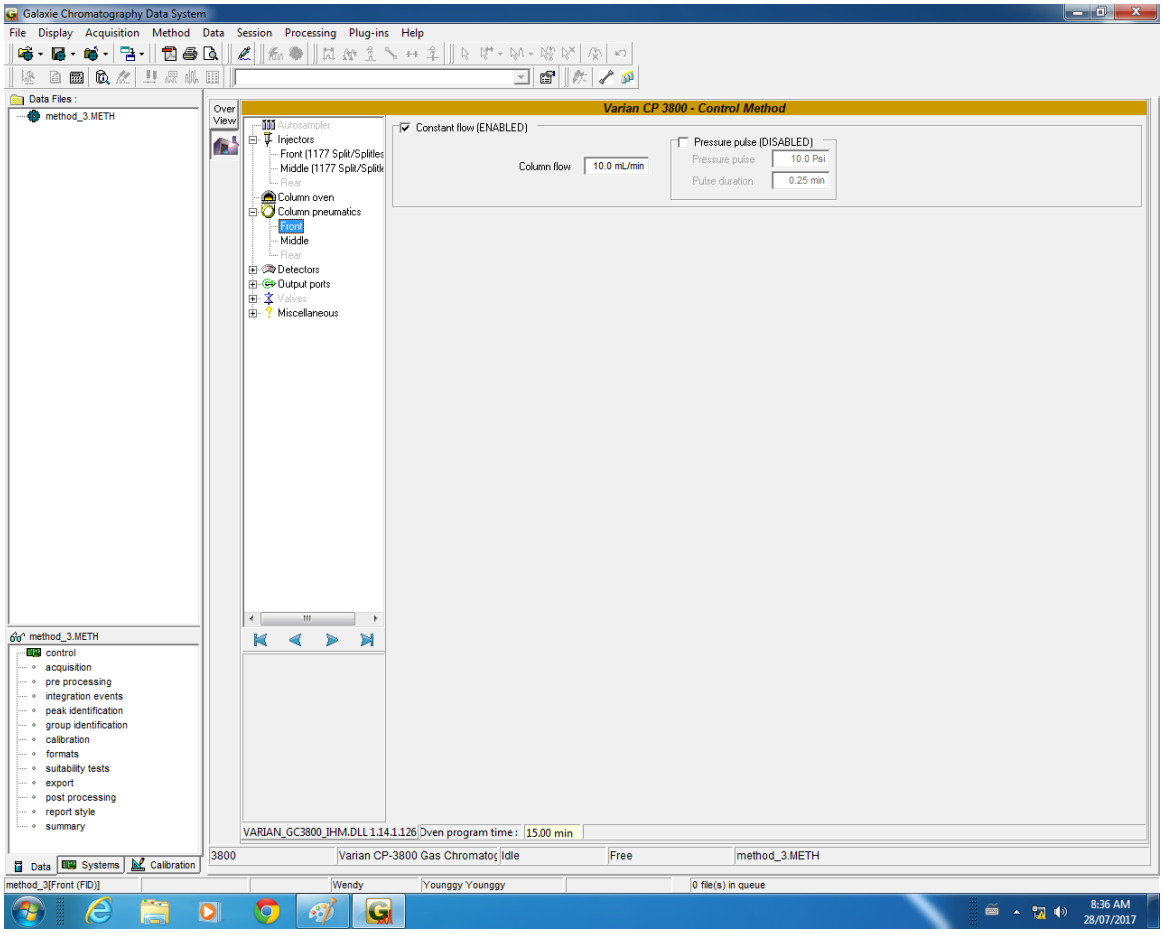

Figure A-3: Column pneumatics, 10 mL/min.

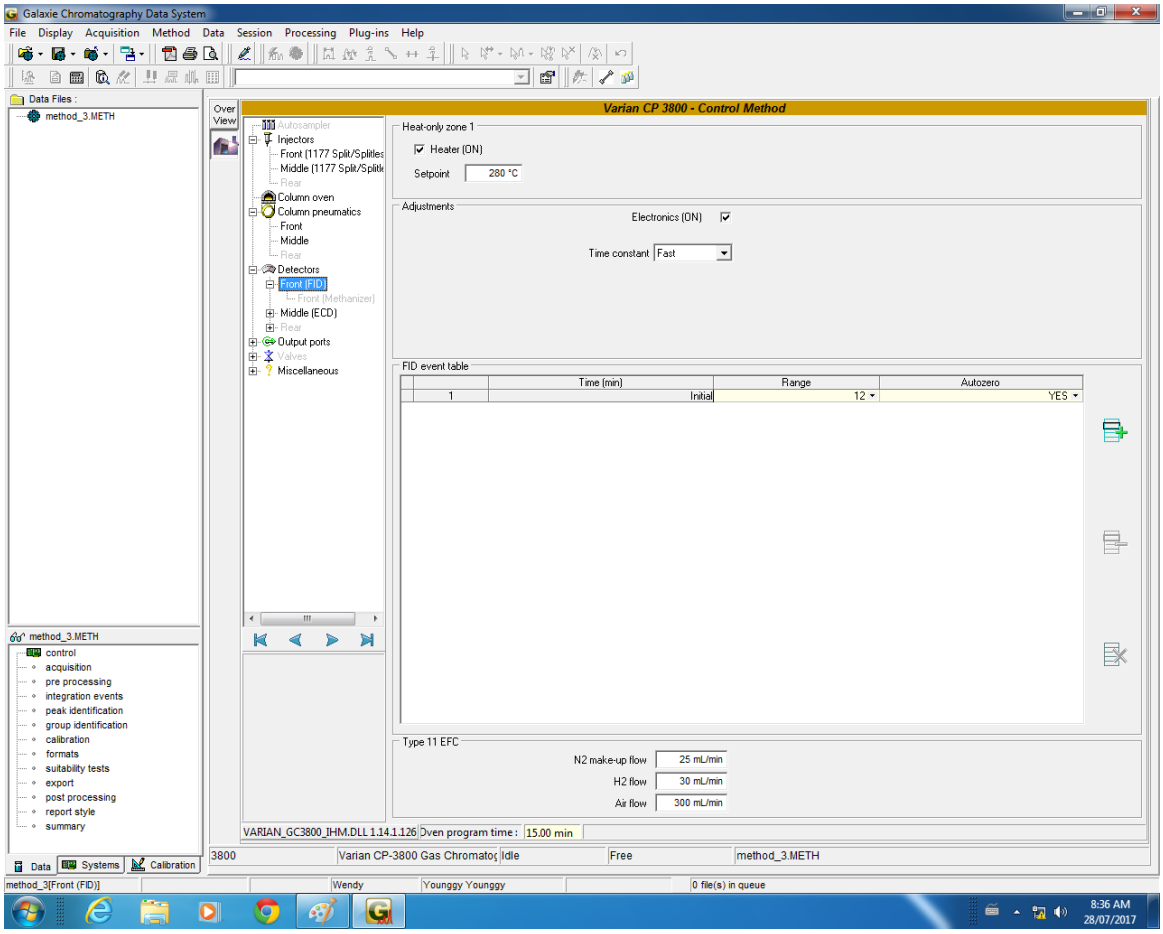

Figure A-4: Detector gas flow settings: 25mL/min N_2, 30mL/min H_2, 200mL/min air.

Appendix B – Experimental Data for Model Calibration (Chapter 2)

Table B-1: Linear Sweep Voltammetry for Model Fitting

Anode Potential (V vs Ag/AgCl)	Anode Potential (V vs SHE)	Current (mA)	Current Density (mA/m^3)
-0.489	-0.278	0.0000	0.0000
-0.399	-0.188	1.9565	55.8986
-0.398	-0.187	1.6146	46.1306
-0.397	-0.186	1.5100	43.1423
-0.396	-0.185	1.4738	42.1089
-0.395	-0.184	1.4732	42.0914
-0.394	-0.183	1.4925	42.6414
-0.393	-0.182	1.5214	43.4686
-0.392	-0.181	1.5548	44.4231
-0.391	-0.180	1.5896	45.4180
-0.390	-0.179	1.6237	46.3911
-0.389	-0.178	1.6567	47.3346
-0.388	-0.177	1.6882	48.2351
-0.387	-0.176	1.7182	49.0903
-0.386	-0.175	1.7467	49.9054
-0.385	-0.174	1.7739	50.6829
-0.384	-0.173	1.7996	51.4174
-0.383	-0.172	1.8252	52.1477
-0.382	-0.171	1.8492	52.8329
-0.381	-0.170	1.8726	53.5040
-0.380	-0.169	1.8957	54.1620
-0.379	-0.168	1.9181	54.8037
-0.378	-0.167	1.9401	55.4323
-0.377	-0.166	1.9614	56.0386
-0.376	-0.165	1.9822	56.6349
-0.375	-0.164	2.0034	57.2394
-0.374	-0.163	2.0242	57.8329
-0.373	-0.162	2.0448	58.4231
-0.372	-0.161	2.0654	59.0120
-0.371	-0.160	2.0856	59.5886
-0.370	-0.159	2.1060	60.1706
-0.369	-0.158	2.1260	60.7431
-0.368	-0.157	2.1460	61.3137
-0.367	-0.156	2.1660	61.8860
-0.366	-0.155	2.1857	62.4474
-0.365	-0.154	2.2055	63.0134
-0.364	-0.153	2.2250	63.5706
-0.363	-0.152	2.2443	64.1229
-0.362	-0.151	2.2639	64.6826
-0.361	-0.150	2.2835	65.2437
-0.360	-0.149	2.3030	65.8009
-0.359	-0.148	2.3224	66.3554
-0.358	-0.147	2.3416	66.9034
-0.357	-0.146	2.3608	67.4520
-0.356	-0.145	2.3799	67.9980
-0.355	-0.144	2.3992	68.5491
-0.354	-0.143	2.4185	69.1009
-0.353	-0.142	2.4377	69.6480
-0.352	-0.141	2.4571	70.2014
-0.351	-0.140	2.4757	70.7331
-0.350	-0.139	2.4948	71.2806
-0.349	-0.138	2.5139	71.8254
-0.348	-0.137	2.5330	72.3720
-0.347	-0.136	2.5521	72.9163
-0.346	-0.135	2.5709	73.4537
-0.345	-0.134	2.5898	73.9951
-0.344	-0.133	2.6090	74.5440
-0.343	-0.132	2.6281	75.0883
-0.342	-0.131	2.6469	75.6260
-0.341	-0.130	2.6659	76.1697
-0.340	-0.129	2.6849	76.7100
-0.339	-0.128	2.7037	77.2480
-0.338	-0.127	2.7223	77.7806
-0.337	-0.126	2.7414	78.3251
-0.336	-0.125	2.7603	78.8643
-0.335	-0.124	2.7791	79.4040
-0.334	-0.123	2.7980	79.9437
-0.333	-0.122	2.8169	80.4817
-0.332	-0.121	2.8360	81.0280
-0.331	-0.120	2.8550	81.5717
-0.330	-0.119	2.8739	82.1109
-0.329	-0.118	2.8926	82.6443
-0.328	-0.117	2.9110	83.1717
-0.327	-0.116	2.9298	83.7097
-0.326	-0.115	2.9483	84.2357
-0.325	-0.114	2.9665	84.7560
-0.324	-0.113	2.9855	85.2997
-0.323	-0.112	3.0039	85.8260
-0.322	-0.111	3.0227	86.3631
-0.321	-0.110	3.0413	86.8929
-0.320	-0.109	3.0598	87.4220
-0.319	-0.108	3.0786	87.9603
-0.318	-0.107	3.0969	88.4814
-0.317	-0.106	3.1149	88.9960
-0.316	-0.105	3.1331	89.5169
-0.315	-0.104	3.1512	90.0351
-0.314	-0.103	3.1694	90.5534
-0.313	-0.102	3.1874	91.0683
-0.312	-0.101	3.2053	91.5797
-0.311	-0.100	3.2237	92.1049
-0.310	-0.099	3.2419	92.6254
-0.309	-0.098	3.2600	93.1426
-0.308	-0.097	3.2783	93.6654
-0.307	-0.096	3.2963	94.1806
-0.306	-0.095	3.3152	94.7203
-0.305	-0.094	3.3336	95.2446

-0.304	-0.093	3.3509	95.7403	-0.253	-0.042	4.2043	120.1234
-0.303	-0.092	3.3690	96.2577	-0.252	-0.041	4.2194	120.5529
-0.302	-0.091	3.3870	96.7720	-0.251	-0.040	4.2344	120.9826
-0.301	-0.090	3.4049	97.2814	-0.250	-0.039	4.2495	121.4143
-0.300	-0.089	3.4225	97.7849	-0.249	-0.038	4.2641	121.8326
-0.299	-0.088	3.4398	98.2809	-0.248	-0.037	4.2788	122.2520
-0.298	-0.087	3.4579	98.7977	-0.247	-0.036	4.2938	122.6809
-0.297	-0.086	3.4757	99.3049	-0.246	-0.035	4.3083	123.0937
-0.296	-0.085	3.4931	99.8040	-0.245	-0.034	4.3229	123.5123
-0.295	-0.084	3.5105	100.3003	-0.244	-0.033	4.3371	123.9174
-0.294	-0.083	3.5280	100.8009	-0.243	-0.032	4.3513	124.3226
-0.293	-0.082	3.5454	101.2977	-0.242	-0.031	4.3658	124.7363
-0.292	-0.081	3.5628	101.7934	-0.241	-0.030	4.3806	125.1586
-0.291	-0.080	3.5805	102.2997	-0.240	-0.029	4.3947	125.5623
-0.290	-0.079	3.5983	102.8097	-0.239	-0.028	4.4089	125.9680
-0.289	-0.078	3.6155	103.2986	-0.238	-0.027	4.4231	126.3754
-0.288	-0.077	3.6326	103.7880	-0.237	-0.026	4.4381	126.8040
-0.287	-0.076	3.6495	104.2720	-0.236	-0.025	4.4514	127.1840
-0.286	-0.075	3.6670	104.7700	-0.235	-0.024	4.4638	127.5360
-0.285	-0.074	3.6840	105.2577	-0.234	-0.023	4.4780	127.9423
-0.284	-0.073	3.7011	105.7449	-0.233	-0.022	4.4924	128.3540
-0.283	-0.072	3.7183	106.2374	-0.232	-0.021	4.5065	128.7580
-0.282	-0.071	3.7353	106.7223	-0.231	-0.020	4.5206	129.1609
-0.281	-0.070	3.7524	107.2123	-0.230	-0.019	4.5343	129.5520
-0.280	-0.069	3.7693	107.6949	-0.229	-0.018	4.5484	129.9551
-0.279	-0.068	3.7863	108.1789	-0.228	-0.017	4.5618	130.3374
-0.278	-0.067	3.8035	108.6703	-0.227	-0.016	4.5749	130.7109
-0.277	-0.066	3.8221	109.2017	-0.226	-0.015	4.5885	131.0989
-0.276	-0.065	3.8391	109.6891	-0.225	-0.014	4.6020	131.4860
-0.275	-0.064	3.8557	110.1617	-0.224	-0.013	4.6133	131.8074
-0.274	-0.063	3.8720	110.6274	-0.223	-0.012	4.6259	132.1686
-0.273	-0.062	3.8883	111.0951	-0.222	-0.011	4.6382	132.5194
-0.272	-0.061	3.9050	111.5709	-0.221	-0.010	4.6502	132.8626
-0.271	-0.060	3.9215	112.0414	-0.220	-0.009	4.6642	133.2617
-0.270	-0.059	3.9375	112.5003	-0.219	-0.008	4.6772	133.6340
-0.269	-0.058	3.9531	112.9446	-0.218	-0.007	4.6891	133.9751
-0.268	-0.057	3.9700	113.4271	-0.217	-0.006	4.7012	134.3209
-0.267	-0.056	3.9857	113.8777	-0.216	-0.005	4.7143	134.6934
-0.266	-0.055	4.0020	114.3440	-0.215	-0.004	4.7269	135.0551
-0.265	-0.054	4.0181	114.8020	-0.214	-0.003	4.7394	135.4126
-0.264	-0.053	4.0334	115.2391	-0.213	-0.002	4.7520	135.7709
-0.263	-0.052	4.0496	115.7037	-0.212	-0.001	4.7641	136.1171
-0.262	-0.051	4.0656	116.1600	-0.211	0.000	4.7778	136.5074
-0.261	-0.050	4.0814	116.6126	-0.210	0.001	4.7889	136.8249
-0.260	-0.049	4.0975	117.0714	-0.209	0.002	4.8007	137.1617
-0.259	-0.048	4.1127	117.5069	-0.208	0.003	4.8124	137.4983
-0.258	-0.047	4.1278	117.9374	-0.207	0.004	4.8244	137.8391
-0.257	-0.046	4.1431	118.3749	-0.206	0.005	4.8366	138.1897
-0.256	-0.045	4.1595	118.8414	-0.205	0.006	4.8479	138.5123
-0.255	-0.044	4.1742	119.2623	-0.204	0.007	4.8584	138.8109
-0.254	-0.043	4.1887	119.6757	-0.203	0.008	4.8701	139.1463

-0.202	0.009	4.8816	139.4729	-0.151	0.060	5.3139	151.8266
-0.201	0.010	4.8919	139.7686	-0.150	0.061	5.3186	151.9611
-0.200	0.011	4.9046	140.1300	-0.149	0.062	5.3236	152.1037
-0.199	0.012	4.9177	140.5066	-0.148	0.063	5.3284	152.2389
-0.198	0.013	4.9291	140.8311	-0.147	0.064	5.3324	152.3551
-0.197	0.014	4.9403	141.1506	-0.146	0.065	5.3362	152.4626
-0.196	0.015	4.9522	141.4900	-0.145	0.066	5.3405	152.5851
-0.195	0.016	4.9619	141.7677	-0.144	0.067	5.3447	152.7066
-0.194	0.017	4.9732	142.0906	-0.143	0.068	5.3488	152.8237
-0.193	0.018	4.9825	142.3569	-0.142	0.069	5.3521	152.9177
-0.192	0.019	4.9903	142.5809	-0.141	0.070	5.3550	153.0011
-0.191	0.020	5.0017	142.9049	-0.140	0.071	5.3583	153.0949
-0.190	0.021	5.0126	143.2183	-0.139	0.072	5.3609	153.1683
-0.189	0.022	5.0221	143.4886	-0.138	0.073	5.3635	153.2426
-0.188	0.023	5.0323	143.7786	-0.137	0.074	5.3658	153.3094
-0.187	0.024	5.0428	144.0806	-0.136	0.075	5.3674	153.3554
-0.186	0.025	5.0531	144.3743	-0.135	0.076	5.3696	153.4183
-0.185	0.026	5.0629	144.6537	-0.134	0.077	5.3718	153.4797
-0.184	0.027	5.0718	144.9086	-0.133	0.078	5.3739	153.5403
-0.183	0.028	5.0809	145.1677	-0.132	0.079	5.3742	153.5489
-0.182	0.029	5.0905	145.4429	-0.131	0.080	5.3760	153.6003
-0.181	0.030	5.0986	145.6740	-0.130	0.081	5.3771	153.6326
-0.180	0.031	5.1076	145.9311	-0.129	0.082	5.3775	153.6440
-0.179	0.032	5.1155	146.1569	-0.128	0.083	5.3785	153.6703
-0.178	0.033	5.1241	146.4026	-0.127	0.084	5.3786	153.6729
-0.177	0.034	5.1332	146.6634	-0.126	0.085	5.3783	153.6660
-0.176	0.035	5.1417	146.9060	-0.125	0.086	5.3777	153.6489
-0.175	0.036	5.1493	147.1234	-0.124	0.087	5.3764	153.6114
-0.174	0.037	5.1578	147.3663	-0.123	0.088	5.3746	153.5586
-0.173	0.038	5.1663	147.6077	-0.122	0.089	5.3736	153.5309
-0.172	0.039	5.1746	147.8454	-0.121	0.090	5.3674	153.3534
-0.171	0.040	5.1823	148.0666	-0.120	0.091	5.3572	153.0634
-0.170	0.041	5.1907	148.3069	-0.119	0.092	5.3588	153.1089
-0.169	0.042	5.1982	148.5189	-0.118	0.093	5.3580	153.0851
-0.168	0.043	5.2061	148.7449	-0.117	0.094	5.3554	153.0117
-0.167	0.044	5.2141	148.9734	-0.116	0.095	5.3519	152.9109
-0.166	0.045	5.2225	149.2149	-0.115	0.096	5.3473	152.7789
-0.165	0.046	5.2298	149.4217	-0.114	0.097	5.3421	152.6306
-0.164	0.047	5.2350	149.5706	-0.113	0.098	5.3367	152.4780
-0.163	0.048	5.2409	149.7409	-0.112	0.099	5.3303	152.2954
-0.162	0.049	5.2491	149.9729	-0.111	0.100	5.3226	152.0729
-0.161	0.050	5.2573	150.2074	-0.110	0.101	5.3148	151.8503
-0.160	0.051	5.2638	150.3943	-0.109	0.102	5.3030	151.5140
-0.159	0.052	5.2698	150.5643	-0.108	0.103	5.2920	151.2009
-0.158	0.053	5.2772	150.7774	-0.107	0.104	5.2795	150.8426
-0.157	0.054	5.2824	150.9263	-0.106	0.105	5.2657	150.4477
-0.156	0.055	5.2853	151.0074	-0.105	0.106	5.2520	150.0583
-0.155	0.056	5.2912	151.1769	-0.104	0.107	5.2371	149.6323
-0.154	0.057	5.2971	151.3449	-0.103	0.108	5.2209	149.1677
-0.153	0.058	5.3027	151.5069	-0.102	0.109	5.2020	148.6297
-0.152	0.059	5.3085	151.6700	-0.101	0.110	5.1817	148.0489

-0.100	0.111	5.1591	147.4040	-0.049	0.162	4.2195	120.5560
-0.099	0.112	5.1341	146.6880	-0.048	0.163	4.2255	120.7277
-0.098	0.113	5.1082	145.9491	-0.047	0.164	4.2320	120.9146
-0.097	0.114	5.0801	145.1466	-0.046	0.165	4.2364	121.0386
-0.096	0.115	5.0497	144.2780	-0.045	0.166	4.2422	121.2063
-0.095	0.116	5.0172	143.3483	-0.044	0.167	4.2472	121.3477
-0.094	0.117	4.9825	142.3557	-0.043	0.168	4.2541	121.5451
-0.093	0.118	4.9499	141.4269	-0.042	0.169	4.2611	121.7457
-0.092	0.119	4.9166	140.4737	-0.041	0.170	4.2679	121.9397
-0.091	0.120	4.8820	139.4860	-0.040	0.171	4.2743	122.1231
-0.090	0.121	4.8470	138.4851	-0.039	0.172	4.2797	122.2769
-0.089	0.122	4.8105	137.4420	-0.038	0.173	4.2857	122.4489
-0.088	0.123	4.7748	136.4220	-0.037	0.174	4.2924	122.6389
-0.087	0.124	4.7370	135.3420	-0.036	0.175	4.2993	122.8366
-0.086	0.125	4.6983	134.2383	-0.035	0.176	4.3055	123.0129
-0.085	0.126	4.6576	133.0743	-0.034	0.177	4.3116	123.1871
-0.084	0.127	4.6165	131.9006	-0.033	0.178	4.3171	123.3457
-0.083	0.128	4.5754	130.7249	-0.032	0.179	4.3230	123.5140
-0.082	0.129	4.5358	129.5931	-0.031	0.180	4.3291	123.6889
-0.081	0.130	4.4975	128.5009	-0.030	0.181	4.3330	123.8006
-0.080	0.131	4.4619	127.4840	-0.029	0.182	4.3392	123.9763
-0.079	0.132	4.4294	126.5554	-0.028	0.183	4.3449	124.1406
-0.078	0.133	4.3988	125.6789	-0.027	0.184	4.3511	124.3160
-0.077	0.134	4.3714	124.8969	-0.026	0.185	4.3587	124.5331
-0.076	0.135	4.3463	124.1803	-0.025	0.186	4.3638	124.6794
-0.075	0.136	4.3229	123.5114	-0.024	0.187	4.3686	124.8177
-0.074	0.137	4.3014	122.8980	-0.023	0.188	4.3742	124.9777
-0.073	0.138	4.2810	122.3143	-0.022	0.189	4.3795	125.1297
-0.072	0.139	4.2619	121.7686	-0.021	0.190	4.3859	125.3126
-0.071	0.140	4.2435	121.2420	-0.020	0.191	4.3921	125.4871
-0.070	0.141	4.2294	120.8411	-0.019	0.192	4.3976	125.6449
-0.069	0.142	4.2153	120.4383	-0.018	0.193	4.4039	125.8249
-0.068	0.143	4.2040	120.1129	-0.017	0.194	4.4068	125.9089
-0.067	0.144	4.1954	119.8691	-0.016	0.195	4.4110	126.0291
-0.066	0.145	4.1877	119.6480	-0.015	0.196	4.4172	126.2046
-0.065	0.146	4.1824	119.4983	-0.014	0.197	4.4216	126.3303
-0.064	0.147	4.1777	119.3631	-0.013	0.198	4.4259	126.4549
-0.063	0.148	4.1749	119.2840	-0.012	0.199	4.4311	126.6040
-0.062	0.149	4.1734	119.2406	-0.011	0.200	4.4362	126.7489
-0.061	0.150	4.1737	119.2491	-0.010	0.201	4.4407	126.8766
-0.060	0.151	4.1708	119.1657	-0.009	0.202	4.4464	127.0389
-0.059	0.152	4.1722	119.2049	-0.008	0.203	4.4501	127.1469
-0.058	0.153	4.1738	119.2500	-0.007	0.204	4.4550	127.2854
-0.057	0.154	4.1759	119.3103	-0.006	0.205	4.4592	127.4049
-0.056	0.155	4.1805	119.4440	-0.005	0.206	4.4640	127.5437
-0.055	0.156	4.1859	119.5966	-0.004	0.207	4.4689	127.6817
-0.054	0.157	4.1906	119.7326	-0.003	0.208	4.4732	127.8046
-0.053	0.158	4.1963	119.8931	-0.002	0.209	4.4778	127.9369
-0.052	0.159	4.2023	120.0649	-0.001	0.210	4.4822	128.0637
-0.051	0.160	4.2077	120.2189	0.000	0.211	4.4860	128.1726
-0.050	0.161	4.2133	120.3809	0.001	0.212	4.4916	128.3317

0.002	0.213	4.4952	128.4340	0.053	0.264	4.5753	130.7226
0.003	0.214	4.4991	128.5466	0.054	0.265	4.5734	130.6680
0.004	0.215	4.5023	128.6380	0.055	0.266	4.5749	130.7126
0.005	0.216	4.5055	128.7280	0.056	0.267	4.5748	130.7080
0.006	0.217	4.5099	128.8551	0.057	0.268	4.5745	130.6989
0.007	0.218	4.5152	129.0054	0.058	0.269	4.5743	130.6934
0.008	0.219	4.5169	129.0537	0.059	0.270	4.5739	130.6829
0.009	0.220	4.5198	129.1374	0.060	0.271	4.5724	130.6411
0.010	0.221	4.5240	129.2583	0.061	0.272	4.5701	130.5729
0.011	0.222	4.5280	129.3706	0.062	0.273	4.5703	130.5806
0.012	0.223	4.5308	129.4506	0.063	0.274	4.5701	130.5740
0.013	0.224	4.5329	129.5100	0.064	0.275	4.5705	130.5866
0.014	0.225	4.5355	129.5857	0.065	0.276	4.5678	130.5094
0.015	0.226	4.5395	129.7000	0.066	0.277	4.5672	130.4906
0.016	0.227	4.5423	129.7811	0.067	0.278	4.5660	130.4569
0.017	0.228	4.5459	129.8831	0.068	0.279	4.5654	130.4403
0.018	0.229	4.5463	129.8949	0.069	0.280	4.5649	130.4266
0.019	0.230	4.5484	129.9529	0.070	0.281	4.5582	130.2331
0.020	0.231	4.5509	130.0266	0.071	0.282	4.5574	130.2126
0.021	0.232	4.5526	130.0746	0.072	0.283	4.5566	130.1883
0.022	0.233	4.5541	130.1160	0.073	0.284	4.5569	130.1980
0.023	0.234	4.5557	130.1623	0.074	0.285	4.5552	130.1474
0.024	0.235	4.5573	130.2091	0.075	0.286	4.5535	130.0991
0.025	0.236	4.5588	130.2503	0.076	0.287	4.5538	130.1086
0.026	0.237	4.5592	130.2623	0.077	0.288	4.5539	130.1114
0.027	0.238	4.5597	130.2766	0.078	0.289	4.5548	130.1380
0.028	0.239	4.5593	130.2666	0.079	0.290	4.5546	130.1314
0.029	0.240	4.5606	130.3037	0.080	0.291	4.5538	130.1086
0.030	0.241	4.5617	130.3334	0.081	0.292	4.5527	130.0769
0.031	0.242	4.5624	130.3531	0.082	0.293	4.5518	130.0520
0.032	0.243	4.5638	130.3949	0.083	0.294	4.5514	130.0394
0.033	0.244	4.5654	130.4397	0.084	0.295	4.5522	130.0620
0.034	0.245	4.5672	130.4926	0.085	0.296	4.5523	130.0669
0.035	0.246	4.5674	130.4966	0.086	0.297	4.5515	130.0423
0.036	0.247	4.5690	130.5429	0.087	0.298	4.5499	129.9957
0.037	0.248	4.5702	130.5760	0.088	0.299	4.5466	129.9040
0.038	0.249	4.5723	130.6380	0.089	0.300	4.5456	129.8737
0.039	0.250	4.5732	130.6614	0.090	0.301	4.5452	129.8629
0.040	0.251	4.5734	130.6694	0.091	0.302	4.5443	129.8363
0.041	0.252	4.5741	130.6874	0.092	0.303	4.5426	129.7883
0.042	0.253	4.5739	130.6840	0.093	0.304	4.5411	129.7460
0.043	0.254	4.5738	130.6791	0.094	0.305	4.5403	129.7237
0.044	0.255	4.5749	130.7106	0.095	0.306	4.5390	129.6869
0.045	0.256	4.5743	130.6946	0.096	0.307	4.5379	129.6551
0.046	0.257	4.5760	130.7423	0.097	0.308	4.5365	129.6151
0.047	0.258	4.5789	130.8263	0.098	0.309	4.5360	129.6003
0.048	0.259	4.5792	130.8331	0.099	0.310	4.5346	129.5594
0.049	0.260	4.5784	130.8100	0.100	0.311	4.5337	129.5343
0.050	0.261	4.5760	130.7420	0.101	0.312	4.5318	129.4794
0.051	0.262	4.5753	130.7217	0.102	0.313	4.5297	129.4186
0.052	0.263	4.5756	130.7306	0.103	0.314	4.5297	129.4197

0.104	0.315	4.5288	129.3934	0.155	0.366	4.4672	127.6349
0.105	0.316	4.5274	129.3540	0.156	0.367	4.4666	127.6171
0.106	0.317	4.5265	129.3280	0.157	0.368	4.4650	127.5723
0.107	0.318	4.5261	129.3174	0.158	0.369	4.4635	127.5277
0.108	0.319	4.5243	129.2649	0.159	0.370	4.4634	127.5254
0.109	0.320	4.5223	129.2086	0.160	0.371	4.4620	127.4843
0.110	0.321	4.5212	129.1757	0.161	0.372	4.4608	127.4526
0.111	0.322	4.5210	129.1709	0.162	0.373	4.4598	127.4223
0.112	0.323	4.5194	129.1257	0.163	0.374	4.4580	127.3711
0.113	0.324	4.5190	129.1149	0.164	0.375	4.4554	127.2977
0.114	0.325	4.5174	129.0677	0.165	0.376	4.4546	127.2746
0.115	0.326	4.5149	128.9960	0.166	0.377	4.4536	127.2451
0.116	0.327	4.5143	128.9794	0.167	0.378	4.4534	127.2386
0.117	0.328	4.5131	128.9449	0.168	0.379	4.4508	127.1643
0.118	0.329	4.5127	128.9334	0.169	0.380	4.4491	127.1171
0.119	0.330	4.5113	128.8943	0.170	0.381	4.4476	127.0743
0.120	0.331	4.5099	128.8546	0.171	0.382	4.4458	127.0231
0.121	0.332	4.5091	128.8311	0.172	0.383	4.4447	126.9917
0.122	0.333	4.5070	128.7700	0.173	0.384	4.4451	127.0020
0.123	0.334	4.5062	128.7477	0.174	0.385	4.4440	126.9714
0.124	0.335	4.5024	128.6409	0.175	0.386	4.4430	126.9429
0.125	0.336	4.5010	128.6000	0.176	0.387	4.4417	126.9051
0.126	0.337	4.5013	128.6091	0.177	0.388	4.4394	126.8411
0.127	0.338	4.5003	128.5791	0.178	0.389	4.4366	126.7591
0.128	0.339	4.4994	128.5549	0.179	0.390	4.4353	126.7240
0.129	0.340	4.4997	128.5631	0.180	0.391	4.4344	126.6969
0.130	0.341	4.4984	128.5260	0.181	0.392	4.4353	126.7220
0.131	0.342	4.4972	128.4920	0.182	0.393	4.4336	126.6743
0.132	0.343	4.4952	128.4334	0.183	0.394	4.4321	126.6303
0.133	0.344	4.4934	128.3814	0.184	0.395	4.4294	126.5546
0.134	0.345	4.4935	128.3857	0.185	0.396	4.4286	126.5306
0.135	0.346	4.4917	128.3337	0.186	0.397	4.4259	126.4529
0.136	0.347	4.4888	128.2523	0.187	0.398	4.4240	126.3997
0.137	0.348	4.4891	128.2606	0.188	0.399	4.4234	126.3831
0.138	0.349	4.4886	128.2454	0.189	0.400	4.4238	126.3954
0.139	0.350	4.4880	128.2277	0.190	0.401	4.4226	126.3611
0.140	0.351	4.4860	128.1700	0.191	0.402	4.4223	126.3511
0.141	0.352	4.4856	128.1589	0.192	0.403	4.4201	126.2883
0.142	0.353	4.4853	128.1509	0.193	0.404	4.4187	126.2471
0.143	0.354	4.4838	128.1091	0.194	0.405	4.4160	126.1706
0.144	0.355	4.4827	128.0760	0.195	0.406	4.4131	126.0891
0.145	0.356	4.4823	128.0663	0.196	0.407	4.4129	126.0840
0.146	0.357	4.4799	127.9966	0.197	0.408	4.4120	126.0569
0.147	0.358	4.4784	127.9540	0.198	0.409	4.4105	126.0129
0.148	0.359	4.4770	127.9140	0.199	0.410	4.4084	125.9549
0.149	0.360	4.4754	127.8694	0.200	0.411	4.4053	125.8643
0.150	0.361	4.4748	127.8506	0.201	0.412	4.4053	125.8657
0.151	0.362	4.4742	127.8346	0.202	0.413	4.4034	125.8109
0.152	0.363	4.4719	127.7694	0.203	0.414	4.4013	125.7506
0.153	0.364	4.4688	127.6794	0.204	0.415	4.4000	125.7154
0.154	0.365	4.4686	127.6754	0.205	0.416	4.3994	125.6971

0.206	0.417	4.3994	125.6963	0.257	0.468	4.3157	123.3051
0.207	0.418	4.3982	125.6631	0.258	0.469	4.3140	123.2563
0.208	0.419	4.3971	125.6326	0.259	0.470	4.3123	123.2080
0.209	0.420	4.3951	125.5740	0.260	0.471	4.3118	123.1943
0.210	0.421	4.3936	125.5303	0.261	0.472	4.3122	123.2051
0.211	0.422	4.3921	125.4886	0.262	0.473	4.3087	123.1063
0.212	0.423	4.3905	125.4429	0.263	0.474	4.3078	123.0797
0.213	0.424	4.3886	125.3889	0.264	0.475	4.3069	123.0551
0.214	0.425	4.3867	125.3343	0.265	0.476	4.3057	123.0200
0.215	0.426	4.3843	125.2649	0.266	0.477	4.3024	122.9243
0.216	0.427	4.3827	125.2200	0.267	0.478	4.3024	122.9254
0.217	0.428	4.3817	125.1909	0.268	0.479	4.2986	122.8163
0.218	0.429	4.3799	125.1400	0.269	0.480	4.2981	122.8020
0.219	0.430	4.3788	125.1089	0.270	0.481	4.2967	122.7637
0.220	0.431	4.3774	125.0677	0.271	0.482	4.2943	122.6943
0.221	0.432	4.3756	125.0174	0.272	0.483	4.2942	122.6917
0.222	0.433	4.3739	124.9683	0.273	0.484	4.2921	122.6306
0.223	0.434	4.3720	124.9134	0.274	0.485	4.2892	122.5480
0.224	0.435	4.3705	124.8709	0.275	0.486	4.2859	122.4554
0.225	0.436	4.3680	124.7997	0.276	0.487	4.2842	122.4060
0.226	0.437	4.3688	124.8220	0.277	0.488	4.2824	122.3529
0.227	0.438	4.3669	124.7697	0.278	0.489	4.2812	122.3197
0.228	0.439	4.3642	124.6909	0.279	0.490	4.2785	122.2420
0.229	0.440	4.3628	124.6500	0.280	0.491	4.2759	122.1671
0.230	0.441	4.3603	124.5786	0.281	0.492	4.2767	122.1900
0.231	0.442	4.3587	124.5349	0.282	0.493	4.2731	122.0877
0.232	0.443	4.3571	124.4880	0.283	0.494	4.2723	122.0669
0.233	0.444	4.3556	124.4460	0.284	0.495	4.2706	122.0171
0.234	0.445	4.3553	124.4366	0.285	0.496	4.2682	121.9497
0.235	0.446	4.3535	124.3860	0.286	0.497	4.2674	121.9254
0.236	0.447	4.3528	124.3660	0.287	0.498	4.2647	121.8489
0.237	0.448	4.3499	124.2837	0.288	0.499	4.2631	121.8034
0.238	0.449	4.3483	124.2369	0.289	0.500	4.2626	121.7897
0.239	0.450	4.3467	124.1909	0.290	0.501	4.2608	121.7357
0.240	0.451	4.3450	124.1434	0.291	0.502	4.2596	121.7029
0.241	0.452	4.3434	124.0980	0.292	0.503	4.2581	121.6603
0.242	0.453	4.3419	124.0551	0.293	0.504	4.2541	121.5454
0.243	0.454	4.3396	123.9877	0.294	0.505	4.2531	121.5169
0.244	0.455	4.3379	123.9411	0.295	0.506	4.2512	121.4637
0.245	0.456	4.3361	123.8894	0.296	0.507	4.2500	121.4294
0.246	0.457	4.3362	123.8923	0.297	0.508	4.2484	121.3820
0.247	0.458	4.3339	123.8257	0.298	0.509	4.2464	121.3266
0.248	0.459	4.3325	123.7857	0.299	0.510	4.2439	121.2543
0.249	0.460	4.3316	123.7611	0.300	0.511	4.2435	121.2426
0.250	0.461	4.3297	123.7051	0.301	0.512	4.2429	121.2249
0.251	0.462	4.3289	123.6823	0.302	0.513	4.2410	121.1700
0.252	0.463	4.3261	123.6026	0.303	0.514	4.2403	121.1517
0.253	0.464	4.3230	123.5134	0.304	0.515	4.2385	121.1009
0.254	0.465	4.3225	123.5011	0.305	0.516	4.2373	121.0649
0.255	0.466	4.3226	123.5029	0.306	0.517	4.2353	121.0077
0.256	0.467	4.3202	123.4337	0.307	0.518	4.2337	120.9634

0.308	0.519	4.2280	120.7991	0.359	0.570	4.1491	118.5469
0.309	0.520	4.2265	120.7571	0.360	0.571	4.1461	118.4600
0.310	0.521	4.2257	120.7340	0.361	0.572	4.1466	118.4734
0.311	0.522	4.2238	120.6797	0.362	0.573	4.1464	118.4689
0.312	0.523	4.2219	120.6269	0.363	0.574	4.1435	118.3863
0.313	0.524	4.2208	120.5954	0.364	0.575	4.1421	118.3457
0.314	0.525	4.2184	120.5246	0.365	0.576	4.1420	118.3426
0.315	0.526	4.2170	120.4846	0.366	0.577	4.1404	118.2971
0.316	0.527	4.2155	120.4437	0.367	0.578	4.1391	118.2594
0.317	0.528	4.2142	120.4043	0.368	0.579	4.1372	118.2057
0.318	0.529	4.2129	120.3697	0.369	0.580	4.1357	118.1614
0.319	0.530	4.2113	120.3223	0.370	0.581	4.1344	118.1263
0.320	0.531	4.2102	120.2923	0.371	0.582	4.1334	118.0969
0.321	0.532	4.2087	120.2486	0.372	0.583	4.1324	118.0683
0.322	0.533	4.2066	120.1897	0.373	0.584	4.1310	118.0289
0.323	0.534	4.2054	120.1551	0.374	0.585	4.1287	117.9623
0.324	0.535	4.2041	120.1183	0.375	0.586	4.1266	117.9034
0.325	0.536	4.2019	120.0543	0.376	0.587	4.1255	117.8706
0.326	0.537	4.2008	120.0214	0.377	0.588	4.1247	117.8474
0.327	0.538	4.1988	119.9646	0.378	0.589	4.1231	117.8017
0.328	0.539	4.1980	119.9426	0.379	0.590	4.1219	117.7677
0.329	0.540	4.1974	119.9263	0.380	0.591	4.1213	117.7517
0.330	0.541	4.1947	119.8474	0.381	0.592	4.1203	117.7217
0.331	0.542	4.1928	119.7937	0.382	0.593	4.1182	117.6637
0.332	0.543	4.1901	119.7166	0.383	0.594	4.1176	117.6449
0.333	0.544	4.1895	119.6989	0.384	0.595	4.1178	117.6503
0.334	0.545	4.1878	119.6520	0.385	0.596	4.1168	117.6214
0.335	0.546	4.1867	119.6200	0.386	0.597	4.1137	117.5346
0.336	0.547	4.1862	119.6063	0.387	0.598	4.1122	117.4917
0.337	0.548	4.1858	119.5940	0.388	0.599	4.1113	117.4663
0.338	0.549	4.1844	119.5534	0.389	0.600	4.1101	117.4323
0.339	0.550	4.1838	119.5380	0.390	0.601	4.1086	117.3897
0.340	0.551	4.1812	119.4614	0.391	0.602	4.1101	117.4320
0.341	0.552	4.1796	119.4174	0.392	0.603	4.1085	117.3843
0.342	0.553	4.1784	119.3814	0.393	0.604	4.1068	117.3369
0.343	0.554	4.1770	119.3423	0.394	0.605	4.1061	117.3169
0.344	0.555	4.1752	119.2914	0.395	0.606	4.1044	117.2674
0.345	0.556	4.1742	119.2640	0.396	0.607	4.1034	117.2409
0.346	0.557	4.1743	119.2649	0.397	0.608	4.1031	117.2311
0.347	0.558	4.1718	119.1940	0.398	0.609	4.1011	117.1749
0.348	0.559	4.1707	119.1640	0.399	0.610	4.0993	117.1214
0.349	0.560	4.1700	119.1423	0.400	0.611	4.0985	117.1011
0.350	0.561	4.1666	119.0457	0.401	0.612	4.0963	117.0357
0.351	0.562	4.1648	118.9934	0.402	0.613	4.0946	116.9877
0.352	0.563	4.1632	118.9480	0.403	0.614	4.0937	116.9634
0.353	0.564	4.1621	118.9174	0.404	0.615	4.0916	116.9034
0.354	0.565	4.1607	118.8769	0.405	0.616	4.0929	116.9400
0.355	0.566	4.1587	118.8200	0.406	0.617	4.0924	116.9269
0.356	0.567	4.1573	118.7789	0.407	0.618	4.0897	116.8491
0.357	0.568	4.1559	118.7386	0.408	0.619	4.0884	116.8114
0.358	0.569	4.1528	118.6500	0.409	0.620	4.0864	116.7540

0.410	0.621	4.0874	116.7829	0.461	0.672	4.0451	115.5729
0.411	0.622	4.0852	116.7203	0.462	0.673	4.0413	115.4643
0.412	0.623	4.0835	116.6711	0.463	0.674	4.0395	115.4151
0.413	0.624	4.0837	116.6766	0.464	0.675	4.0335	115.2431
0.414	0.625	4.0802	116.5780	0.465	0.676	4.0337	115.2494
0.415	0.626	4.0797	116.5620	0.466	0.677	4.0329	115.2254
0.416	0.627	4.0792	116.5497	0.467	0.678	4.0312	115.1780
0.417	0.628	4.0805	116.5863	0.468	0.679	4.0294	115.1266
0.418	0.629	4.0795	116.5566	0.469	0.680	4.0293	115.1217
0.419	0.630	4.0759	116.4551	0.470	0.681	4.0292	115.1197
0.420	0.631	4.0755	116.4431	0.471	0.682	4.0287	115.1043
0.421	0.632	4.0756	116.4463	0.472	0.683	4.0278	115.0794
0.422	0.633	4.0738	116.3954	0.473	0.684	4.0282	115.0920
0.423	0.634	4.0732	116.3760	0.474	0.685	4.0274	115.0694
0.424	0.635	4.0716	116.3300	0.475	0.686	4.0265	115.0426
0.425	0.636	4.0703	116.2929	0.476	0.687	4.0262	115.0329
0.426	0.637	4.0691	116.2611	0.477	0.688	4.0260	115.0280
0.427	0.638	4.0706	116.3034	0.478	0.689	4.0256	115.0183
0.428	0.639	4.0705	116.3006	0.479	0.690	4.0249	114.9966
0.429	0.640	4.0687	116.2494	0.480	0.691	4.0236	114.9600
0.430	0.641	4.0676	116.2163	0.481	0.692	4.0233	114.9503
0.431	0.642	4.0668	116.1951	0.482	0.693	4.0231	114.9446
0.432	0.643	4.0663	116.1811	0.483	0.694	4.0228	114.9369
0.433	0.644	4.0660	116.1700	0.484	0.695	4.0226	114.9323
0.434	0.645	4.0614	116.0403	0.485	0.696	4.0212	114.8914
0.435	0.646	4.0627	116.0766	0.486	0.697	4.0213	114.8951
0.436	0.647	4.0640	116.1134	0.487	0.698	4.0204	114.8686
0.437	0.648	4.0626	116.0740	0.488	0.699	4.0195	114.8414
0.438	0.649	4.0635	116.0991	0.489	0.700	4.0196	114.8469
0.439	0.650	4.0608	116.0214	0.490	0.701	4.0217	114.9060
0.440	0.651	4.0609	116.0263	0.491	0.702	4.0235	114.9557
0.441	0.652	4.0597	115.9900	0.492	0.703	4.0232	114.9483
0.442	0.653	4.0564	115.8974	0.493	0.704	4.0222	114.9206
0.443	0.654	4.0560	115.8849	0.494	0.705	4.0221	114.9163
0.444	0.655	4.0554	115.8680	0.495	0.706	4.0223	114.9214
0.445	0.656	4.0534	115.8114	0.496	0.707	4.0204	114.8694
0.446	0.657	4.0535	115.8154	0.497	0.708	4.0195	114.8440
0.447	0.658	4.0526	115.7877	0.498	0.709	4.0175	114.7863
0.448	0.659	4.0518	115.7654	0.499	0.710	4.0162	114.7486
0.449	0.660	4.0504	115.7269	0.500	0.711	4.0158	114.7371
0.450	0.661	4.0483	115.6666	0.501	0.712	4.0145	114.6994
0.451	0.662	4.0478	115.6520	0.502	0.713	4.0153	114.7240
0.452	0.663	4.0482	115.6629	0.503	0.714	4.0212	114.8903
0.453	0.664	4.0493	115.6934	0.504	0.715	4.0219	114.9106
0.454	0.665	4.0508	115.7366	0.505	0.716	4.0185	114.8146
0.455	0.666	4.0508	115.7360	0.506	0.717	4.0184	114.8111
0.456	0.667	4.0505	115.7289	0.507	0.718	4.0171	114.7749
0.457	0.668	4.0452	115.5763	0.508	0.719	4.0172	114.7763
0.458	0.669	4.0455	115.5843	0.509	0.720	4.0181	114.8026
0.459	0.670	4.0449	115.5689	0.510	0.721	4.0178	114.7934
0.460	0.671	4.0450	115.5717	0.511	0.722	4.0190	114.8297

0.512	0.723	4.0181	114.8040	0.558	0.769	3.9913	114.0380
0.513	0.724	4.0115	114.6134	0.559	0.770	3.9909	114.0266
0.514	0.725	4.0069	114.4837	0.560	0.771	3.9904	114.0109
0.515	0.726	4.0069	114.4831	0.561	0.772	3.9910	114.0286
0.516	0.727	4.0062	114.4614	0.562	0.773	3.9934	114.0977
0.517	0.728	4.0069	114.4820	0.563	0.774	3.9952	114.1489
0.518	0.729	4.0052	114.4334	0.564	0.775	3.9933	114.0951
0.519	0.730	4.0030	114.3726	0.565	0.776	3.9892	113.9771
0.520	0.731	4.0028	114.3646	0.566	0.777	3.9894	113.9829
0.521	0.732	4.0026	114.3591	0.567	0.778	3.9888	113.9666
0.522	0.733	4.0024	114.3534	0.568	0.779	3.9872	113.9186
0.523	0.734	4.0024	114.3531	0.569	0.780	3.9873	113.9231
0.524	0.735	4.0055	114.4414	0.570	0.781	3.9872	113.9194
0.525	0.736	4.0031	114.3749	0.571	0.782	3.9868	113.9080
0.526	0.737	3.9987	114.2480	0.572	0.783	3.9867	113.9049
0.527	0.738	3.9988	114.2520	0.573	0.784	3.9865	113.8989
0.528	0.739	3.9992	114.2626	0.574	0.785	3.9864	113.8957
0.529	0.740	3.9989	114.2531	0.575	0.786	3.9857	113.8760
0.530	0.741	3.9999	114.2823	0.576	0.787	3.9844	113.8403
0.531	0.742	3.9987	114.2477	0.577	0.788	3.9841	113.8317
0.532	0.743	3.9984	114.2406	0.578	0.789	3.9839	113.8243
0.533	0.744	3.9987	114.2491	0.579	0.790	3.9838	113.8214
0.534	0.745	3.9971	114.2017	0.580	0.791	3.9839	113.8254
0.535	0.746	3.9993	114.2643	0.581	0.792	3.9842	113.8343
0.536	0.747	3.9962	114.1757	0.582	0.793	3.9843	113.8377
0.537	0.748	3.9956	114.1589	0.583	0.794	3.9845	113.8414
0.538	0.749	3.9953	114.1517	0.584	0.795	3.9840	113.8294
0.539	0.750	3.9952	114.1497	0.585	0.796	3.9846	113.8451
0.540	0.751	3.9947	114.1349	0.586	0.797	3.9833	113.8080
0.541	0.752	3.9947	114.1340	0.587	0.798	3.9839	113.8260
0.542	0.753	3.9955	114.1569	0.588	0.799	3.9831	113.8023
0.543	0.754	3.9949	114.1391	0.589	0.800	3.9844	113.8411
0.544	0.755	3.9949	114.1389	0.590	0.801	3.9838	113.8231
0.545	0.756	3.9950	114.1431	0.591	0.802	3.9864	113.8977
0.546	0.757	3.9935	114.1003	0.592	0.803	3.9876	113.9300
0.547	0.758	3.9922	114.0640	0.593	0.804	3.9888	113.9643
0.548	0.759	3.9921	114.0597	0.594	0.805	3.9846	113.8454
0.549	0.760	3.9908	114.0234	0.595	0.806	3.9825	113.7869
0.550	0.761	3.9908	114.0223	0.596	0.807	3.9821	113.7731
0.551	0.762	3.9915	114.0414	0.597	0.808	3.9824	113.7840
0.552	0.763	3.9902	114.0057	0.598	0.809	3.9823	113.7786
0.553	0.764	3.9906	114.0157	0.599	0.810	3.9827	113.7906
0.554	0.765	3.9939	114.1117	0.600	0.811	3.9833	113.8094
0.555	0.766	3.9941	114.1180	0.601	0.812	3.9837	113.8191
0.556	0.767	3.9949	114.1391	0.601	0.812	3.9848	113.8526
0.557	0.768	3.9947	114.1351				

Table B-1: Fixed operation for model fitting

Time (days)	Current (mA)	Current Density (mA/m³)
13.16	0.037223983	1.240799417
13.17	0.324061397	10.80204657
13.18	1.02802822	34.26760733
13.20	1.5995197	53.31732333
13.21	1.66986659	55.66221967
13.23	1.70090459	56.69681967
13.24	1.71887036	57.29567867
13.26	1.72675289	57.55842967
13.27	1.73368603	57.78953433
13.28	1.73374787	57.79159567
13.30	1.73716862	57.90562067
13.31	1.73205826	57.73527533
13.33	1.73171312	57.72377067
13.34	1.7310746	57.70248667
13.35	1.73221026	57.740342
13.37	1.73156913	57.718971
13.38	1.73252542	57.75084733
13.40	1.73345003	57.78166767
13.41	1.7332593	57.77531
13.43	1.73722375	57.90745833
13.44	1.74086317	58.02877233
13.45	1.74167752	58.05591733
13.47	1.74632389	58.21079633
13.48	1.74952038	58.317346
13.50	1.75288375	58.42945833
13.51	1.75958034	58.652678
13.52	1.76323149	58.774383
13.54	1.76826213	58.942071
13.55	1.77278966	59.09298867
13.57	1.77961551	59.320517
13.58	1.78986229	59.66207633
13.60	1.79666597	59.88886567
13.61	1.80296972	60.09899067
13.62	1.81537233	60.512411
13.64	1.82931814	60.97727133
13.65	1.840299	61.3433
13.67	1.85703635	61.90121167
13.68	1.87352095	62.45069833
13.70	1.8904347	63.01449
13.71	1.91263873	63.75462433
13.72	1.93953756	64.651252
13.74	1.96616221	65.53874033
13.75	2.00153477	66.71782567
13.77	2.02652533	67.55084433
13.78	2.04835925	68.27864167
13.79	2.06611883	68.87062767
13.81	2.07287092	69.09569733
13.82	2.0739777	69.13259
13.84	2.0803092	69.34364
13.85	2.07703412	69.23447067
13.87	2.07154807	69.05160233
13.88	2.0721348	69.07116
13.89	2.06579454	68.859818
13.91	2.06357427	68.785809
13.92	2.05988642	68.66288067
13.94	2.0590527	68.63509
13.95	2.0626422	68.75474
13.96	2.061099	68.7033
13.98	2.06355713	68.78523767
13.99	2.06755903	68.91863433
14.01	2.06659306	68.88643533
14.02	2.06792913	68.930971
14.04	2.06611436	68.87047867
14.05	2.05998346	68.66611533
14.06	2.05650106	68.55003533
14.08	2.04935707	68.31190233
14.09	2.04706397	68.23546567
14.11	2.04154942	68.05164733
14.12	2.03889646	67.96321533
14.13	2.03826111	67.942037
14.15	2.03733034	67.91101133
14.16	2.03573518	67.85783933
14.18	2.0312665	67.70888333
14.19	2.02678759	67.55958633
14.21	2.02998985	67.66632833
14.22	2.02442408	67.48080267
14.23	2.02704743	67.56824767
14.25	2.01877933	67.29264433
14.26	2.01538447	67.17948233
14.28	2.01212317	67.07077233
14.29	2.00566035	66.855345
14.30	2.00548749	66.849583
14.32	1.99963152	66.654384
14.33	1.99500099	66.500033
14.35	1.9961765	66.53921667
14.36	1.99183095	66.394365
14.38	1.99364666	66.45488867
14.39	1.98995471	66.33182367
14.40	1.98597871	66.19929033
14.42	1.98190026	66.063342
14.43	1.97948851	65.98295033
14.45	1.97760109	65.92003633
14.46	1.97403096	65.801032
14.47	2.00536121	66.84537367
14.49	1.99243948	66.41464933
14.50	1.9914994	66.38331333
14.52	1.98354702	66.118234

14.53	1.98725052	66.241684
14.55	1.98363662	66.12122067
14.56	1.98340267	66.11342233
14.57	1.97611414	65.87047133
14.59	1.96871106	65.623702
14.60	1.96747482	65.582494
14.62	1.96144283	65.38142767
14.63	1.96183119	65.394373
14.64	1.96279436	65.42647867
14.66	1.95975881	65.32529367
14.67	1.95801314	65.26710467
14.69	1.95681453	65.227151
14.70	1.95169989	65.056663
14.72	1.94802452	64.93415067
14.73	1.94846187	64.948729
14.74	1.94602273	64.86742433
14.76	1.94921214	64.973738
14.77	1.94405913	64.801971
14.79	1.9390665	64.63555
14.80	1.93916894	64.63896467
14.81	1.93563364	64.52112133
14.83	1.93325393	64.44179767
14.84	1.92891583	64.29719433
14.86	1.92666743	64.22224767
14.87	1.93153825	64.38460833
14.89	1.92890354	64.29678467
14.90	1.92358717	64.11957233
14.91	1.9450726	64.83575333
14.93	1.94078013	64.692671
14.94	1.93333831	64.44461033
14.96	1.93106364	64.368788
14.97	1.92980431	64.32681033
14.98	1.92358233	64.119411
15.00	1.92257427	64.085809
15.01	1.92133598	64.04453267
15.03	1.91491153	63.83038433
15.04	1.91709436	63.90314533
15.06	1.91428941	63.809647
15.07	1.90972406	63.65746867
15.08	1.90770645	63.590215
15.10	1.90692898	63.56429933
15.11	1.91430654	63.810218
15.13	1.90848522	63.616174
15.14	1.90468468	63.48948933
15.16	1.90590043	63.53001433
15.17	1.90047026	63.34900867
15.18	1.90036874	63.34562467
15.20	1.89756192	63.252064
15.21	1.89744141	63.248047
15.23	1.89024806	63.00826867
15.24	1.88917704	62.972568
15.25	1.88680906	62.89363533
15.27	1.8891193	62.97064333
15.28	1.88265853	62.75528433
15.30	1.89888794	63.29626467
15.31	1.91897042	63.96568067
15.33	1.91978943	63.992981
15.34	1.93606354	64.53545133
15.35	1.92681327	64.227109
15.37	1.92708075	64.236025
15.38	1.93429105	64.47636833
15.40	1.92455053	64.15168433
15.41	1.92247555	64.08251833
15.42	1.92345325	64.11510833
15.44	1.91246234	63.74874467
15.45	1.90220121	63.406707
15.47	1.91129781	63.709927
15.48	1.90430768	63.47692267
15.50	1.92035791	64.01193033
15.51	1.92329008	64.10966933
15.52	1.92394964	64.13165467
15.54	1.9185856	63.95285333
15.55	1.91168785	63.72292833
15.57	1.92209389	64.06979633
15.58	1.91661697	63.88723233
15.59	1.91130843	63.710281
15.61	1.91113874	63.70462467
15.62	1.92838628	64.27954267
15.64	1.92232206	64.077402
15.65	1.91997401	63.99913367
15.67	1.92136168	64.04538933
15.68	1.92202106	64.06736867
15.69	1.91435497	63.81183233
15.71	1.90751702	63.58390067
15.72	1.90155581	63.38519367
15.74	1.91012546	63.67084867
15.75	1.9031981	63.43993667
15.76	1.90088879	63.36295967
15.78	1.89875383	63.29179433
15.79	1.9045718	63.48572667
15.81	1.90548431	63.51614367
15.82	1.90054178	63.35139267
15.84	1.92582775	64.19425833
15.85	1.91260371	63.753457
15.86	1.91188101	63.729367
15.88	1.90101434	63.36714467
15.89	1.89386532	63.128844
15.91	1.89593602	63.19786733
15.92	1.89513378	63.171126
15.93	1.89742856	63.24761867
15.95	1.9043291	63.47763667
15.96	1.89735033	63.245011

15.98	1.89062878	63.02095933
15.99	1.89779997	63.259999
16.01	1.90202948	63.40098267
16.02	1.90080814	63.36027133
16.03	1.89887285	63.29576167
16.05	1.89084094	63.02803133
16.06	1.88771859	62.923953
16.08	1.88781731	62.92724367
16.09	1.87617149	62.53904967
16.10	1.87655464	62.55182133
16.12	1.87565237	62.52174567
16.13	1.87152121	62.38404033
16.15	1.86979808	62.32660267
16.16	1.86534245	62.17808167
16.18	1.85937714	61.979238
16.19	1.85665116	61.888372
16.20	1.85101163	61.70038767
16.22	1.84937343	61.645781
16.23	1.84338633	61.446211
16.25	1.83987916	61.32930533
16.26	1.83705557	61.23518567
16.27	1.8429121	61.43040333
16.29	1.83582287	61.19409567
16.30	1.83164869	61.05495633
16.32	1.83001217	61.00040567
16.33	1.83204059	61.06801967
16.35	1.833665	61.12216667
16.36	1.84251536	61.41717867
16.37	1.83969047	61.32301567
16.39	1.83702763	61.23425433
16.40	1.83439404	61.146468
16.42	1.8256966	60.85655333
16.43	1.8241385	60.80461667
16.44	1.81635898	60.54529933
16.46	1.81302335	60.43411167
16.47	1.80946495	60.31549833
16.49	1.80579647	60.19321567
16.50	1.79761723	59.92057433
16.52	1.79527644	59.842548
16.53	1.79601293	59.86709767
16.54	1.88815277	62.93842567
16.56	1.87597498	62.53249933
16.57	1.86446309	62.14876967
16.59	1.85444634	61.814878
16.60	1.84473153	61.491051
16.61	1.83538459	61.17948633
16.63	1.84806213	61.602071
16.64	1.84581615	61.527205
16.66	1.8302625	61.00875
16.67	1.82176866	60.725622
16.69	1.82019491	60.67316367
16.70	1.80105586	60.03519533
16.71	1.79876219	59.95873967
16.73	1.79121476	59.70715867
16.74	1.77064352	59.02145067
16.76	1.75362732	58.454244
16.77	1.73921958	57.973986
16.79	1.73134953	57.711651
16.80	1.71364471	57.12149033
16.81	1.69167202	56.38906733
16.83	1.67335831	55.77861033
16.84	1.64722018	54.90733933
16.86	1.64622478	54.87415933
16.87	1.6356349	54.52116333
16.88	1.6048342	53.49447333
16.90	1.59303788	53.10126267
16.91	1.57569926	52.52330867
16.93	1.57992765	52.664255
16.94	1.55928424	51.97614133
16.96	1.5391537	51.30512333
16.97	1.53484857	51.161619
16.98	1.50900614	50.30020467
17.00	1.50408065	50.13602167
17.01	1.49538666	49.846222
17.03	1.49429897	49.80996567
17.04	1.46619957	48.873319
17.05	1.44918244	48.30608133
17.07	1.4290737	47.63579
17.08	1.41743738	47.24791267
17.10	1.39964456	46.65481867
17.11	1.37048392	45.68279733
17.13	1.34775657	44.925219
17.14	1.32923666	44.30788867
17.15	1.32632833	44.21094433
17.17	1.30115934	43.371978
17.18	1.27595002	42.53166733
17.20	1.25257196	41.75239867
17.21	1.23896394	41.298798
17.22	1.2163288	40.54429333
17.24	1.21742794	40.58093133
17.25	1.2098101	40.32700333
17.27	1.2221043	40.73681
17.28	1.22529157	40.84305233
17.30	1.18889464	39.62982133
17.31	1.14803892	38.267964
17.32	1.11139016	37.04633867
17.34	1.09299673	36.43322433
17.35	1.07364636	35.788212
17.37	1.06145646	35.381882
17.38	1.12005295	37.33509833
17.39	1.0826014	36.08671333
17.41	1.06912851	35.637617

17.42	1.04387393	34.79579767	17.75	0.76261186	25.42039533
17.44	1.01692602	33.897534	17.76	0.753940223	25.13134077
17.45	1.00761931	33.58731033	17.78	0.745782722	24.85942407
17.47	0.97711077	32.570359	17.79	0.743756909	24.79189697
17.48	0.976120587	32.5373529	17.81	0.735190045	24.50633483
17.49	0.949511211	31.6503737	17.82	0.731768645	24.39228817
17.51	0.927428063	30.91426877	17.83	0.722322986	24.07743287
17.52	0.9145597	30.48532333	17.85	0.71688965	23.89632167
17.54	0.907518994	30.25063313	17.86	0.703770155	23.45900517
17.55	0.894743856	29.8247952	17.88	0.698041171	23.26803903
17.56	0.901705958	30.05686527	17.89	0.686086807	22.86956023
17.58	0.894421712	29.81405707	17.90	0.724630244	24.15434147
17.59	0.885883812	29.5294604	17.92	0.69085774	23.02859133
17.61	0.874110684	29.1370228	17.93	0.6831937	22.77312333
17.62	0.860038679	28.66795597	17.95	0.674019102	22.4673034
17.64	0.844034553	28.1344851	17.96	0.661058258	22.03527527
17.65	0.84710056	28.23668533	17.98	0.656476058	21.88253527
17.66	0.828426331	27.61421103	17.99	0.651837606	21.7279202
17.68	0.811072253	27.03574177	18.00	0.650292682	21.67642273
17.69	0.797119737	26.5706579	18.02	0.649577519	21.65258397
17.71	0.787832495	26.26108317	18.03	0.650723791	21.69079303
17.72	0.77706282	25.902094	18.05	0.646006782	21.5335594
17.73	0.769645255	25.65484183	18.06	0.680382131	22.67940437

Appendix C – Experimental Data for Junction Potential Estimation (Chapter 4)

Table C-1: 0.5M Ammonium Bicarbonate

	Average Conductivity (mS/cm)	Conductivity (mS/cm)	Measured JP (V)	Conductivity (mS/cm)	Measured JP (V)	Conductivity (mS/cm)	Measured JP (V)
HC (AEM)	40.267	40.000		40.300		40.500	
1:500	0.137	0.133	0.11573553	0.152	0.11674310	0.128	0.12468595
1:250	0.245	0.263	0.10671664	0.240	0.10692711	0.231	0.11471810
1:100	0.584	0.603	0.09057211	0.564	0.09284882	0.586	0.09825018
1:50	1.118	1.113	0.07771820	1.132	0.08025551	1.110	0.08587644
1:25	2.113	2.140	0.06470247	2.120	0.06842941	2.080	0.07343210
1:10	5.000	4.950	0.04774056	5.070	0.05086727	4.980	0.05796283
HC (CEM)	40.267	40.000		40.300		40.500	
1:500	0.144	0.126	0.13513095	0.171	0.13690167	0.135	0.13136762
1:250	0.260	0.264	0.13205337	0.243	0.12977728	0.272	0.12160784
1:100	0.596	0.566	0.10821674	0.621	0.10445408	0.600	0.10158041
1:50	1.139	1.088	0.09118289	1.221	0.08646077	1.107	0.08518768
1:25	2.117	2.080	0.07340183	2.180	0.07079667	2.090	0.06851220
1:10	4.957	4.860	0.05073374	4.980	0.04859708	5.030	0.04549511

Table C-2: 1M Ammonium Bicarbonate

	Average Conductivity (mS/cm)	Conductivity (mS/cm)	Measured JP (V)	Conductivity (mS/cm)	Measured JP (V)	Conductivity (mS/cm)	Measured JP (V)
HC (AEM)	70.467	71.600		70.100		69.700	
1:500	0.242	0.238	0.11730187	0.245	0.12165581	0.244	0.12880325
1:250	0.464	0.480	0.10735687	0.462	0.11138418	0.451	0.11796047
1:100	1.136	1.154	0.08811704	1.139	0.09279705	1.115	0.10237475
1:50	2.119	2.200	0.07430569	2.180	0.07920277	1.978	0.08746314
1:25	3.963	4.060	0.06184061	4.180	0.06684738	3.650	0.07297354
1:10	9.313	9.470	0.04381600	9.750	0.04865784	8.720	0.05298802
HC (CEM)	70.850	71.600		70.100			
1:500	0.250	0.279	0.12887239	0.248	0.13384937	0.224	0.13424866
1:250	0.489	0.554	0.12344130	0.456	0.12633725	0.457	0.11926370
1:100	1.166	1.325	0.10145229	1.142	0.10277227	1.031	0.09893778
1:50	2.137	2.180	0.08834425	2.180	0.08590000	2.050	0.08040785
1:25	4.050	4.150	0.07100269	4.170	0.06859271	3.830	0.06445854
1:10	9.383	9.540	0.04842652	9.620	0.04603798	8.990	0.04229058

Table C-3: 2M Ammonium Bicarbonate

	Average Conductivity (mS/cm)	Conductivity (mS/cm)	Measured JP (V)	Conductivity (mS/cm)	Measured JP (V)	Conductivity (mS/cm)	Measured JP (V)
HC (AEM)	115.367	114.700		115.200		116.200	
1:500	0.452	0.447	0.11877796	0.444	0.12753555	0.466	0.14396073
1:250	0.877	0.858	0.10651865	0.878	0.11523373	0.895	0.11440216
1:100	2.057	2.020	0.09066412	2.020	0.09385224	2.130	0.09585389
1:50	3.897	3.830	0.07696968	3.880	0.07289278	3.980	0.08172277
1:25	7.377	7.160	0.06436556	7.420	0.06320367	7.550	0.06698577
1:10	16.893	16.110	0.04680291	17.280	0.04640924	17.290	0.04829865
HC (CEM)	115.967	116.500		115.200		116.200	
1:500	0.470	0.492	0.14217952	0.456	0.12593932	0.461	0.13128206
1:250	0.884	0.837	0.12250000	0.888	0.10590360	0.927	0.11303150
1:100	2.100	2.130	0.10010000	2.120	0.08852058	2.050	0.09243838
1:50	3.917	3.940	0.08410000	3.930	0.07715841	3.880	0.07542825
1:25	7.207	6.700	0.07110000	7.490	0.06424397	7.430	0.05886196
1:10	17.137	17.210	0.04760000	17.340	0.04495428	16.860	0.03884724

Table C-4: 1M Ammonium Carbonate

	Average Conductivity (mS/cm)	Conductivity (mS/cm)	Measured JP (V)	Conductivity (mS/cm)	Measured JP (V)	Conductivity (mS/cm)	Measured JP (V)
HC (AEM)	51.000	51.200		50.900		50.900	
1:500	0.164	0.170	0.13740288	0.154	0.09790956	0.167	0.09495024
1:250	0.315	0.313	0.12573045	0.318	0.09025567	0.313	0.08833654
1:100	0.750	0.752	0.10248822	0.762	0.07769343	0.735	0.07563608
1:50	1.402	1.458	0.08783281	1.403	0.06714585	1.345	0.06635522
1:25	2.763	2.820	0.06853880	2.720	0.05779057	2.750	0.05573678
1:10	6.527	6.580	0.04748849	6.520	0.04430488	6.480	0.04234968
HC (CEM)	51.000	51.200		50.900		50.900	
1:500	0.166	0.172	0.14155366	0.160	0.13096971	0.165	0.13518350
1:250	0.319	0.327	0.13197537	0.315	0.12104840	0.314	0.12450559
1:100	0.753	0.759	0.11329924	0.732	0.10135171	0.768	0.10244089
1:50	1.442	1.454	0.09772205	1.438	0.08479901	1.433	0.08613620
1:25	2.660	2.830	0.08021983	2.380	0.06729763	2.770	0.06861029
1:10	6.457	6.460	0.05834910	6.420	0.04582029	6.490	0.04609065